UNIVERSIDADE DE SÃO PAULO
FACULDADE DE ODONTOLOGIA DE RIBEIRÃO PRETO
PROGRAMA DE PÓS-GRADUAÇÃO EM BIOLOGIA ORAL

RAYANA LONGO BIGHETTI TREVISAN

Efeito da superfície de titânio com nanotopografia sobre a interação entre osteoblastos e osteoclastos

Ribeirão Preto
2022

RAYANA LONGO BIGHETTI TREVISAN

Efeito da superfície de titânio com nanotopografia sobre a interação entre osteoblastos e osteoclastos

Tese apresentada à Faculdade de Odontologia de Ribeirão Preto da Universidade de São Paulo, para obtenção do título de Doutora em Ciências junto ao Programa de Pós-Graduação em Biologia Oral.

Orientador: Prof. Dr. Márcio Mateus Beloti

VERSÃO ORIGINAL

Ribeirão Preto

2022

FICHA CATALOGRÁFICA

Elaborada pela Biblioteca Central do Campus USP - Ribeirão Preto

Bighetti-Trevisan, Rayana Longo

Efeito da superfície de titânio com nanotopografia sobre a interação entre osteoblastos e osteoclastos. / Rayana Longo Bighetti Trevisan; Orientador, Prof. Dr. Márcio Mateus Beloti. Ribeirão Preto, 2022.

130p. : il. ; 30 cm

Tese apresentada à Faculdade de Odontologia de Ribeirão Preto da Universidade de São Paulo, para obtenção do título de Doutora em Ciências junto ao Programa de Pós-Graduação em Biologia Oral.

Versão Original

1. Histona. 2. Nanotopografia. 3. Osso. 4. Osteoblasto. 5. Osteoclasto. 6. Titânio.

FOLHA DE APROVAÇÃO

Bighetti-Trevisan, R.L. **Efeito da superfície de titânio com nanotopografia sobre a interação entre osteoblastos e osteoclastos**

Tese apresentada à Faculdade de Odontologia de Ribeirão Preto da Universidade de São Paulo, para obtenção do título de Doutora em Ciências junto ao Programa de Pós-Graduação em Biologia Oral.

BANCA EXAMINADORA

Prof(a). Dr(a). _____

Instituição:_____

Julgamento: _____Assinatura_____

Prof(a). Dr(a). _____

Instituição:_____

Julgamento: _____Assinatura_____

Prof(a). Dr(a). _____

Instituição:_____

Julgamento: _____Assinatura_____

Este trabalho foi realizado nos Laboratórios de Cultura de Células, de Biologia Molecular e LAB 3D BIO da Faculdade de Odontologia de Ribeirão Preto da Universidade de São Paulo e no Department of Biochemistry and Vermont Cancer Center, University of Vermont Larner College of Medicine, com auxílio financeiro da Fundação de Amparo à Pesquisa do Estado de São Paulo (FAPESP) nas modalidades Bolsa de Doutorado (Processo nº 2017/23888-8), Bolsa de Estágio de Pesquisa no Exterior (BEPE, Processo nº 2019/09349-2) e Auxílio Regular à Pesquisa (Processo nº 2018/17356-6), da Coordenação de Aperfeiçoamento de Pessoal de Nível Superior – Brasil (CAPES) Código de Financiamento 001 e do Conselho Nacional de Desenvolvimento Científico e Tecnológico - CNPq (Processo nº 303464/2016-0).

O sonho

Sonhe com aquilo que você quer ser,
porque você possui apenas uma vida
e nela só se tem uma chance
de fazer aquilo que quer.

Tenha felicidade bastante para fazê-la doce.
Dificuldades para fazê-la forte.
Tristeza para fazê-la humana.
E esperança suficiente para fazê-la feliz.

As pessoas mais felizes não têm as melhores coisas.
Elas sabem fazer o melhor das oportunidades
que aparecem em seus caminhos.

A felicidade aparece para aqueles que choram.
Para aqueles que se machucam
Para aqueles que buscam e tentam sempre.
E para aqueles que reconhecem
a importância das pessoas que passaram por suas vidas.

Clarice Lispector

Dedicatória

Dedico

Ao grande companheiro, que enfrentou comigo todos os obstáculos, dificuldades, ansiedade, medo e incertezas; que foi alicerce nos momentos de insegurança; que trouxe o riso nos momentos de tristeza; que celebrou comigo cada pequena conquista alcançada durante esse período. Quão sortuda sou por ter o melhor amigo, companheiro e amor em uma só pessoa. A você **Junior**, dedico essa conquista! A Deus agradeço a benção concedida pelo nosso encontro!

"As pessoas mais felizes não têm as melhores coisas.
Elas sabem fazer o melhor das oportunidades que aparecem em seus caminhos."

Clarice Lispector

Agradecimentos

Agradeço

A **Deus**, por ser meu grande guia, por proteger meus caminhos e abençoar minha vida.

Aos meus pais, **Telma Aparecida Longo Bighetti** e **Carlos César Bighetti**, e ao meu irmão **Raony Longo Bighetti**, agradeço por tanto amor, carinho e atenção nos momentos de dificuldade, pela paciência, força, por todos os valores ensinados durante a vida, essenciais na construção de meu caráter e essência, e por sempre terem acreditado em mim e em meus sonhos.

Ao meu orientador, Prof. Dr. **Márcio Mateus Beloti**, agradeço imensamente por ter me aceitado como sua aluna de doutorado, por todos os ensinamentos transmitidos, pelas oportunidades a mim disponibilizadas, pela grande contribuição em minha formação profissional, pelo brilhantismo e carinho na condução de todo o nosso trabalho e pelos grandes exemplos de organização, disciplina, excelência na escrita científica e comprometimento. Serei eternamente grata por esse período, inesquecível, e por tudo o que aprendi estando ao seu lado; o levarei para sempre em minha memória e meu coração.

Aos Profs. Drs. **Adalberto Luiz Rosa** e **Paulo Tambasco de Oliveira** pelos grandes ensinamentos, pelas valorosas contribuições no desenvolvimento desse trabalho e em minha formação profissional; por todo apoio, confiança e especialmente pela grande oportunidade de trabalhar ao lado de vocês. Foi uma grande honra poder conviver e aprender tanto durante todos esses anos.

Às Profas. Dras. **Emanuela Prado Ferraz**, **Larissa Moreira Spinola de Castro-Raucci** e **Luciana Oliveira de Almeida** pela grande amizade e carinho, pelas valorosas oportunidades de aprendizado e parceria, por contribuírem grandemente em minha formação docente e pelos grandes exemplos de vida, resiliência, persistência e coragem.

Às Profas. Dras. **Andréia Machado Leopoldino** e **Manoela Domingues Martins** por terem me recebido com tanto carinho em seus respectivos grupos de

pesquisa, pelos grandes ensinamentos, por terem participado sobremaneira de minha formação científica e pessoal durante os valorosos momentos compartilhados com extraordinários exemplos de ética, honestidade e amor.

À Profa. Dra. **Janet Stein** por ter me supervisionado com tanto entusiasmo durante o estágio na Universidade de Vermont, pelos grandes ensinamentos e pelo fabuloso exemplo profissional.

Aos Profs. Drs. **Jonathan Gordon** e **Wilson Araújo da Silva Junior** agradeço por terem sido meus maiores exemplos durante o aprendizado de Bioinformática, pelo grande incentivo e por terem acreditado em minha capacidade, antes mesmo de começar.

Às Profas. Dras. **Karina Fittipaldi Bombonato Prado, Selma Siéssere** e **Simone Cecilio Hallak Regalo** pelas valorosas contribuições em minha formação docente, pelos ensinamentos e agradáveis momentos vividos durante minha passagem no Departamento de Biologia Básica e Oral.

Aos técnicos dos laboratórios LAB 3D BIO, Biologia Molecular, Anatomia, Histologia e Cultura de Células, **Adriana Luisa Gonçalves de Almeida, Fabíola Singaretti de Oliveira, Luiz Gustavo de Sousa, Milla Tavares Ricoldi** e **Roger Rodrigo Fernandes**, pela companhia ao longo desses anos, por toda ajuda na realização desse trabalho e pelos bons momentos compartilhados.

Em especial aos grandes amigos, **Alice Corrêa Silva Souza, Amanda Leal Rocha**, **Ana Luiza Viana Sousa, Daniela Zangrande, Isadora Almeida Poscidonio, Laís Ranieri Makrakis, Lucas Ribeiro Teixeira, Marcela Galvão Tucci, Maria Beatriz Cal Alonso, Marta Maria Giamatei Contente**, **Otávio Guilherme Gonçalves de Almeida**, **Renato Carvalho** e **Vitor Mori**, pela preciosa amizade, apoio e força ao longo da pós-graduação e da vida.

Aos companheiros de laboratório, **Alann Thaffarell Portilho de Souza**, **Ana Patrícia Espaladori Eskenazi**, **Antônio Secco Martorano**, **Denise Weffort**, **Gabriela Guaraldo Campos Tótoli**, **Georgia Kors Quiles**, **Gileade Pereira Freitas,**

Helena Bacha Lopes, Jaqueline Isadora Reis Ramos, Jéssica Emanuella Rocha Moura Paz, **João Lisboa de Sousa Filho**, **Letícia Faustino Adolpho**, **Luciana Tabajara Parreiras e Silva**, **Marcelle Beathriz Fernandes da Silva**, **Maria Paula Oliveira Gomes**, **Paola Gomes Souza**, **Robson Diego Calixto** e **Thaís Moré Milan**, pelos bons momentos vividos durante minha passagem no *Bone Research Lab*.

À secretária do Programa de Pós-Graduação em Biologia Oral, **Imaculada Jainaira Miguel**, por toda ajuda, palavras de conforto e amizade essenciais durante a minha passagem pela pós-graduação. Obrigada por tudo!

À secretária do Departamento de Biologia Básica e Oral, **Clélia Aparecida Celino**, pelos bons momentos compartilhados durante minha passagem no Departamento de Biologia Básica e Oral.

À **FAPESP** pelo apoio financeiro nas modalidades Bolsa de Doutorado (Processo nº 2017/23888-8), BEPE (Processo nº 2019/09349-2) e Auxílio Regular à Pesquisa (Processo nº 2018/17356-6).

À **CAPES**, pelo apoio financeiro. Código de Financiamento 001.

Ao **CNPq** pela Bolsa de Produtividade em Pesquisa (Orientador) (Processo nº 303464/2016-0).

À Faculdade de Odontologia de Ribeirão Preto da Universidade de São Paulo por ter me acolhido durante a realização da Graduação e dos cursos de Pós-Graduação.

A todos os familiares e àqueles que contribuíram direta e indiretamente para a realização desse sonho. Meus sinceros agradecimentos!

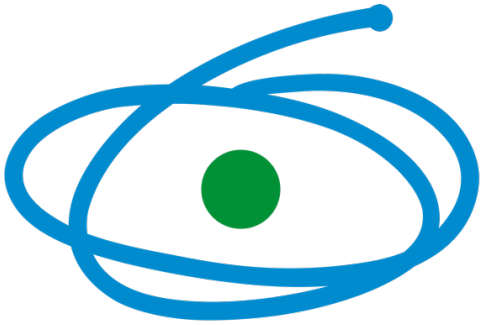

O presente trabalho foi realizado com os seguintes apoios:

- Bolsa de Doutorado (Processo nº 2017/23888-8), BEPE (Processo nº 2019/09349-2) e Auxílio Regular à Pesquisa (Processo nº 2018/17356-6) da Fundação de Amparo à Pesquisa do Estado de São Paulo (FAPESP).

- Bolsa de Doutorado com apoio da Coordenação de Aperfeiçoamento de Pessoal de Nível Superior - Brasil (CAPES) - Código de Financiamento 001.

- Bolsa de Produtividade em Pesquisa (Orientador) CNPq (Processo nº 303464/2016-0).

Resumo

RESUMO

Bighetti-Trevisan RL. **Efeito da superfície de titânio com nanotopografia sobre a interação entre osteoblastos e osteoclastos.** Tese (Doutorado). Ribeirão Preto. Faculdade de Odontologia de Ribeirão Preto, Universidade de São Paulo, 2022.130p.

O processo de remodelação óssea, fundamental para a manutenção da osseointegração de implantes de titânio (Ti), compreende o equilíbrio entre a reabsorção de tecido ósseo por osteoclastos e a formação desse tecido por osteoblastos. Diversos estudos realizados por nosso grupo de pesquisa evidenciaram o papel da superfície de Ti com nanotopografia, obtida por condicionamento químico com solução de H_2SO_4/H_2O_2, na diferenciação osteoblástica, em diferentes condições. Entretanto, ainda não foram investigados os efeitos dessa superfície sobre a diferenciação e atividade osteoclásticas, e sobre a interação destas células com osteoblastos. Nesse contexto, nossa hipótese é que a nanotopografia, além de favorecer a diferenciação osteoblástica, é capaz de modular a diferenciação osteoclástica e a interação osteoblasto/osteoclasto. Assim, esse estudo teve como objetivo determinar a influência da superfície de Ti com nanotopografia (Ti Nano), comparada com a superfície de Ti usinada (Ti Controle), na interação entre osteoblastos e osteoclastos. Células pré-osteoblásticas (MC3T3-E1) e macrófagos (RAW 264.7) foram plaqueadas em ambas as superfícies de Ti e em insertos a 10.000 células/disco e cultivadas sob condições osteogênicas e osteoclastogênicas por 5 dias. No dia 5, os insertos contendo os osteoblastos foram posicionados nas culturas de osteoclastos e os insertos contendo osteoclastos foram posicionados nas culturas de osteoblastos, estabelecendo assim co-culturas indiretas, que foram mantidas por 2 dias. Os controles foram células não co-cultivadas crescidas sobre ambas as superfícies de Ti. Ensaios com meio condicionado por osteoblastos crescidos sobre Ti Nano e Ti Controle, utilizados em culturas de osteoclastos cultivados sobre poliestireno também foram realizados, com a mesma densidade celular e intervalos de cultura. Os resultados referentes ao efeito de osteoclastos em osteoblastos crescidos sobre as diferentes superfícies demostraram, através de RNASeq (DESeq2: FC>1,7; p≤0,05) que os osteoclastos regulam negativamente a expressão de genes relacionados à osteogênese e regulam positivamente genes relacionados à modificação de histonas e organização da cromatina em osteoblastos cultivados em ambas as superfícies. Os osteoclastos também inibiram (p≤0,05) a expressão gênica e proteica de marcadores osteogênicos, e tal efeito foi reduzido pelo Ti Nano. Em relação ao mecanismo envolvido, observou-se aumento na expressão das proteínas H3K9me2, H3K27me3 e EZH2 em ambas as superfícies de Ti em condições de cocultura (p≤0,05). O ensaio ChIP revelou acúmulo de H3K9me2 reprimindo a região promotora de *Alpl* e H3K27me3 reprimindo *Runx2*, *Alpl*, *Ibsp* e *Opg* em osteoblastos na presença de osteoclastos, o que foi atenuado por Ti Nano. A imunofluorescência corroborou o ensaio ChIP, exibindo menos RUNX2 e ALP e mais H3K27me3 em osteoblastos em condições de co-cultura de forma menos pronunciada em Ti Nano. Os resultados referentes ao efeito de osteoblastos em osteoclastos crescidos sobre Ti Nano e Ti Controle e na presença de meio condicionado demostraram, através de análises de expressão gênica, que a nanotopografia favorece a diferenciação osteoclástica (p≤0,05), que foi potencializada pela presença dos osteoblastos, com aumento da expressão dos marcadores *Rank*, *Ctsk*, *Tnf-α* e da via de sinalização Rank/Rankl

como *cFos*, *Mitf*, *Nfatc1*, e *Traf6* (p≤0,05); entretanto, os osteoclastos apresentaram menor atividade, uma vez que houve diminuição da marcação de TRAP e da expressão das proteínas CTSK e TRAP, principalmente sobre Ti Nano na presença dos osteoblastos. Em conclusão, o Ti Nano pode favorecer resultados clínicos em termos de osseointegração de implantes, uma vez que a nanotopografia favorece a diferenciação osteoblástica, protege osteoblastos do efeito deletério de osteoclastos e modula a diferenciação osteoclástica, evidenciando um possível papel sobre o processo de remodelação óssea. Através desses achados, novas abordagens terapêuticas podem ser desenvolvidas, utilizando estratégias capazes de modular as atividades de osteoblastos e osteoclastos por diferentes nanotopografias, com objetivo de favorecer a interação entre biomateriais e o tecido ósseo.

Palavras-chave: histona, nanotopografia, osso, osteoblasto, osteoclasto, titânio.

Abstract

ABSTRACT

Bighetti-Trevisan RL. **Effect of titanium with nanotopography on the interaction between osteoblasts and osteoclasts.** Thesis (Doctor's Degree). Ribeirão Preto. School of Dentistry of Ribeirão Preto, University of São Paulo, 2022. 130p.

The bone remodeling process, essential for the maintenance of osseointegration of titanium (Ti) implants, comprises the balance between the resorption of bone tissue by osteoclasts and the formation by osteoblasts. Several studies developed by our research group demonstrated the role of the Ti surface with nanotopography, obtained by chemical conditioning with a H_2SO_4/H_2O_2 solution, in osteoblast differentiation under different conditions. However, the effects of this surface on osteoclast differentiation and activity, and their interaction with osteoblasts have not been investigated yet. In this context, our hypothesis is that nanotopography, in addition to favor osteoblast differentiation, is capable of modulating osteoclast differentiation and the osteoblast/osteoclast interaction. Thus, the aim of this study was to determine the influence of the Ti surface with nanotopography (Ti Nano), compared to the machined Ti surface (Ti Control), on the interaction between osteoblasts and osteoclasts. Pre-osteoblastic cells (MC3T3-E1) and macrophages (RAW 264.7) were plated on both Ti surfaces and on inserts at 10,000 cells/disc or insert and cultured under osteogenic and osteoclastogenic conditions for 5 days. On day 5, inserts containing osteoblasts were placed in osteoclastic cultures and inserts containing osteoclasts were placed in osteoblastic cultures, thus establishing indirect co-cultures, which were maintained for 2 days. Controls were non-co-cultured cells grown on both Ti surfaces. Assays with conditioned media by osteoblasts grown on Ti Nano and Ti Control, used in osteoclast cultures grown on polystyrene were also performed, with the same cell density and time points. Regarding the effect of osteoclasts on osteoblasts grown on Ti surfaces, the RNASeq (DESeq2: FC>1.7; $p \leq 0.05$) evidenced that osteoclasts downregulated the expression of genes related to osteogenesis and upregulated genes related to histone modification and chromatin organization in osteoblasts cultured on both Ti Nano and Ti Control. Osteoclasts also inhibited ($p \leq 0.05$) gene and protein expression of osteogenic markers, and this effect was reduced by Ti Nano. Regarding the mechanism involved, an increase in the expression of H3K9me2, H3K27me3 and EZH2 proteins was observed on both Ti surfaces under co-culture conditions ($p \leq 0.05$). The ChIP assay revealed accumulation of H3K9me2 repressing the promoter region of *Alpl* and H3K27me3 repressing *Runx2*, *Alpl*, *Ibsp* and *Opg* in osteoblasts in the presence of osteoclasts, which was attenuated by Ti Nano. Immunofluorescence corroborated the ChIP assay, exhibiting less RUNX2 and ALP and more H3K27me3 staining in osteoblasts under co-culture conditions in a less pronounced way on Ti Nano. The results of the effect of osteoblasts on osteoclasts grown on Ti Nano and Ti Control and in the presence of conditioned medium showed, through gene expression analysis, that nanotopography favored osteoclast differentiation ($p \leq 0.05$), which was potentiated by the presence of osteoblasts, with an increased expression of markers such as *Rank*, *Ctsk*, *Tnf-*α and genes related to Rank/Rankl signaling pathway such as *cFos*, *Mitf*, *Nfatc1*, and *Traf6* ($p \leq 0.05$); however, osteoclasts showed lower activity, as indicated by reduced TRAP staining and protein expression of CTSK and TRAP, mainly on Ti Nano in the presence of osteoblasts. In conclusion, Ti Nano may favor clinical results in terms of implants osseointegration, since nanotopography favors osteoblast differentiation, protects osteoblasts from the deleterious effect of osteoclasts and

modulates osteoclast differentiation, evidencing a possible role in the bone remodeling process. Through these findings, new therapeutic approaches can be developed using strategies capable of modulating the activities of osteoblasts and osteoclasts by different nanotopographies, in order to favor the interaction between biomaterials and bone tissue.

Keywords: histone, nanotopography, bone, osteoblast, osteoclast, titanium.

Sumário

SUMÁRIO

Lista de Figuras

LISTA DE FIGURAS

CAPÍTULO 1

CAPÍTULO 2

Lista de Tabelas

LISTA DE TABELAS

CAPÍTULO 1

CAPÍTULO 2

1. Introdução

1. INTRODUÇÃO

As pesquisas nas áreas de Odontologia e Ortopedia têm como um dos focos as interações entre implantes de titânio (Ti) e tecido ósseo, eventos fundamentais para o processo de osseointegração (BRANEMARK, 1983; HOU et al., 2022; MAVROGENIS et al., 2009; SILVERWOOD et al., 2016). A topografia das superfícies de implantes tem sido considerada um fator que influencia a osseointegração por estimular a osteogênese ao regular a diferenciação de células osteoprogenitoras, resultando na formação de matriz extracelular mineralizada e neoformação óssea (DALBY et al., 2007; DE OLIVEIRA et al., 2007; REN et al., 2021; SOUZA et al., 2019). Entretanto, o processo de osseointegração baseia-se não somente na osteogênese, mas também na remodelação óssea, compreendida pelo equilíbrio entre a atividade de reabsorção de tecido ósseo por osteoclastos e a formação desse tecido por osteoblastos (NAGASAWA et al., 2016; UENAKA et al., 2022).

A remodelação óssea, regulada por contínuos ciclos de reabsorção e formação ósseas, é um processo fisiológico natural e depende de uma complexa interação entre osteoblastos e osteoclastos (ERIKSEN, 2010; KIM et al., 2020; TU; CHEN; SHIE, 2015; ZHANG et al., 2022). Enquanto osteoblastos são derivados de células-tronco mesenquimais, osteoclastos são derivados de linhagens celulares hematopoiéticas e formados pela fusão predominantemente de macrófagos após contato com o estroma ou células osteoblásticas, gerando assim células multinucleadas responsáveis pela reabsorção óssea (MATSUO; IRIE, 2008; YOUNG et al., 2015). Os osteoblastos sintetizam citocinas e fatores de crescimento que regulam a formação e atividade de osteoclastos, incluindo o ligante do receptor ativador do fator nuclear Kappa B (RANKL) e o fator estimulante de colônias de macrófagos (M-CSF) que induzem a osteoclastogênese. Desde a identificação do gene que codifica o RANKL, formas solúveis de RANKL e de M-CSF têm sido utilizadas para obtenção de células osteoclásticas *in vitro* na ausência de osteoblastos, simplificando a análise dos eventos envolvidos na diferenciação osteoclástica (CIAPETTI et al., 2017; COSTA-RODRIGUES et al., 2016; MATSUO; IRIE, 2008).

Os mecanismos de favorecimento ou indução da diferenciação osteoblástica por características topográficas e químicas de superfícies do Ti têm sido amplamente abordados na literatura (DE OLIVEIRA et al., 2007; CASTRO-RAUCCI

et al., 2016; MARTIN et al., 1995; MENDONÇA et al., 2010; MORANDINI RODRIGUES et al., 2022). Nosso grupo de pesquisa investiga a interação entre osteoblastos e uma superfície de Ti com nanotopografia (Ti Nano) extensamente caracterizada, obtida pelo tratamento com solução de H_2SO_4/H_2O_2, baseado em desoxidação e reoxidação controladas (VARIOLA et al., 2008; YI et al., 2006). Trata-se de um procedimento simples, extremamente reprodutível e de baixo custo, que gera uma superfície com rugosidade de superfície três vezes maior quando comparada à superfície não tratada (Ti Controle), espessura da camada de óxido de Ti (TiO_2) aumentada de 5 nm para 32-40 nm, redução da presença de contaminantes como silício e nitrogênio e com nanocavidades de aproximadamente 22 nm (YI et al., 2006). As várias investigações realizadas ao longo dos anos produziram resultados que mostram que a nanotopografia é capaz de induzir a diferenciação de osteoblastos em condições osteogênicas e não-osteogênicas (DE OLIVEIRA et al., 2007; ROSA et al., 2014). Também demonstramos que o potencial osteogênico da nanotopografia envolve, pelo menos, três mecanismos celulares: (1) a modulação da via de sinalização de integrinas (LOPES et al., 2019; ROSA et al., 2014), (2) a modulação da via de sinalização de proteínas ósseas morfogenéticas (BMPs) por uma combinação de aumento da produção endógena de BMP-2 e de redução da expressão de alguns microRNAs, responsáveis pela inibição das proteínas intracelulares SMAD1 e SMAD4, ambas transdutoras do sinal osteogênico da BMP-2 (KATO et al., 2014; CASTRO-RAUCCI et al., 2016) e (3) modulação da via de sinalização de Wnt (ABUNA et al., 2019, 2020).

As investigações da interação entre osteoblastos e osteoclastos na presença de diferentes biomateriais por meio de modelos de culturas isoladas ou co-culturas de células osteoblásticas em combinação com precursores de osteoclastos (células mononucleares de sangue periférico ou monócitos/macrófagos isolados), na presença ou ausência de RANKL ou M-CSF, têm sido extensamente reportadas (CIAPETTI et al., 2017; COSTA-RODRIGUES et al., 2016; DETSCH; MAYR; ZIEGLER, 2008; HE et al., 2022; YOUNG et al., 2015). Em estudo utilizando as linhagens MC3T3-E1 (células osteoblásticas) e RAW 264.7 (macrófagos isolados) observou-se que o cimento de silicato de cálcio reduziu o potencial de diferenciação das células RAW 264.7 por inibição da expressão gênica e proteica do receptor ativador do fator nuclear Kappa B (RANK); além disso, essa linhagem atuou na indução da diferenciação osteoblástica das células da linhagem MC3T3-E1 por aumentar a expressão de BMP-2, ativando sua via de sinalização, resultando em

maior deposição de matriz mineralizada (TU; CHEN; SHIE, 2015). Em estudo recente utilizando a linhagem RAW 264.7, observou-se que uma superfície de Ti nanoporosa inibiu a diferenciação osteoclástica através da fosforilação de FAK mediada por integrina e sua via MAPK. Os autores ainda observaram que a expressão de clastocinas, por osteoclastos e citocinas, por macrófagos, pode ser afetada por essa superfície, e que essas alterações podem ser benéficas para o processo de regeneração óssea (HE et al., 2022). No entanto, o efeito da superfície de Ti Nano sobre a diferenciação e atividade osteoclásticas e sobre sua interação com osteoblastos permanecia desconhecido.

Considerando a relevância da atividade osteoclástica e da interação osteoblasto/osteoclasto na resposta do tecido ósseo ao Ti e o potencial osteogênico da nanotopografia, demostramos, pela primeira vez, através de estudo baseado em cultura de células da linhagem RAW 264.7 isoladas e em co-cultura com células da linhagem MC3T3-E1, e na cultura de células da linhagem MC3T3-E1 isoladas e em co-cultura com células da linhagem RAW 264.7, o impacto do Ti com nanotopografia sobre o *crosstalk* entre osteoblastos e osteoclastos. Concluímos no capítulo 1 que, apesar de osteoclastos inibirem osteoblastos cultivados tanto no Ti Controle quanto no Ti Nano, a nanotopografia atenuou o efeito negativo dos osteoclastos sobre a diferenciação osteoblástica, ao impedir o aumento do acúmulo de histonas que medeiam a repressão da expressão gênica nas regiões promotoras do fator de transcrição relacionado ao gene runt 2 (*Runx2*) e fosfatase alcalina (*Alpl*), genes essenciais para a diferenciação osteoblástica. No capítulo 2 demonstramos que a nanotopografia favorece a diferenciação osteoclástica, que foi favorecida pela presença dos osteoblastos. Entretanto, apesar dos osteoclastos apresentarem a expressão de marcadores específicos da diferenciação celular aumentada, essas células exibiram menor atividade, evidenciada pela diminuição da marcação da fosfatase ácida resistente ao tartarato (TRAP) e da expressão proteica, principalmente quando crescidos sobre a nanotopografia e na presença de osteoblastos. Nós acreditamos que os resultados gerados por este estudo contribuirão para o desenvolvimento de novas abordagens terapêuticas utilizando estratégias capazes de modular as atividades de osteoblastos e osteoclastos, visando o equilíbrio do processo de remodelação e assim favorecendo a interação entre biomateriais e o tecido ósseo.

2. Proposição

2. PROPOSIÇÃO

Determinar a influência do Ti Nano, comparado ao Ti Controle, na interação entre osteoblastos e osteoclastos.

Capítulo 1

CAPÍTULO 1 – EFEITO DE OSTEOCLASTOS SOBRE OSTEOBLASTOS CRESCIDOS NO TI NANO

Este capítulo é apresentado em formato de artigo científico, publicado no periódico Biomaterials Advances (IF = 7.328, doi: 10.1016/j.msec.2021.112548), cuja autorização para uso nesta tese é apresentada no Anexo A.

1.1 OBJETIVO

- Avaliar o papel do Ti Nano sobre os efeitos de osteoclastos em osteoblastos por meio da regulação de histonas.

1.2 ARTIGO CIENTÍFICO

ARTICLE IN PRESS

MSC-112548; No of Pages 13

Biomaterials Advances xxx (xxxx) xxx

Contents lists available at ScienceDirect

Biomaterials Advances

journal homepage: www.elsevier.com/locate/bioadv

Titanium with nanotopography attenuates the osteoclast-induced disruption of osteoblast differentiation by regulating histone methylation

Rayana L. Bighetti-Trevisan [a], Luciana O. Almeida [a], Larissa M.S. Castro-Raucci [b], Jonathan A.R. Gordon [c], Coralee E. Tye [c], Gary S. Stein [c], Jane B. Lian [c], Janet L. Stein [c], Adalberto L. Rosa [a], Marcio M. Beloti [a,*]

[a] Bone Research Lab, School of Dentistry of Ribeirão Preto, University of São Paulo, Ribeirão Preto, SP, Brazil
[b] School of Dentistry, University of Ribeirão Preto, Ribeirão Preto, SP, Brazil
[c] Department of Biochemistry and Vermont Cancer Center, University of Vermont Larner College of Medicine, Burlington, VT, USA

ARTICLE INFO

Keywords:
Histone
Nanotopography
Osteoblast
Osteoclast
Titanium

ABSTRACT

The bone remodeling process is crucial for titanium (Ti) osseointegration and involves the crosstalk between osteoclasts and osteoblasts. Considering the high osteogenic potential of Ti with nanotopography (Ti Nano) and that osteoclasts inhibit osteoblast differentiation, we hypothesized that nanotopography attenuate the osteoclast-induced disruption of osteoblast differentiation. Osteoblasts were co-cultured with osteoclasts on Ti Nano and Ti Control and non-co-cultured osteoblasts were used as control. Gene expression analysis using RNAseq showed that osteoclasts downregulated the expression of osteoblast marker genes and upregulated genes related to histone modification and chromatin organization in osteoblasts grown on both Ti surfaces. Osteoclasts also inhibited the mRNA and protein expression of osteoblast markers, and such effect was attenuated by Ti Nano. Also, osteoclasts increased the protein expression of H3K9me2, H3K27me3 and EZH2 in osteoblasts grown on both Ti surfaces. ChIP assay revealed that osteoclasts increased accumulation of H3K27me3 that represses the promoter regions of *Runx2* and *Alpl* in osteoblasts grown on Ti Control, which was reduced by Ti Nano. In conclusion, these data show that despite osteoclast inhibition of osteoblasts grown on both Ti Control and Ti Nano, the nanotopography attenuates the osteoclast-induced disruption of osteoblast differentiation by preventing the increase of H3K27me3 accumulation that represses the promoter regions of some key osteoblast marker genes. These findings highlight the epigenetic mechanisms triggered by nanotopography to protect osteoblasts from the deleterious effects of osteoclasts, which modulate the process of bone remodeling and may benefit the osseointegration of Ti implants.

1. Introduction

A focus of biomaterial investigation is the interactions between titanium (Ti) implants and bone tissue, an essential component of osseointegration [1–4]. To improve the integrative ability of Ti, modifications of implant surfaces have been made, such as functionalization with molecules and creation of different topographies. These modifications affect signaling pathways and cellular events involved in cell adhesion and proliferation, as well as osteoprogenitor cell differentiation, which ultimately regulate the formation of mineralized extracellular matrix [5–9].

Chemical conditioning with H_2SO_4/H_2O_2 solution creates a Ti surface with nanotopography that reduces the contaminants, increases the oxide layer (TiO_2) from 5 to 32-40 nm and generates nano-sized pits of 20-22 nm average diameters [6,10,11]. This nanotopography favors cell adhesion and osteoblast differentiation by modulating several signaling pathways such as integrins, bone morphogenetic proteins (BMPs) and Wnt [6,7,11–14]. To date, there are no investigations on the effects of this nanotopography on the crosstalk between osteoblasts and osteoclasts, which may have a direct impact on bone remodeling and consequently on Ti osseointegration.

Bone remodeling is a physiological process regulated by continuous cycles of bone resorption and formation and depends on complex interactions between osteoblasts and osteoclasts [15]. Osteoblasts are derived from mesenchymal stem cells and osteoclasts are derived from hematopoietic cells through the fusion of macrophages after contact with stromal or osteoblastic cells, thus forming multinucleated cells [16,17]. Osteoblasts synthesize cytokines and growth factors that regulate the formation and activity of osteoclasts, including receptor activator of nuclear factor Kappa B ligand (RANKL) and macrophage colony stimulating factor (M-CSF); osteoclasts secrete sphingosine 1 phosphate (S1P), collagen triple helix repeat containing 1 (CTHRC1) and complement component C (C3) that stimulate while semaphorin 4D (SEMA4D) and sclerostin (SCL) inhibit osteoblast differentiation [16,18–21]. Such fine balance of the interactions between osteoblasts and osteoclasts is regulated by several cell mechanisms, including epigenetic modifications.

* Corresponding author at: School of Dentistry of Ribeirão Preto, University of São Paulo, Av. do Café, s/n, 14040-904 Ribeirão Preto, SP, Brazil.
E-mail address: mmbeloti@usp.br (M.M. Beloti).

http://dx.doi.org/10.1016/j.msec.2021.112548
Received 28 July 2021; Received in revised form 11 October 2021; Accepted 9 November 2021
Available online xxxx

Please cite this article as: R.L. Bighetti-Trevisan, L.O. Almeida, L.M.S. Castro-Raucci, et al., Titanium with nanotopography attenuates the osteoclast-induced disruption of osteoblast..., Biomaterials Advances, http://dx.doi.org/10.1016/j.msec.2021.112548

Epigenetic modifications comprise changes in response to environmental stimuli without alterations of the DNA sequence. The phenomenon is based on chemical modifications of proteins and DNA resulting in a diversity of chromatin accessibility [22]. Histone methylation, a mechanism that contributes to chromatin dynamics and occurs through enzymes that catalyze the addition of methyl groups to lysine and arginine residues of histones, is associated with changes in the activation and repression of gene expression. Depending on the histone and the residue that will undergo, these changes can participate in the regulation of several tumors and acting on cell differentiation [22–25]. Histones H3K9 and H3K27 methylations, which are associated with a highly compacted and transcriptionally repressed chromatin, inhibit gene transcription and the osteoblast differentiation [26–28]. Such inhibitory effects of histone methylation on osteoblast differentiation are underexplored in the crosstalk between osteoblasts and osteoclasts, especially in the context of Ti osseointegration.

Considering the high osteogenic potential of Ti with nanotopography and that osteoclasts inhibit osteoblast differentiation, we hypothesized that this nanotopography inhibits the deleterious effects of osteoclasts on osteoblasts by regulating histone modifications. To test this hypothesis, we established a co-culture model in which osteoblasts were grown on Ti discs and osteoclasts were cultured into inserts positioned above the discs, thus sharing the same microenvironment. Our results demonstrated that this nanotopography attenuated the disruption of osteoblast differentiation induced by osteoclasts by reducing the accumulation of methylated histones that repress the promoter regions of some osteoblast marker genes.

2. Materials and methods

2.1. Materials and reagents

Discs of commercially pure grade II Ti (1.0 mm thickness and 13 mm in diameter) were purchased from Realum (São Paulo, São Paulo, Brazil) and silicon carbides from Norton (Guarulhos, São Paulo, Brazil). MC3T3-E1 and RAW 264.7 cell lines were obtained from American Type Culture Collection (ATCC) (Manassas, Virginia, USA). Minimum essential medium alpha-modification (α-MEM), Dulbeccco's modified eagle medium (DMEM), fetal bovine serum (FBS), penicillin-streptomycin, TRIzol reagent and immunoprecipitation kit dynabeads protein G were purchased from Thermo Fisher Scientific (Waltham, Massachusetts, USA). β-glycerophosphate, L-ascorbic acid, bovine serum albumin, Tween® 20, bone morphogenetic protein receptor type 1A antibody (anti-BMPR1A, SAB1302614), Hoechst 33258 (bisBenzimide H 33258 solution), phenylmethanesulfonyl fluoride and ethyl alcohol pure were purchased from Sigma-Aldrich (St. Louis, Missouri, USA). Runt related transcription factor 2 (anti-RUNX2, 8486S), dimethyl-histone H3 (Lys9) (anti-H3K9me2, D85B4), tri-methyl-histone H3 (Lys27) (anti-H3K27me3, C36B11), enhancer of zeste 2 polycomb repressive complex 2 subunit (anti-EZH2, D2C9) and secondary horseradish peroxidase-conjugated goat anti-rabbit IgG (7074S) antibodies were purchased from Cell Signaling (Beverly, Massachusetts, USA). Alkaline phosphatase (anti-ALPL, ab108337) and anti-RUNX2 (ab76956) were purchased from Abcam (Cambridge, Massachusetts, United Kingdom) and glyceraldehyde-3-phosphate dehydrogenase (anti-GAPDH, sc-25,778) and anti-ALPL (sc-137,213) from Santa Cruz Technology (Dallas, Texas, USA). Red-fluorescent Alexa Fluor 594-conjugated goat anti-mouse secondary antibody (A11005) and green-fluorescent Alexa Fluor 488-conjugated goat anti-rabbit secondary antibody (A11008) were purchased from Molecular Probes (Eugene, Oregon, USA). Twenty-four-well ThinCert™ cell culture inserts and 24-well plates were purchased from Greiner Bio-One (Frickenhausen, Baden-Württemberg, Germany), Millex GV filter (0.22 μm), ethanol, formaldehyde, sulfuric acid (95–97%) and hydrogen peroxide (30%) from Merck Millipore (Darmstadt, Hesse, Germany) and RANKL from Peprotech (Rocky Hill, Connecticut, USA). SMARTer® Stranded Total RNA Hi Mammalian Sample Prep Kit was purchased from Takara (Mountain View, California, USA) and Qubit® RNA HS assay kit from Life Technologies (Carlsbad, California, USA). High-capacity cDNA reverse transcription kit and Fast SYBR green master mix reagent was obtained from Applied Biosystems (Foster City, California, USA). Protease inhibitor tablets and MG132 proteasome inhibitor were acquired from Roche Applied Science (Indianapolis, Indiana, USA). *Trans*-blot turbo PVDF membrane, nonfat powdered milk and Clarity western ECL substrate were purchased from Bio-Rad Laboratories (Hercules, California, USA). MinElute PCR purification kit was purchased from QIAGEN (Hilden, Nordrhein-Westfalen, Germany). UNC1999 was purchased from Cayman Chemical (Ann Arbor, Michigan, USA).

2.2. Ti surface modification and characterization

The discs of Ti (Realum) were polished with silicon carbide (320 and 600 grit) (Norton), cleaned in 70% ethanol (Merck) and washed by sonication in distilled water. The discs were conditioned for 4 h, at room temperature, with a mixture of 10 N H_2SO_4 (Merck) and 30% aqueous H_2O_2 (Merck) to obtain the nanotopography (Ti Nano) [10]. Non-conditioned discs were used as control (Ti Control). Before cell culture experiments, all discs were cleaned by sonication, air-dried and autoclaved. The surfaces were characterized by field emission scanning electron microscopy (SEM) operated at 5 kV (Inspect S50, FEI, Hillsboro, Oregon, USA) and by atomic force microscopy (AFM) using an AFM Bruker Multimode 8 Microscope (Bruker, Santa Barbara, California, USA) operated in air using the contact mode and a contact probe DNP-10 (Bruker) with tip radius of 20 nm and spring constant of 0.35 N/m. The AFM images were treated, and the surface area ($n = 5$) were calculated using the software NanoScope Analysis 1.5 (Bruker).

2.3. Effect of osteoclasts on osteoblasts grown on Ti Nano

2.3.1. Cell cultures

MC3T3-E1 pre-osteoblastic cells were cultured in α-MEM (Gibco - Thermo Fisher Scientific), supplemented with 10% FBS (Gibco - Thermo Fisher Scientific), 100 U/mL penicillin (Gibco - Thermo Fisher Scientific) and 100 μg/mL streptomycin (Gibco - Thermo Fisher Scientific) and RAW 264.7 macrophage cells were cultured in DMEM (Gibco - Thermo Fisher Scientific), supplemented with 10% FBS (Gibco - Thermo Fisher Scientific), 100 U/mL penicillin (Gibco - Thermo Fisher Scientific) and 100 μg/mL streptomycin (Gibco - Thermo Fisher Scientific), both non-inducing differentiation media, and kept at 37 °C in a humid atmosphere containing 5% CO_2 and 95% atmospheric air. After subconfluence, MC3T3-E1 cells were plated on Ti Nano and Ti Control discs and RAW 264.7 cells on 24-well ThinCert (Greiner Bio-One), in 24-well culture plates (Greiner Bio-One) at a density of 1×10^4 cells/well or insert. MC3T3-E1 cells were cultured in osteogenic medium, constituted by α-MEM (Gibco - Thermo Fisher Scientific), supplemented with 10% FBS (Gibco - Thermo Fisher Scientific), 100 U/mL penicillin (Gibco - Thermo Fisher Scientific), 100 μg/mL streptomycin (Gibco - Thermo Fisher Scientific), 7 mM β-glycerophosphate (Sigma-Aldrich) and 5 μg/mL L-ascorbic acid (Sigma-Aldrich) for 5 days and RAW 264.7 cells were cultured in osteoclastogenic medium, constituted by DMEM (Gibco - Thermo Fisher Scientific), supplemented with 10% FBS (Gibco - Thermo Fisher Scientific), 100 U/mL penicillin (Gibco - Thermo Fisher Scientific), 100 μg/mL streptomycin (Gibco - Thermo Fisher Scientific) and 50 ng/mL of RANKL (Peprotech) also for 5 days, and they were kept separated during this time. On day 5, the inserts containing the osteoclasts were positioned above osteoblast cultures, thereby establishing an indirect co-culture system. The osteoblast-osteoclast co-cultures were kept in α-MEM (Gibco - Thermo Fisher Scientific), supplemented with 10% FBS (Gibco - Thermo Fisher Scientific), 100 U/mL penicillin (Gibco - Thermo Fisher Scientific), 100 μg/mL streptomycin (Gibco - Thermo Fisher Scientific), 7 mM β-glycerophosphate (Sigma-Aldrich), 5 μg/mL L-ascorbic acid (Sigma-Aldrich) and 50 ng/mL of RANKL (Peprotech) for another 2 days, completing 7 days of culture in differentiation media. The co-culture medium was α-MEM supplemented with osteoblast and osteoclast differentiation factors, since DMEM reduced osteoblast differentiation compared to α-MEM, while α-MEM did not affect osteoclast differentiation

compared to DMEM (data not shown). The controls were non-co-cultured osteoblasts grown on both Ti surfaces.

2.3.2. RNA isolation and library preparation

On day 7 (2 days of co-culture), the total RNA was isolated from the osteoblasts using TRizol reagent (Invitrogen - Thermo Fisher Scientific), according to the manufacturer's specifications. RNA integrity was assessed by Bioanalyzer (Agilent, Santa Clara, California, USA). RNA-Seq libraries were built with the SMARTer® Stranded Total RNA Hi Mammalian Sample Prep Kit (Takara) according to the manufacturer's protocol. The quality and quantification of RNA-Seq libraries were determined by Bioanalyzer (Agilent) and Qubit® (Life Technologies). The RNA-Seq libraries were single-end sequenced considering 75-bp single-end reads using a Hi-Seq 1500 Platform (Illumina, Hayward, California, USA) and three biological replicates ($n = 3$) of each sample.

2.3.3. RNA-Seq analysis

The dataset analysis was performed using the Galaxy Platform and RStudio [29,30]. The quality control of raw reads was done using FastQC and the alignment to reference genome mm10 using STAR [31,32]. The process data from high-throughput sequencing assays (expression counts) was performed using HTSeq with gene annotations (Gencode m23) [33, 34]. Differential expression was analyzed by DESeq2 [35]. The GO enrichment analyses were performed using Gene Ontology (GO Ontology database Released 2019-12-09) and PANTHER Overrepresentation Test (Released 20,190,711) [36–38]. To consider differential gene expression, the cutoff for significant fold change was >1.7, and adjusted *p*-value <0.05.

2.3.4. mRNA expression by real-time polymerase chain reaction (RT-qPCR)

On day 7 (2 days of co-culture), RT-qPCR was carried out to evaluate the gene expression of runt related transcription factor 2 (*Runx2*), distal-less homeobox 5 (*Dlx5*), alkaline phosphatase (*Alpl*), bone sialoprotein (*Ibsp*), osteocalcin (*Bglap*), osteoprotegerin (*Opg*), bone morphogenetic protein receptor type 1A (*Bmpr1a*), inhibitor of DNA binding 3 (*Id3*), jun D proto-oncogene (*Jund*) and matrix metallopeptidase 13 (*Mmp13*). The total RNA collected from osteoblasts was quantified and the cDNA was done using high-capacity cDNA reverse transcription kit (Applied Biosystems) following the manufacturer's instructions. The real-time PCR reactions were done with Fast SYBR green master mix reagent (Applied Biosystems) and the selected primers (Supplementary Material 1, Table s1). The results were normalized to actin-beta (*Actb*) and calibrated by non-co-cultured osteoblasts grown on Ti Control. The data ($n = 3$) were calculated according to the comparative $2^{-\Delta\Delta Ct}$ method [39].

2.3.5. Protein expression by western blotting

The protein expression of RUNX2, ALPL and BMPR1A was detected by western blotting on day 7 (2 days of co-culture). Cells were lysed with 150 μL of buffer constituted by 1 × protease inhibitor mixture (Roche Applied Science), 1 mM phenylmethanesulfonyl fluoride (Sigma-Aldrich) and 25 mM MG132 proteasome inhibitor (Roche Applied Science). Briefly, 50 μg of total protein was denatured, separated in 10% SDS polyacrylamide electrophoresis gel and transferred to a trans-blot turbo PVDF membrane (Bio-Rad Laboratories). The membrane was blocked for 1 h in Tris-buffered saline with 0.1% Tween® 20 (Sigma-Aldrich), containing 5% non-fat powdered milk (Bio-Rad Laboratories), probed with primary antibodies anti-RUNX2 (1:2000, Cell Signaling), anti-ALPL (1:3000, Abcam) and anti-BMPR1A (1:250, Sigma-Aldrich) overnight at 4 °C, and incubated with secondary horseradish peroxidase-conjugated antibody goat anti-rabbit IgG (1:2000, Cell Signaling) for 1 h at room temperature. The proteins were detected using Clarity Western ECL Substrate (Bio-Rad Laboratories) and the images were acquired using G-Box gel imaging (Syngene, Cambridge, UK). The proteins were quantified ($n = 3$) by counting pixels through Image-J software (National Institutes of Health, Bethesda, Maryland, USA), normalized to GAPDH (Santa Cruz Technology) and calibrated by non-co-cultured osteoblasts grown on Ti Control.

2.3.6. In situ ALPL activity by Fast red staining

The *in situ* ALPL activity was evaluated on day 7 (2 days of co-culture) using Fast red staining, as previously described [13]. Macroscopic images were digitally obtained with a stereomicroscope coupled to a high-resolution digital camera Leica DC 300F (Leica Biosystem, Wetzlar, Hesse, Germany) and ALPL staining was quantified ($n = 4$) by counting pixels using LASV 4.0 Image Analysis Software (Leica Biosystem). The data are presented as percentage of the area of the disc.

2.4. Effect of osteoclasts on methylated histones H3K9 and H3K27 accumulation in osteoblasts grown on Ti Nano

2.4.1. Protein expression by western blotting

The protein expression of H3K9me2, H3K27me3 and EZH2 was detected by western blotting on day 7 (2 days of co-culture). The membrane was blocked for 1 h in Tris-buffered saline with 0.1% Tween® 20 (Sigma-Aldrich), containing 5% bovine serum albumin (Sigma-Aldrich), probed with primary antibodies anti-H3K9me2 (1:1000, Cell Signaling), anti-H3K27me3 (1:1000, Cell Signaling) and anti-EZH2 (1:1000, Cell Signaling) overnight at 4 °C and incubated with secondary horseradish peroxidase-conjugated antibody goat anti-rabbit IgG (1:2000, Cell Signaling) for 1 h at room temperature. The proteins were detected as described above in Section 2.3.5.

2.4.2. Chromatin immunoprecipitation (ChIP) assay

The ChIP assay was carried out on day 7 (2 days of co-culture) as described elsewhere [40]. The osteoblasts were cross-linked with 1% formaldehyde (Merck) and lysed, and the DNA-protein complexes were immunoprecipitated with anti-H3K9me2 (Cell Signaling), anti-H3K27me3 (Cell Signaling) antibodies and protein G dynabeads kit (Invitrogen - Thermo Fisher Scientific). The DNA was extracted and purified with MinElute PCR purification kit (QIAGEN) after DNA-protein crosslink reversion. The PCR reactions were performed using the sequence primers for *Runx2*, *Alpl*, *Ibsp*, *Id3, Bglap* and *Jund* (Supplementary Material 1, Table s2) and the products were analyzed through 7% acrylamide gel, quantified by counting pixels through Image-J software (National Institutes of Health), normalized to positive control (INPUT) and calibrated by non-co-cultured osteoblasts grown on Ti Control.

2.4.3. Protein co-immunolocalization by immunofluorescence

On day 7 (2 days of co-culture), the RUNX2, ALPL and H3K27me3 proteins were evaluated by indirect immunofluorescence with anti-RUNX2 (1:100, Abcam), anti-ALPL (1:50, Santa Cruz Technology) and anti-H3K27me3 (1:200, Cell Signaling) antibodies, followed by a mixture of the red-fluorescent Alexa Fluor 594-conjugated goat anti-mouse secondary antibody (1:200, Molecular Probes) to detect the RUNX2 and ALPL and green-fluorescent Alexa Fluor 488-conjugated goat anti-rabbit secondary antibody to detect anti-H3K27me3 (1:200, Molecular Probes). Nuclei were detected with Hoechst 33258 solution (1:1000, Sigma-Aldrich). The samples were analyzed and randomly photographed in two areas per disc with an epifluorescence microscope ZEISS, ApoTome.2 (Carl Zeiss, Oberkochen, Baden-Württemberg, Germany).

2.5. Statistical analysis

The data of Ti surface area were compared using Student's *t*-test while the data of mRNA expression by RT-qPCR, protein expression by western blotting and *in situ* ALPL activity by Fast red staining were compared by two-way ANOVA followed by the Holm-Sidak post-test when appropriate. All analyses were made using the SigmaPlot software (Systat Software Inc., San Jose, California, USA) and the level of significance was set at 5% ($p \leq 0.05$).

3. Results

3.1. Characterization of Ti surfaces

The Ti Control exhibited a polished surface (Fig. 1A) while the Ti Nano (Fig. 1B) generated by H_2SO_4/H_2O_2 treatment presented nanopores distributed over the entire surface as observed under SEM. The surface area of Ti Nano (21.96 ± 0.52) was greater ($p = 0.001$) compared to Ti Control (14.44 ± 0.89) as determined by AFM (Fig. 1 C-F).

3.2. Osteoclasts induce differential expression of genes in osteoblasts grown on Ti Nano

Changes in gene expression of osteoblasts grown on both Ti Control and Ti Nano, either in the presence or absence of osteoclasts, were identified (Fig. 2). The relationship between samples during this interaction was evidenced by both principal component analysis (PCA, Fig. 2A) and Euclidean distance analysis (Fig. 2B). Irrespective of Ti surface, the presence of osteoclasts generated separation from the samples cultured in the absence of osteoclasts in the first principal component (PC1, x-axis, 79% of variance, Fig. 2A). The y-axis (PC2) shows 11% of variance and the samples of osteoblasts co-cultured with osteoclasts on Ti Nano were separately clustered from the osteoblasts co-cultured with osteoclasts on Ti Control (Fig. 2A). No relevant differences were noted between non-co-cultured osteoblast grown on Ti Nano compared to non-co-cultured osteoblasts grown on Ti Control (Fig. 2A). The Euclidean distance analysis (Fig. 2B) corroborates the findings of PCA, indicating the great variance between osteoblasts grown in the presence of osteoclasts on both Ti Control and Ti Nano compared to the variance between non-co-cultured osteoblasts.

The Volcano plots showed the patterns of global gene expression and compared osteoblasts grown on Ti Control either in the presence or absence of osteoclasts (Fig. 2C), osteoblasts grown on Ti Nano either in the presence

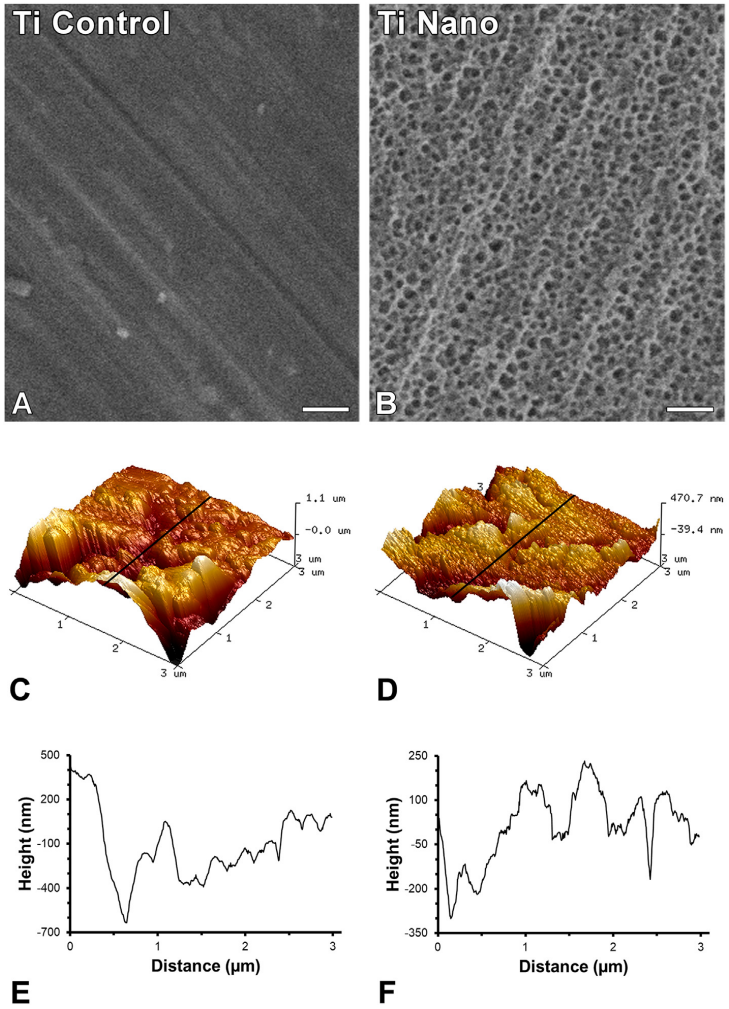

Fig. 1. Surface topography of titanium (Ti) discs. Scanning electron micrographies of polished Ti (A, Ti Control) and Ti with nanotopography (B, Ti Nano). Three-dimensional surface topography generated by atomic force microscopy and the corresponding line profile of Ti Control (C, E) and Ti Nano (D, F). Scale bars (A and B) = 100 nm. The reader is referred to the web version of this article for the colour representation of this figure.

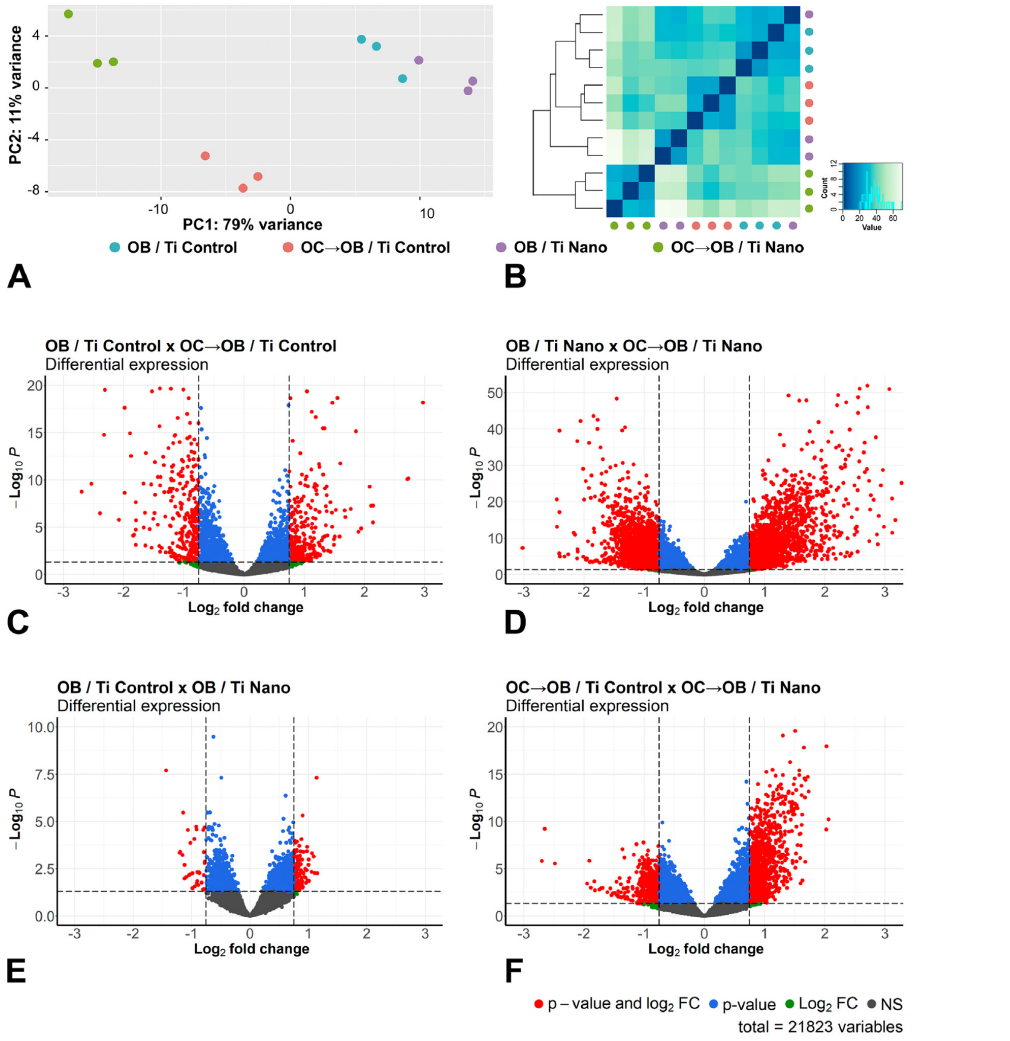

Fig. 2. Osteoclasts induce differential expression of genes in osteoblasts grown on titanium with nanotopography (Ti Nano) compared to polished titanium (Ti Control). Principal component analysis (A) and Euclidean distance metric plot (B) with dots in different colors representing osteoblasts grown on Ti Control (OB / Ti Control), osteoblasts grown on Ti Control in the presence of osteoclasts (OC → OB / Ti Control), osteoblasts grown on Ti Nano (OB / Ti Nano) and osteoblasts grown on Ti Nano in the presence of osteoclasts (OC → OB / Ti Nano) ($n = 3$); the first component (PC1) showed 79% of variance and the second component (PC2) showed 11% (A). Volcano plots of the RNA-Seq data showing the differential gene expression (n = 3) by comparing OB / Ti Control with OC → OB / Ti Control (C), OB / Ti Nano with OC → OB / Ti Nano (D), OB / Ti Control with OB / Ti Nano (E) and OC → OB / Ti Control with OC → OB / Ti Nano (F). The upregulated genes are represented as red dots on the right and the downregulated ones as red dots on the left, which means that these genes presented statistically significant differences (adjusted *p*-value) and magnitude of fold change (FC). Blue dots indicate genes that only presented statistically significant differences (adjusted p-value), green dots, the genes that only presented magnitude of FC and the grey ones indicate genes without both statistically significant differences and magnitude of FC (CF). (For interpretation of the references to colour in this figure legend, the reader is referred to the web version of this article.)

or absence of osteoclasts (Fig. 2D), osteoblasts grown on Ti Control and Ti Nano (Fig. 2E) and osteoblasts grown in the presence of osteoclasts on Ti Control and Ti Nano (Fig. 2F). The comparison of osteoblasts grown on Ti Control either in the presence or absence of osteoclasts showed that the presence of osteoclasts upregulated 305 and downregulated 322 genes (Fig. 2C). By comparing osteoblasts grown on Ti Nano either in the presence or absence of osteoclasts, we found that the presence of osteoclasts upregulated 1825 and downregulated 1629 genes, quite a large difference from the Ti control (Fig. 2D). Osteoblasts grown on either Ti Control or Ti Nano showed that nanotopography upregulated 116 and downregulated 34 genes (Fig. 2E). By comparing osteoblasts grown in the presence of osteoclasts on Ti Control and Ti Nano, nanotopography upregulated 934 and downregulated 471 genes (Fig. 2F) indicating that osteoblasts grown on Ti Nano are more responsive to osteoclasts than the ones grown on Ti Control. These data are summarized in Supplementary Material 1, Table s3.

The Heatmap shows a total of 4328 genes of osteoblasts that were regulated by both Ti surfaces and the presence or absence of osteoclasts (Fig. 3A). Hierarchical clustering of these differentially expressed genes was performed and GO analysis identified biological processes involved in osteoblast differentiation and regulation of chromatin organization (Fig. 3A,B). Cluster 1 presented a total of 223 genes highly expressed in non-co-cultured osteoblasts and a complete change in the pattern of gene expression when grown in the presence of osteoclasts, both being more evident on Ti Nano (Fig. 3A). Among the regulated genes, GO identified genes involved in an essential biological process termed "regulation of osteoblast differentiation" including *Wnt4* and *Wnt7b*, which are involved in bone formation and enhancement of fracture healing, *Id1* and *Id3*, both targets modulated by the BMP signaling pathway, *Jund* that stimulates the osteocalcin gene transcription and *Gli1*, a hedgehog gene directly regulated by *Runx2* (Fig. 3B) [41–46]. Cluster 3 presented 1388 genes with low expression in osteoblasts grown on Ti Nano, which were upregulated by the presence of osteoclasts, while no relevant regulation was observed in osteoblasts grown on Ti Control irrespective of the presence of osteoclasts (Fig. 3A).

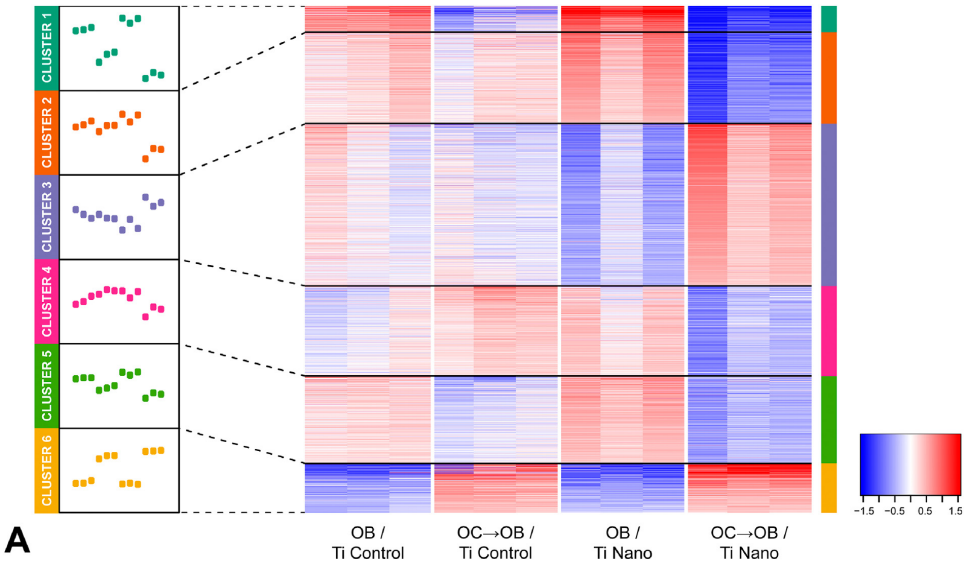

A

B

ID	Name	*p* value	Gene
Cluster 1 (223 genes)			
GO:0045667	regulation of osteoblast differentiation	1.99E-04	*Wnt4, Wnt7b, Id1, Id3, JunD, Gli1, Cebpa*
Cluster 3 (1388 genes)			
GO:1902275	regulation of chromatin organization	1.50E-04	*Sirt1, Snai2, Mettl4, Kdm4c, Kdm5a, Kmt8b, Tasor, Ogt, Mphosph8, Mtf2*
GO:0016570	histone modification	1.49E-04	*Kmt3a, Kdm5a, Mysm1, Kdm6a, Bmi1, Kmt5b, Kdm7a, Kmt2c*
GO:0045944	positive regulation of transcription by RNA polymerase II	6.57E-06	*Kmt2h, Kmt8b, Bmpr1a, Bmpr2, Fzd5*
Cluster 4 (771 genes)			
GO:0035148	tube formation	2.96E-04	*Rarg, Notch1*
GO:1901607	alpha-amino acid biosynthetic process	6.74E-04	*Alpl, Col4a2, Itgb5*
GO:0009888	tissue development	5.26E-04	*Bglap, Vim, Bmp8a, Mustn1*
GO:0030198	extracellular matrix organization	7.01E-04	*Lgals3, Col5a1, Col4a2, Efemp2, Emilin1, Fbln2*
Cluster 5 (747 genes)			
GO:0034645	cellular macromolecule biosynthetic process	1.14E-05	*Xbp1*
GO:0044267	cellular protein metabolic process	7.59E-05	*Dot1l*
Cluster 6 (419 genes)			
GO:0001558	regulation of cell growth	1.02E-04	*Fn1, Sema3e, Grem1*
GO:0000188	inactivation of MAPK activity	5.54E-04	*Cav1, Dusp4, Dusp1*
GO:0048589	developmental growth	3.51E-04	*Spry2*
GO:0001503	ossification	1.43E-03	*Mmp13, Igfbp5, Fat4, Spp1*

Fig. 3. Osteoclasts induce differential expression of genes in osteoblasts grown on titanium with nanotopography (Ti Nano) compared to polished titanium (Ti Control). Heatmap showing the differential gene expression of osteoblasts grown on Ti Control (OB / Ti Control), osteoblasts grown on Ti Control in the presence of osteoclasts (OC → OB / Ti Control), osteoblasts grown on Ti Nano (OB / Ti Nano) and osteoblasts grown on Ti Nano in the presence of osteoclasts (OC → OB / Ti Nano) ($n = 3$). Six clusters were defined, and the line plots indicate the gene expression dynamics of each cluster (A). The clusters were submitted to GO analysis and selected GO terms and genes are presented in the table (B). The reader is referred to the web version of this article for the colour representation of this figure.

GO identified genes linked to “regulation of chromatin organization” and “histone modification” that have well-known roles in bone biology, including *Sirt1*, a regulator of bone mass and *Kdm5a* that inhibits bone formation [47,48]. The genes encoding the receptors *Bmpr1a*, *Bmpr2* and *Fzd5*, involved with BMP and Wnt signaling pathways, are included in the GO category “positive regulation of transcription by RNA polymerase II” (Fig. 3B). Cluster 4 presented a total of 771 genes that were downregulated by osteoclasts in osteoblasts grown on Ti Nano, while on Ti Control, osteoclasts induced a slight upregulation of these genes (Fig. 3A). Among these, GO identified the following genes: *Rarg* that influences the development of trabecular bone mass and hematopoiesis; *Notch1*, an essential receptor involved in Notch signaling that regulates skeletal cell proliferation and differentiation; *Alpl*, a marker of early osteoblast differentiation that is crucial for bone formation; *Bglap* that encodes the most abundant non-collagenous protein in the bone matrix; *Mustn1* that represents a pan-musculoskeletal cell marker that precedes *Sox9* in cartilage; and *Col5a1*, a gene activated by osterix during osteoblast differentiation, that is related to “tube formation”, “alpha-amino acid biosynthetic process”, “tissue development” and “extracellular matrix organization” (Fig. 3B) [49–55]. Cluster 5 presented a total of 747 genes that were downregulated by osteoclasts in osteoblasts cultured on both Ti surfaces, with more pronounced effect on Ti Nano (Fig. 3A). *Xbp1* encodes a protein that targets Osterix and *Dot1l* that plays an important role in prenatal and postnatal chondrocyte development and trabecular bone maintenance; each of these genes are included in the GO categories “cellular macromolecule biosynthetic process” and “cellular protein metabolic process” respectively (Fig. 3B) [56–58]. Cluster 6 presented a total of 419 genes that were upregulated by osteoclasts in osteoblasts cultured on both Ti surfaces, with more pronounced effect on Ti Nano (Fig. 3A). Among these, GO identified *Grem1*, a BMP antagonist associated with “regulation of cell growth”, *Cav1* that negatively regulates osteoblasts and cementoblasts associated with “inactivation of MAPK activity”, *Spry2* that is involved in proliferation and differentiation of osteoblasts, included in “developmental growth”; *Mmp13*, a marker of bone matrix remodeling and *Spp1*, a bone sialoprotein involved in osteoclast attachment to mineralized bone matrix, both associated with “Ossification” [59–63].

3.3. Ti Nano attenuates the osteoclast-induced disruption of osteoblast differentiation

To investigate if Ti Nano attenuates the negative effect of osteoclasts on osteoblasts, we measured the mRNA and protein expressions of key bone markers and the *in situ* ALPL activity (Fig. 4). The gene expression of *Runx2* and *Bmpr1a* in osteoblasts was upregulated ($p = 0.001$ for both) by Ti Nano, and the presence of osteoclasts downregulated their expressions on Ti Control ($p = 0.001$ for both genes) and upregulated on Ti Nano ($p = 0.001$; $p = 0.04$) (Fig. 4A). The gene expression of *Dlx5*, *Ibsp* and *Opg* in osteoblasts was upregulated ($p = 0.005$; $p = 0.001$; $p = 0.001$, respectively) by Ti Nano and the presence of osteoclasts downregulated their expressions ($p = 0.001$ for all three) in a more pronounced way on Ti Control (Fig. 4A). The gene expression of *Alpl* and *Bglap* in osteoblasts was inhibited ($p = 0.001$ for both genes) by Ti Nano and the presence of osteoclasts downregulated their expressions ($p = 0.001$ for both genes) in a more pronounced way on Ti Control (Fig. 4A). The gene expression of *Id3* in osteoblasts was not affected ($p = 0.990$) by Ti surfaces and the presence of osteoclasts downregulated its expression on Ti Control and Ti Nano ($p = 0.001$ for both surfaces) (Fig. 4A). The gene expression of *Jund* in osteoblasts was not affected ($p = 0.319$) by Ti surfaces and the presence of osteoclasts downregulated its expression on Ti Control ($p = 0.021$) and Ti Nano ($p = 0.001$) (Fig. 4A). The gene expression of *Mmp13* in osteoblasts was not affected ($p = 0.551$) by Ti surfaces and the presence of osteoclasts downregulated its expression on Ti Control and upregulated on Ti Nano ($p = 0.001$ for both surfaces) (Fig. 4A). The protein expression of RUNX2 in osteoblasts was upregulated ($p = 0.001$) by Ti Nano and the presence of osteoclasts downregulated its expression on Ti Control and Ti Nano ($p = 0.001$ for both) in a more pronounced way on Ti Control (Fig. 4B). The protein expression of ALPL in osteoblasts was upregulated ($p = 0.001$) by Ti Nano and the presence of osteoclasts downregulated its expression on Ti Control and upregulated on Ti Nano ($p = 0.001$ for both) (Fig. 4C). The protein expression of BMPR1A in osteoblasts was inhibited ($p = 0.001$) by Ti Nano and the presence of osteoclasts downregulated its expression on Ti Control and upregulated on Ti Nano ($p = 0.001$ for both) (Fig. 4C). The ALPL activity in osteoblasts was increased ($p = 0.001$) by Ti Nano and the presence of osteoclasts downregulated its activity on Ti Control and Ti Nano ($p = 0.001$ for both) in a more pronounced way on Ti Control (Fig. 4E).

3.4. Ti Nano attenuates the osteoclast-induced disruption of osteoblast differentiation by reducing accumulation of the methylated histones

The RNA-Seq analysis, especially cluster 3, identified genes strongly associated with regulation of chromatin organization and histone modification, and the downregulation of osteoblast markers induced by osteoclasts, which was attenuated by Ti Nano. We used this experimental design to evaluate the mechanisms involved in the regulation of the crosstalk between osteoclasts and osteoblasts that were mediated by the nanotopography. Initially, we evaluated the the expression of H3K9me2 (Fig. 5A), H3K27me3 (Fig. 5B) and EZH2 (Fig. 5C). The protein expression of H3K9me2 in osteoblasts was increased by Ti Nano ($p = 0.004$) and the presence of osteoclasts did not affect its expression on Ti Control ($p = 0.130$) and upregulated it on Ti Nano ($p = 0.001$) (Fig. 5A). The protein expression of H3K27me3 in osteoblasts was increased by Ti Nano ($p = 0.018$) and the presence of osteoclasts upregulated its expression on Ti Control ($p = 0.001$) and Ti Nano ($p = 0.020$) (Fig. 5B). The protein expression of EZH2 in osteoblasts was increased by Ti Nano ($p = 0.004$) and the presence of osteoclasts upregulated its expression on Ti Control ($p = 0.007$) and Ti Nano ($p = 0.014$) (Fig. 5C).

Based on these findings, the ChIP assay (Fig. 5D-H) was performed to identify if the higher expression of H3K9me2 and H3K27me3 induced by osteoclasts contributes to the downregulation of osteoblast markers through chromatin condensation at the promoters, which prevents gene expression. Osteoclasts induced a high accumulation of H3K27me3, repressing the promoter regions of *Runx2* and *Alpl* of osteoblasts grown on Ti Control compared to Ti Nano (Fig. 5D-F). Irrespective of the presence of osteoclasts, the Ti Nano prevented the accumulation of H3K9me2 and H3K27me3 in the promoter regions of *Ibsp* and *Id3* of the osteoblasts (Fig. 5D,G,H). On Ti Control, only the accumulation of H3K9me2 in these regions was inhibited by the presence of osteoclasts (Fig. 5D,G,H). No methylation of histones H3K9 or H3K27 was identified in the promoter regions of *Bglap* and *Jund* (Fig. 5D). As H3K27me3 seemed to be more involved in the regulation of osteoblast differentiation by osteoclasts on Ti Nano, we used an immunofluorescence assay that corroborated the ChIP data and showed that osteoclasts increased the expression of H3K27me3 (Fig. 6A, B), which reduced the expression of RUNX2 (Fig. 6A) and ALPL (Fig. 6B) in osteoblasts grown on both Ti surfaces, but in a less pronounced way on Ti Nano. These results indicate the protective role of Ti Nano on osteoblasts, since this nanotopography attenuated the osteoclast-induced disruption of osteoblast differentiation by reducing the accumulation of H3K9 and H3K27, mainly H3K27, methylated histones.

4. Discussion

Several studies have shown the relevance of implant surface topography to the process of osseointegration. This event is characterized by the establishment of a direct interface between bone and the biomaterial, resulting in functional stability, load support and decreased risk of failure, thus maintaining the longevity of the implanted material and the health of the adjacent tissues [3,17,64]. Ti has been widely used to produce implants and the nanotopography generated by chemical conditioning with H_2SO_4/H_2O_2 favors osteoblast differentiation by modulating several cellular signaling pathways [6,7,11–14]. Considering the importance of bone remodeling to the Ti osseointegration, we demonstrated that nanotopography attenuated the negative effect of osteoclasts on osteoblast differentiation by

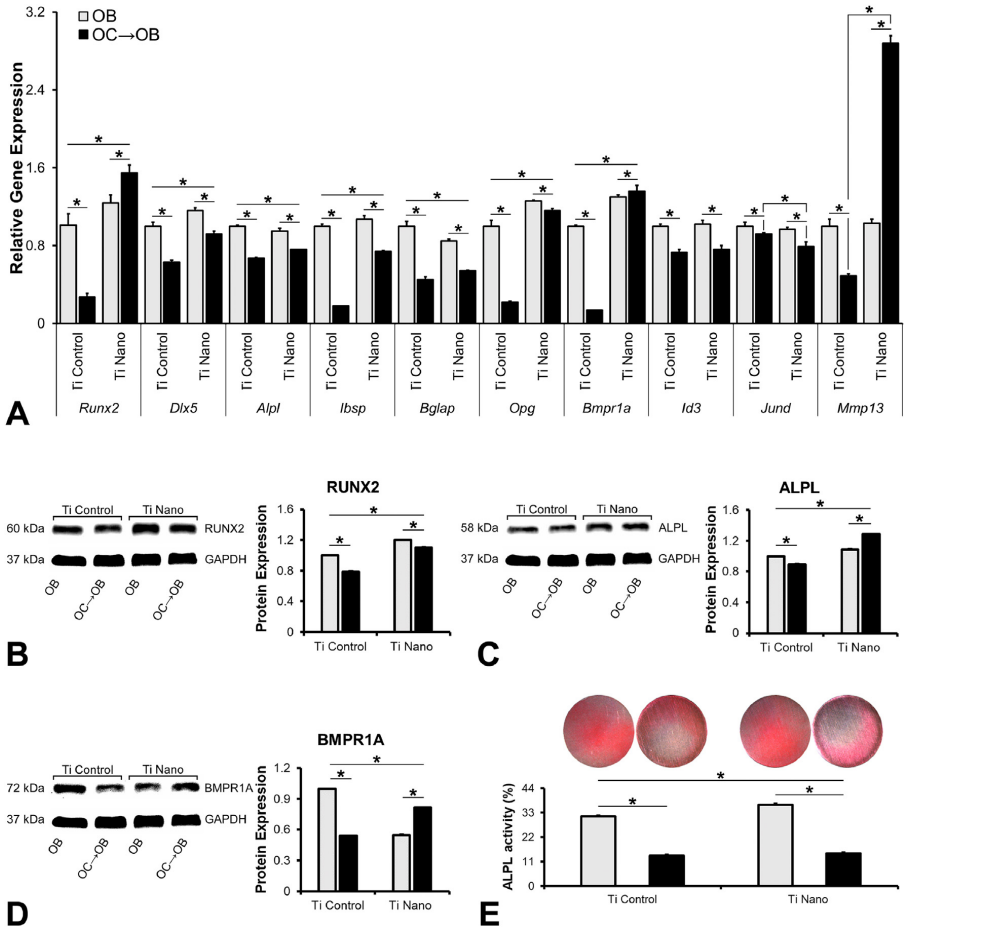

Fig. 4. Titanium with nanotopography (Ti Nano) attenuates osteoclast-induced disruption of osteoblast differentiation. Gene expression of the bone markers *Runx2*, *Dlx5*, *Alpl*, *Ibsp*, *Bglap*, *Opg*, *Bmpr1a*, *Id3*, *Jund* and *Mmp13* (A), protein expression of RUNX2 (B), ALPL (C) and BMPR1A (D) and *in situ* ALPL activity (E) of osteoblasts (OB) grown on polished titanium (Ti Control), osteoblasts grown in the presence of osteoclasts (OC → OB) on Ti Control, OB grown on Ti Nano and OC → OB on Ti Nano. The data of gene expression (n = 3), protein expression (n = 3) and *in situ* ALPL activity ($n = 4$) are presented as mean ± standard deviation and asterisks (*) indicate statistically significant differences ($p \leq 0.05$). The reader is referred to the web version of this article for the colour representation of this figure.

reducing the accumulation of H3K27me3 in the promoter regions of *Runx2* and *Alpl* (Fig. 7), which adds further explanation to the high osteogenic potential of this Ti surface.

To investigate the impact of the osteoclasts on osteoblasts grown on Ti Nano, we initiated a transcriptome analysis that revealed different patterns of gene expression by osteoblasts depending on Ti surfaces and the presence of osteoclasts. The downregulation of transcripts from the essential biological process "regulation of osteoblast differentiation" was induced by osteoclasts irrespective of the Ti surface. Indeed, some studies have indicated that osteoclasts secrete microRNA-enriched exosomes that are transferred to osteoblasts, inhibiting osteoblast differentiation and activity [65,66]. This mechanism highlights the relevance of exosomes secreted by osteoclasts on bone loss and could be, at least in part, involved in the inhibitory action of osteoclasts on osteoblast differentiation observed here. It was also identified an upregulation of genes involved with "histone modification" and "regulation of chromatin organization" in the presence of osteoclasts that were more pronounced in osteoblasts grown on Ti Nano compared to Ti Control. These results indicate that osteoclasts trigger post-translational modifications of chromatin and histones in osteoblasts, which is corroborated by studies that link epigenetic modifications with bone development [22,26,28].

The Ti Nano favored osteoblast differentiation compared to Ti Control, as evidenced by gene and protein expression of osteoblastic markers as well as ALPL activity, corroborating our previous studies [6,7,12–14]. As expected, osteoclasts inhibited osteoblast differentiation and interestingly this effect was more pronounced in cells grown on Ti Control compared to Ti Nano. It has been shown that exosomes derived from osteoclasts contain miR-23a-5p that suppresses osteoblast activity through a connecting site between this miRNA and *Runx2* [67]. These data demonstrate that osteoclasts reduced not only *Runx2*, but many genes and proteins associated with osteoblast differentiation and activity, again in a more marked way in cells grown on Ti Control than on Ti Nano. It is noteworthy that *Bmpr1a*, a receptor that mediates the BMP signaling pathway was downregulated by osteoclasts in osteoblasts grown on Ti Control, which was

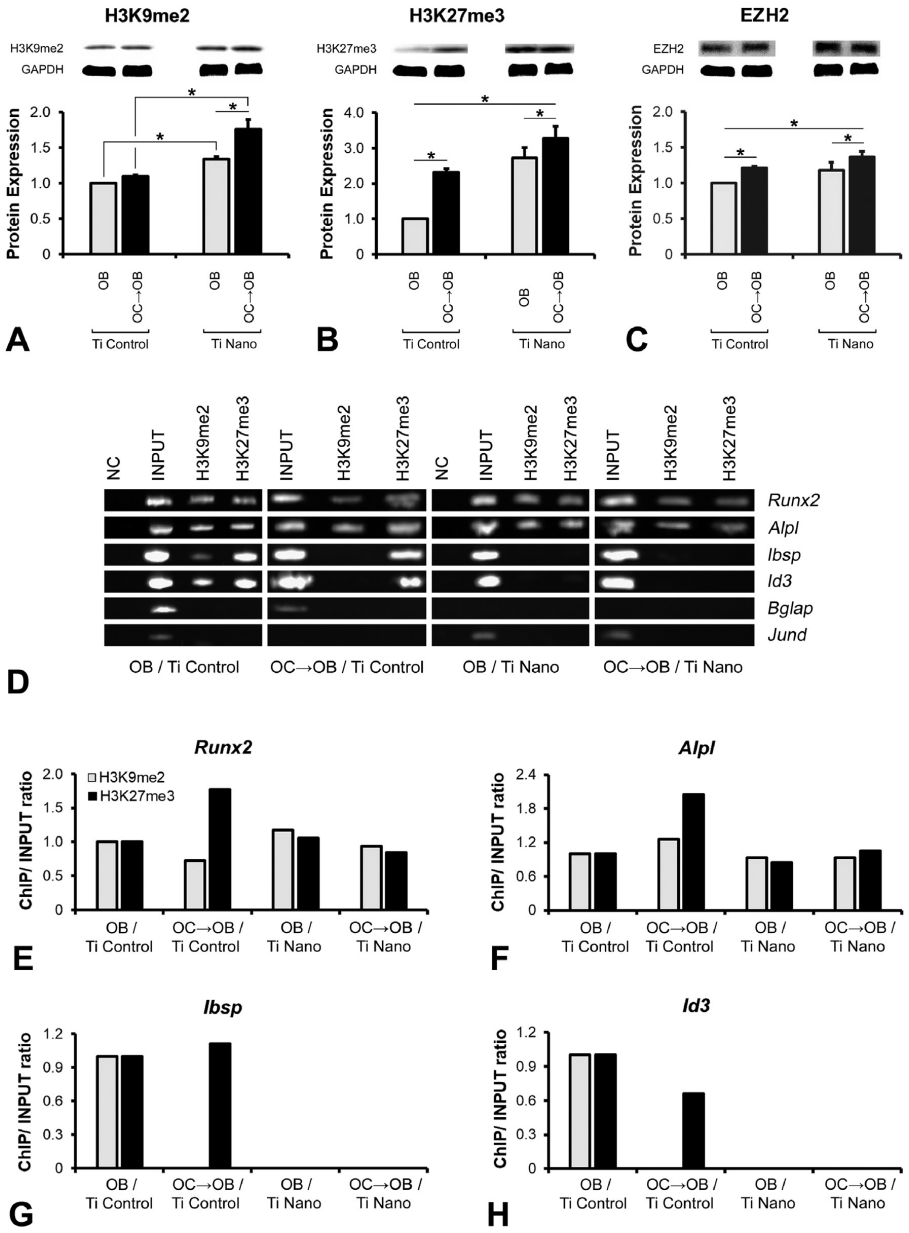

Fig. 5. Titanium with nanotopography (Ti Nano) attenuate osteoclast-induced disruption of osteoblast differentiation by reducing the methylated histone accumulation. Protein expression of H3K9me2 (A), H327me3 (B) and EZH2 (C) of osteoblasts (OB) grown on polished titanium (Ti Control), osteoblasts grown in the presence of osteoclasts (OC → OB) on Ti Control, OB grown on Ti Nano and OC → OB on Ti Nano. Binding of the H3K9me2 and H3K27me3 to the promoter regions of the bone markers *Runx2*, *Alpl*, *Ibsp*, *Id3*, *Bglap* and *Jund* in OB grown on Ti Control, OC → OB on Ti Control, OB grown on Ti Nano and OC → OB on Ti Nano (DH). Representative values from the PCR quantification of the genes, *Runx2*, *Alpl*, *Ibsp* and *Id3*, regulated by histone methylation (*E*-H). NC lanes represent samples immunoprecipitated with anti-IgG antibody, INPUT samples consist of total DNA, and H3K9me2 and H3K27me3 lanes refer to DNA immunoprecipitated with anti-H3K9me2 and anti-H3K27me3 antibodies (D). The data of protein expression (n = 3) are presented as mean ± standard deviation and asterisks (*) indicate statistically significant differences ($p \leq 0.05$).

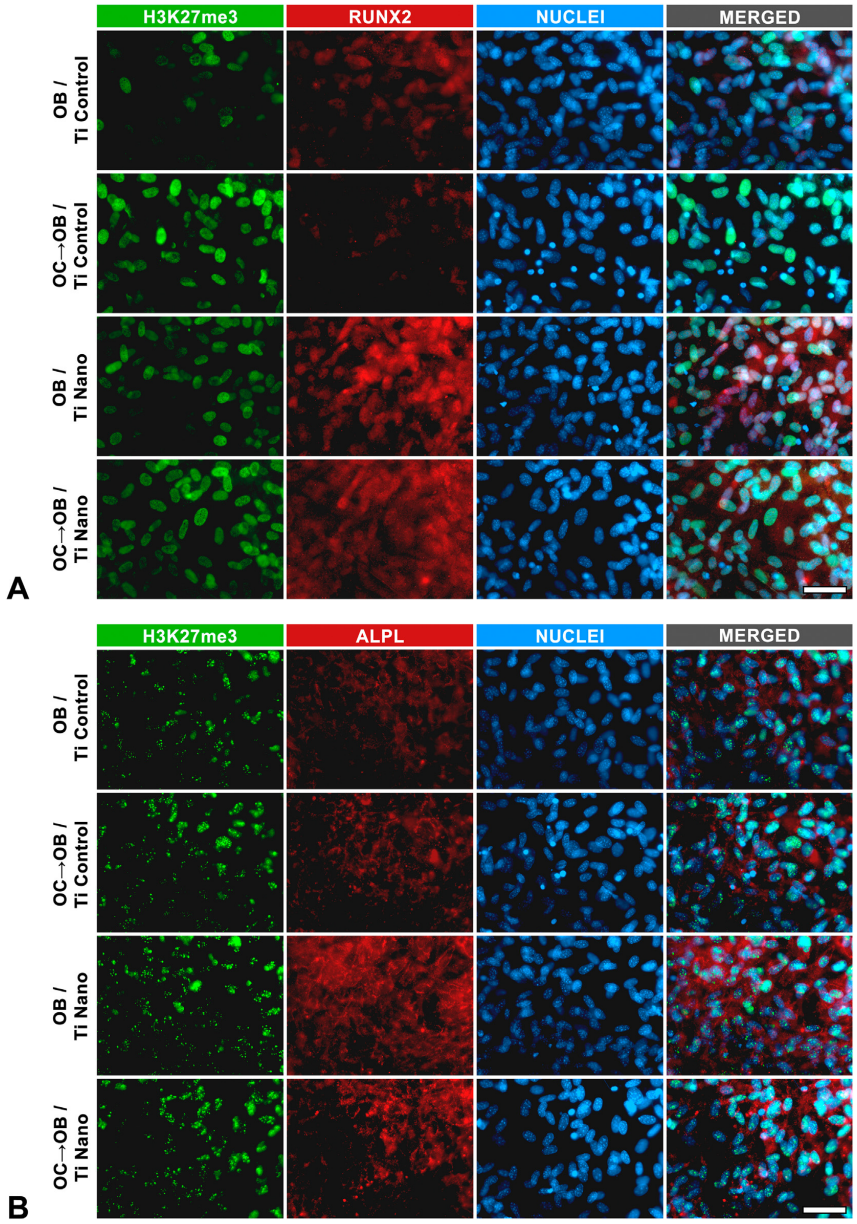

Fig. 6. Titanium with nanotopography (Ti Nano) attenuate osteoclast-induced disruption of osteoblast differentiation by reducing the methylated histone accumulation. Co-immunolocalization of H3K27me3 and RUNX2 (A), and H3K27me3 and ALPL (B) in osteoblasts (OB) grown on polished titanium (Ti Control), osteoblasts grown in the presence of osteoclasts (OC → OB) on Ti Control, OB grown on Ti Nano and OC → OB on Ti Nano. Scale bars (A and B) = 50 μm. The reader is referred to the web version of this article for the colour representation of this figure.

prevented by Ti Nano. Because the knockdown of *Bmpr1a* generates a striking inhibition of the osteogenic potential, bone quality and bone strength, these results suggest a compensatory mechanism when osteoblasts are grown on Ti Nano in the presence of osteoclasts, as the nanotopography induces osteoblast differentiation, at least in part, by the increase of BMP-2 production and BMP signaling pathway modulation [13,68]. Another interesting finding is the upregulation of *Mmp13* induced by osteoclasts in osteoblasts cultured on Ti Nano. MMP13 is a member of the matrix metalloproteinases that acts on bone remodeling and cartilage degradation due to its particular ability to cleave type II collagen. This upregulation

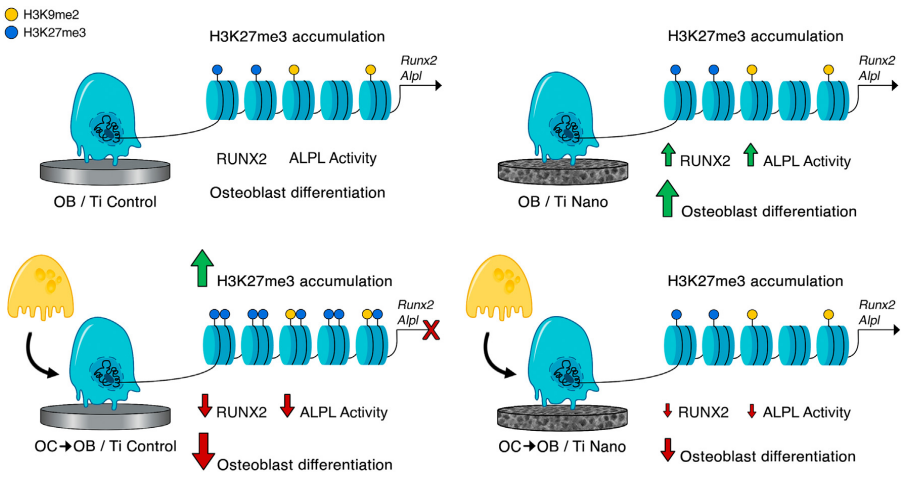

Fig. 7. Schematic representation of the main findings of this study. It is demonstrated that osteoclasts inhibit osteoblast differentiation of cells grown on both Ti Control and Ti Nano and that Ti Nano attenuates the osteoclast-induced disruption of osteoblast differentiation by preventing the accumulation of H3K27me3 in the promoter regions of *Runx2* and *Alpl*. The reader is referred to the web version of this article for the colour representation of this figure.

suggests that nanotopography could be associated not only with the increased osteoblast differentiation but also with high osteoclast activity leading to an enhancement of the bone remodeling process [69].

As the RNA-Seq and GO results showed differential patterns of expression of genes related to chromatin dynamics in osteoblasts depending on both the Ti surface topography and the presence of osteoclasts, we hypothesized that the inhibition of osteoblast differentiation induced by osteoclasts grown on Ti surfaces, which was attenuated by nanotopography, is due to histone modifications. Indeed, the expression of methylated histones H3K9me2 and H3K27me3, and EZH2, the enzyme that catalyzes the addition of methyl groups to histone H3 at Lys 27 (H3K27), was higher in osteoblasts grown on both Ti surfaces under the influence of osteoclasts. Methylation of histone proteins, a post-translational modification, is a remarkable epigenetic modification involved in bone development by regulating gene expression through chromatin compaction that represses gene transcription [22,27,28]. Despite H3K27me3 global distribution was higher in osteoblasts grown on both Ti surfaces under the influence of osteoclasts, the ChIP data showed that osteoclasts enhanced the accumulation of histone H3K27me3 in the promoter regions of key osteoblast marker genes, mainly *Runx2* and *Alpl*, on Ti Control, suppressing the gene expression of *Runx2, Alpl*, *Ibsp*, and *Id3*, which was attenuated on Ti Nano. The co-immunolocalization confirmed that the increase of H3K27me3 reduced the protein expression of RUNX2 and ALPL in a more pronounced way in osteoblasts grown on Ti Control in the presence of osteoclasts. Attesting that this mechanism of histone modification is involved in the protective effect of nanotopography on osteoblasts, the treatment with UNC1999, an EZH2 inhibitor, reversed both H3K27me3 increase and RUNX2 reduction induced by osteoclasts in osteoblasts grown on Ti Nano (Supplementary Material 2). In agreement with these findings, it has been demonstrated that the increase in the H3K27 trimethylation resulted in a repression of *Runx2* and *Spp1* through a decrease in EZH2 phosphorylation and that H3K9me2 repressed the regulatory regions of *Twist* in primary osteogenic mesenchyme from calvaria [26,70]. Considering the relevance of this mechanism to the bone-biomaterial interactions, further studies are needed to decipher which factors secreted by osteoclasts are inducing the accumulation of H3K27me3 in the *Runx2* and *Alpl* promoter regions of osteoblasts.

In conclusion, to the best of our knowledge, this study is the first to show the impact of the Ti Nano on the crosstalk between osteoblasts and osteoclasts. Despite osteoclasts inhibiting osteoblasts grown on both Ti Control and Ti Nano, the nanotopography attenuated the osteoclast-induced disruption of osteoblast differentiation by preventing the increase of H3K27me3 accumulation, which mediate repression of gene expression, in the promoter regions of *Runx2* and *Alpl*. These findings shed light on the epigenetic mechanisms triggered by nanotopography to protect osteoblasts from the deleterious effects of osteoclasts, generating a fine balance of the process of bone remodeling that may benefit the osseointegration of Ti implants.

CRediT authorship contribution statement

Rayana L. Bighetti-Trevisan: Conceptualization, Methodology, Investigation, Formal analysis, Writing – Original Draft, Visualization. **Luciana O. Almeida**, **Larissa M. S. Castro-Raucci**, **Jonathan A. R. Gordon** and **Coralee E. Tye**: Methodology, Investigation, Formal analysis, Writing – Review & Editing. **Gary S. Stein**, **Jane B. Lian** and **Janet L. Stein**: Conceptualization, Formal analysis, Writing – Review & Editing, Funding acquisition. **Adalberto L. Rosa** and **Marcio M. Beloti**: Conceptualization, Formal analysis, Writing – Original Draft, Writing – Review & Editing, Funding acquisition.

Data availability

Data supporting the findings of this study are available upon request to the corresponding author.

Declaration of competing interest

The authors declare that they have no known competing financial interests or personal relationships that could have appeared to influence the work reported in this paper.

Acknowledgments

The authors would like to thank Fabiola S. Oliveira and Roger R. Fernandes for their technical assistance during the experiments. The next-generation sequencing was performed in the Vermont Integrative Genomics Resource Massively Parallel Sequencing Facility and was supported by the University of Vermont Cancer Center, Lake Champlain Cancer Research Organization, UVM College of Agriculture and Life Sciences, and the UVM Larner College of Medicine.

Funding sources

This study was supported by the State of São Paulo Research Foundation (FAPESP, Brazil) [grant numbers 2019/09349-2, 2018/17356-6 and 2017/23888-8]; National Council for Scientific and Technological Development (CNPq, Brazil) [grant number 303464/2016-0]; Coordination of Improvement of Higher Education Personnel (CAPES, Brazil); and National Institutes of Health (USA) [grant numbers R01AR039588 and R01DE029311].

Appendix A. Supplementary data

Supplementary data to this article can be found online at https://doi.org/10.1016/j.msec.2021.112548.

References

[1] P.I. Brånemark, Osseointegration and its experimental background, J. Prosthet. Dent. 50 (1983) 399–410, https://doi.org/10.1016/s0022-3913(83)80101-2.
[2] C.M. Serre, G. Boivin, K.J. Obrant, L. Linder, Osseointegration of titanium implants in the tibia. Electron microscopy of biopsies from 4 patients, Acta Orthop. Scand. 65 (1994) 323–327, https://doi.org/10.3109/17453679408995462.
[3] R.K. Silverwood, P.G. Fairhurst, T. Sjöström, F. Welsh, Y. Sun, G. Li, B. Yu, P.S. Young, B. Su, R.M.D. Meek, M.J. Dalby, P.M. Tsimbouri, Analysis of osteoclastogenesis/osteoblastogenesis on nanotopographical titania surfaces, Adv. Healthc. Mater. 5 (2016) 947–955, https://doi.org/10.1002/adhm.201500664.
[4] S. Lee, Y.Y. Chang, J. Lee, S.K. Madhurakkat Perikamana, E.M. Kim, Y.H. Jung, J.H. Yun, H. Shin, Surface engineering of titanium alloy using metal-polyphenol network coating with magnesium ions for improved osseointegration, Biomater. Sci. 8 (2020) 3404–3417, https://doi.org/10.1039/d0bm00566e.
[5] P.T. Oliveira, A. Nanci, Nanotexturing of titanium-based surfaces upregulates expression of bone sialoprotein and osteopontin by cultured osteogenic cells, Biomaterials 25 (2004) 403–413, https://doi.org/10.1016/s0142-9612(03)00539-8.
[6] P.T. Oliveira, S.F. Zalzal, M.M. Beloti, A.L. Rosa, A. Nanci, Enhancement of in vitro osteogenesis on titanium by chemically produced nanotopography, J. Biomed. Mater. Res. A 80 (2007) 554–564, https://doi.org/10.1002/jbm.a.30955.
[7] A.L. Rosa, R.B. Kato, L.M.S. Castro Raucci, L.N. Teixeira, F.S. de Oliveira, L.S. Bellesini, P.T. de Oliveira, M.Q. Hassan, M.M. Beloti, Nanotopography drives stem cell fate toward osteoblast differentiation through α1β1 integrin signaling pathway, J. Cell. Biochem. 115 (2014) 540–548, https://doi.org/10.1002/jcb.24688.
[8] Y. Liu, Y. Wang, X. Cheng, Y. Zheng, M. Lyu, P. Di, Y. Lin, MiR-181d-5p regulates implant surface roughness-induced osteogenic differentiation of bone marrow stem cells, Mater. Sci. Eng. C Mater. Biol. Appl. 121 (2021), 111801, https://doi.org/10.1016/j.msec.2020.111801.
[9] J. Tang, L. Chen, D. Yan, Z. Shen, B. Wang, S. Weng, Z. Wu, Z. Xie, J. Shao, L. Yang, L. Shen, Surface functionalization with proanthocyanidins provides an anti-oxidant defense mechanism that improves the long-term stability and osteogenesis of titanium implants, Int. J. Nanomedicine 15 (2020) 1643–1659, https://doi.org/10.2147/IJN.S231339.
[10] J.-H. Yi, C. Bernard, F. Variola, S.F. Zalzal, J.D. Wuest, F. Rosei, A. Nanci, Characterization of a bioactive nanotextured surface created by controlled chemical oxidation of titanium, Surf. Sci. 600 (2006) 4613–4621, https://doi.org/10.1016/j.susc.2006.07.053.
[11] D. Guadarrama Bello, A. Fouillen, A. Badia, A. Nanci, Nanoporosity stimulates cell spreading and focal adhesion formation in cells with mutated paxillin, ACS Appl. Mater. Interfaces 12 (2020) 14924–14932, https://doi.org/10.1021/acsami.0c01172.
[12] R.B. Kato, B. Roy, F.S. De Oliveira, E.P. Ferraz, P.T. De Oliveira, A.G. Kemper, M.Q. Hassan, A.L. Rosa, M.M. Beloti, Nanotopography directs mesenchymal stem cells to osteoblast lineage through regulation of microRNA-SMAD-BMP-2 circuit, J. Cell. Physiol. 229 (2014) 1690–1696, https://doi.org/10.1002/jcp.24614.
[13] L.M.S. Castro-Raucci, M.S. Francischini, L.N. Teixeira, E.P. Ferraz, H.B. Lopes, P.T. de Oliveira, M.Q. Hassan, A.L. Rosa, M.M. Beloti, Titanium with nanotopography induces osteoblast differentiation by regulating endogenous bone morphogenetic protein expression and signaling pathway, J. Cell. Biochem. 117 (2016) 1718–1726, https://doi.org/10.1002/jcb.25469.
[14] R.P.F. Abuna, F.S. Oliveira, H.B. Lopes, G.P. Freitas, R.R. Fernandes, A.L. Rosa, M.M. Beloti, The Wnt/β-catenin signaling pathway is regulated by titanium with nanotopography to induce osteoblast differentiation, 184 (2019), 110513, https://doi.org/10.1016/j.colsurfb.2019.110513.
[15] E.F. Eriksen, Cellular mechanisms of bone remodeling, Rev. Endocr. Metab. Disord. 11 (2010) 219–227, https://doi.org/10.1007/s11154-010-9153-1.
[16] K. Matsuo, N. Irie, Osteoclast–osteoblast communication, Arch. Biochem. Biophys. 473 (2008) 201–209, https://doi.org/10.1016/j.abb.2008.03.027.
[17] P.S. Young, P.M. Tsimbouri, N. Gadegaard, R.M.D. Meek, M.J. Dalby, Osteoclastogenesis/osteoblastogenesis using human bone marrow-derived cocultures on nanotopographical polymer surfaces, Nanomedicine 10 (2015) 949–957, https://doi.org/10.2217/nnm.14.146.
[18] N. Kusu, J. Laurikkala, M. Imanishi, H. Usui, M. Konishi, A. Miyake, I. Thesleff, N. Itoh, Sclerostin is a novel secreted osteoclast-derived bone morphogenetic protein antagonist with unique ligand specificity, J. Biol. Chem. 278 (2003) 24113–24117, https://doi.org/10.1074/jbc.M301716200.
[19] T. Negishi-Koga, M. Shinohara, N. Komatsu, H. Bito, T. Kodama, R.H. Friedel, H. Takayanagi, Suppression of bone formation by osteoclastic expression of semaphorin 4D, Nat. Med. 17 (2011) 1473–1480, https://doi.org/10.1038/nm.2489.
[20] Y. Zhang, S.E. Chen, J. Shao, J.J.J.P. van den Beucken, Combinatorial surface roughness effects on osteoclastogenesis and osteogenesis, ACS Appl. Mater. Interfaces 10 (2018) 36652–36663, https://doi.org/10.1021/acsami.8b10992.
[21] J.M. Kim, C. Lin, Z. Stavre, M.B. Greenblatt, J.H. Shim, Osteoblast-osteoclast communication and bone homeostasis, Cells 9 (2020) 2073, https://doi.org/10.3390/cells9092073.
[22] J.A.R. Gordon, J.L. Stein, J.J. Westendorf, A.J. van Wijnen, Chromatin modifiers and histone modifications in bone formation, regeneration, and therapeutic intervention for bone-related disease, Bone 81 (2015) 739–745, https://doi.org/10.1016/j.bone.2015.03.011.
[23] W. Mu, J. Starmer, D. Yee, T. Magnuson, EZH2 variants differentially regulate polycomb repressive complex 2 in histone methylation and cell differentiation, Epigenetics Chromatin 11 (2018) 71, https://doi.org/10.1186/s13072-018-0242-9.
[24] Y. Li, D. Guo, R. Sun, P. Chen, Q. Qian, H. Fan, Methylation patterns of Lys9 and Lys27 on histone H3 correlate with patient outcome in gastric cancer, Dig. Dis. Sci. 64 (2019) 439–446, https://doi.org/10.1007/s10620-018-5341-8.
[25] C.S. Tellez, M.A. Picchi, D. Juri, K. Do, D.H. Desai, S.G. Amin, J.A. Hutt, P.T. Filipczak, S.A. Belinsky, Chromatin remodeling by the histone methyltransferase EZH2 drives lung pre-malignancy and is a target for cancer prevention, Clin. Epigenetics 13 (2021) 44, https://doi.org/10.1186/s13148-021-01034-4.
[26] Y. Wei, Y.H. Chen, L.Y. Li, J. Lang, S.P. Yeh, B. Shi, C.C. Yang, J.Y. Yang, C.Y. Lin, C.C. Lai, M.C. Hung, CDK1-dependent phosphorylation of EZH2 suppresses methylation of H3K27 and promotes osteogenic differentiation of human mesenchymal stem cells, Nat. Cell Biol. 13 (2011) 87–94, https://doi.org/10.1038/ncb2139.
[27] P. Deng, Q.M. Chen, C. Hong, C.Y. Wang, Histone methyltransferases and demethylases: regulators in balancing osteogenic and adipogenic differentiation of mesenchymal stem cells, Int. J. Oral Sci. 7 (2015) 197–204, https://doi.org/10.1038/ijos.2015.41.
[28] M. Montecino, M.E. Carrasco, G. Nardocci, Epigenetic control of osteogenic lineage commitment, Front. Cell Dev. Biol. 8 (2021), 611197, https://doi.org/10.3389/fcell.2020.611197.
[29] E. Afgan, D. Baker, M. van den Beek, D. Blankenberg, D. Bouvier, M. Cech, J. Chilton, D. Clements, N. Coraor, C. Eberhard, B. Gruning, A. Guerler, J. Hillman-Jackson, G.Von Kuster, E. Rasche, N. Soranzo, N. Turaga, J. Taylor, A. Nekrutenko, J. Goecks, The galaxy platform for accessible, reproducible and collaborative biomedical analyses: 2016 update, Nucleic Acids Res. 44 (2016) W3–W10, https://doi.org/10.1093/nar/gkw343.
[30] RStudio, Integrated development for R, http://www.rstudio.com. (Accessed 14 January 2020).
[31] S. Anders, FastQC: a quality control tool for high throughput sequence data, http://www.bioinformatics.babraham.ac.uk/projects/fastqc. (Accessed 14 January 2020).
[32] A. Dobin, C.A. Davis, F. Schlesinger, J. Drenkow, C. Zaleski, S. Jha, P. Batut, M. Chaisson, T.R. Gingeras, STAR: ultrafast universal RNA-seq aligner, Bioinformatics 29 (2013) 15–21, https://doi.org/10.1093/bioinformatics/bts635.
[33] J. Harrow, A. Frankish, J.M. Gonzalez, E. Tapanari, M. Diekhans, F. Kokocinski, B.L. Aken, D. Barrell, A. Zadissa, S. Searle, I. Barnes, A. Bignell, V. Boychenko, T. Hunt, M. Kay, G. Mukherjee, J. Rajan, G. Despacio-Reyes, G. Saunders, C. Steward, R. Harte, M. Lin, C. Howald, A. Tanzer, T. Derrien, J. Chrast, N. Walters, S. Balasubramanian, B. Pei, M. Tress, J.M. Rodriguez, I. Ezkurdia, J. van Baren, M. Brent, D. Haussler, M. Kellis, A. Valencia, A. Reymond, M. Gerstein, R. Guigó, T.J. Hubbard, GENCODE: the reference human genome annotation for the ENCODE project, Genome Res. 22 (2012) 1760–1774, https://doi.org/10.1101/gr.135350.111.
[34] S. Anders, P.T. Pyl, W. Huber, HTSeq–a python framework to work with high-throughput sequencing data, Bioinformatics 31 (2015) 166–169, https://doi.org/10.1093/bioinformatics/btu638.
[35] M.I. Love, W. Huber, A. Anders, Moderated estimation of fold change and dispersion for RNA-seq data with DESeq2, Genome Biol. 15 (2014) 550, https://doi.org/10.1186/s13059-014-0550-8.
[36] M. Ashburner, C.A. Ball, J.A. Blake, D. Botstein, H. Butler, J.M. Cherry, A.P. Davis, K. Dolinski, S.S. Dwight, J.T. Eppig, M.A. Harris, D.P. Hill, L. Issel-Tarver, A. Kasarskis, S. Lewis, J.C. Matese, J.E. Richardson, M. Ringwald, G.M. Rubin, G. Sherlock, Gene ontology: tool for the unification of biology. The gene ontology consortium, Nat. Genet. 25 (2000) 25–29, https://doi.org/10.1038/75556.
[37] H. Mi, A. Muruganujan, D. Ebert, X. Huang, P.D. Thomas, PANTHER version 14: more genomes, a new PANTHER GO-slim and improvements in enrichment analysis tools, Nucleic Acids Res. 47 (2019) D419–D426, https://doi.org/10.1093/nar/gky1038.
[38] The Gene Ontology Consortium, The gene ontology resource: 20 years and still going strong, Nucleic Acids Res. 47 (2019) D330–D338, https://doi.org/10.1093/nar/gky1055.
[39] K.J. Livak, T.D. Schmittgen, Analysis of relative gene expression data using real-time quantitative PCR and the 2(-Delta Delta C(T)) method, Methods 25 (2001) 402–408, https://doi.org/10.1006/meth.2001.1262.
[40] L.O. Almeida, R.N. Goto, C.R. Pestana, S.A. Uyemura, S. Gutkind, C. Curti, A.M. Leopoldino, SET overexpression decreases cell detoxification efficiency: ALDH2 and GSTP1 are downregulated, DDR is impaired and DNA damage accumulates, FEBS J. 279 (2012) 4615–4628, https://doi.org/10.1111/febs.12047.
[41] O. Akhouayri, R. St-Amaud, Differential mechanisms of transcriptional regulation of the mouse osteocalcin gene by Jun family members, Calcif. Tissue Int. 80 (2007) 123–131, https://doi.org/10.1007/s00223-006-0102-7.
[42] S. Kobaku, S. Ohte, H. Sasanuma, M. Shin, K. Yoneyama, E. Murata, K. Kanomata, J. Nojima, Y. Ono, T. Yoda, T. Fukuda, T. Katagiri, Supression of BMP-smad signaling axis-induced osteoblastic differentiation by small C-terminal domain phosphatase 1, a smad phosphatase, Mol. Endocrinol. 25 (2011) 474–481, https://doi.org/10.1210/me.2010-0305.

[43] K. Vrijens, W. Lin, J. Cui, D. Farmer, J. Low, E. Pronier, F.Y. Zeng, A.A. Shelat, K. Guy, M.R. Taylor, T. Chen, M.F. Roussel, Identification of small molecule activators of BMP signaling, PLoS One 8 (2013), e59045, https://doi.org/10.1371/journal.pone.0059045.

[44] B. Yu, J. Chang, Y. Liu, J. Li, K. Kevork, K. Al-Hezaimi, D.T. Graves, N.H. Park, C.Y. Wang, Wnt4 signaling prevents skeletal aging and inflammation by inhibiting nuclear factor-kappaB, Nat. Med. 20 (2014) 1009–1017, https://doi.org/10.1038/nm.3586.

[45] T. Komori, Regulation of proliferation, differentiation and functions of osteoblasts by runx 2, Int. J. Mol. Sci. 20 (2019) 1694, https://doi.org/10.3390/ijms20071694.

[46] D. Song, G. He, F. Song, Z. Wang, X. Liu, L. Liao, J. Ni, M.J. Silva, F. Long, Inducible expression of Wnt7b promotes bone formation in aged mice and enhances fracture healing, Bone Res. 8 (2020) 4, https://doi.org/10.1038/s41413-019-0081-8.

[47] K. Zainabadi, C.J. Liu, A.L.M. Caldwell, L. Guarente, SIRT1 is a positive regulator of in vivo bone mass and a therapeutic target for osteoporosis, PLoS One 12 (2017), e0185236, https://doi.org/10.1371/journal.pone.0185236.

[48] C. Wang, J. Wang, J. Li, G. Hu, S. Shan, Q. Li, X. Zhang, KDM5A controls bone morphogenic protein 2-induced osteogenic differentiation of bone mesenchymal stem cells during osteoporosis, Cell Death Dis. 7 (2016), e2335, https://doi.org/10.1038/cddis.2016.238.

[49] R.H. Christenson, Biochemical markers of bone metabolism: an overview, Clin. Biochem. 30 (1997) 573–593, https://doi.org/10.1016/s0009-9120(97)00113-6.

[50] Y.F. Wu, N. Matsuo, H. Sumiyoshi, H. Yoshioka, Sp7/Osterix is involved in the up-regulation of the mouse pro-α1(V) collagen gene (Col5a1) in osteoblastic cells, Matrix Biol. 29 (2010) 701–706, https://doi.org/10.1016/j.matbio.2010.09.002.

[51] A.C. Green, V. Rudolf-Stringer, L. Straszkowski, G. Tjin, B. Crimeen-Irwin, M. Walia, T.J. Martin, N.A. Sims, L.E. Purton, Retinoic acid receptor γ activity in mesenchymal stem cells regulates endochondral bone, angiogenesis, and B lymphopoiesis, J. Bone Miner. Res. 33 (2018) 2202–2213, https://doi.org/10.1002/jbmr.3558.

[52] M. Hadjiargyrou, Mustn1: a developmentally regulated pan-musculoskeletal cell marker and regulatory gene, Int. J. Mol. Sci. 19 (2018) 206, https://doi.org/10.3390/ijms19010206.

[53] N. Dirckx, M.C. Moorer, T.L. Clemens, R.C. Riddle, The role of osteoblasts in energy homeostasis, Nat. Rev. Endocrinol. 15 (2019) 651–665, https://doi.org/10.1038/s41574-019-0246-y.

[54] S. Novak, E. Roeder, B.P. Sinder, D.J. Adams, C.W. Siebel, D. Grcevic, K.D. Hankenson, B.G. Matthews, I. Kalajzic, Modulation of Notch1 signaling regulates bone fracture healing, J. Orthop. Res. 38 (2020) 2350–2361, https://doi.org/10.1002/jor.24650.

[55] C. Wehner, S. Lettner, A. Moritz, O. Andrukhov, X. Rausch-Fan, Effect of bisphosphonate treatment of titanium surfaces on alkaline phosphatase activity in osteoblasts: a systematic review and meta-analysis, BMC Oral Health 20 (2020) 125, https://doi.org/10.1186/s12903-020-01089-4.

[56] K. Nakashima, X. Zhou, G. Kunkel, Z. Zhang, J.M. Deng, R.R. Behringer, B. de Crombrugghe, The novel zinc finger-containing transcription factor osterix is required for osteoblast differentiation and bone formation, Cell 108 (2002) 17–29, https://doi.org/10.1016/s0092-8674(01)00622-5.

[57] T. Tohmonda, Y. Miyauchi, R. Ghosh, M. Yoda, S. Uchikawa, J. Takito, H. Morioka, M. Nakamura, T. Iwawaki, K. Chiba, Y. Toyama, F. Urano, K. Horiuchi, The IRE1α-XBP1 pathway is essential for osteoblast differentiation through promoting transcription of osterix, EMBO Rep. 12 (2011) 451–457, https://doi.org/10.1038/embor.2011.34.

[58] S.Y. Jo, M.S. Domowicz, J.G. Henry, N.B. Schwartz, The role of Dot1l in prenatal and postnatal murine chondrocytes and trabecular bone, JBMR Plus 4 (2019), e10254, https://doi.org/10.1002/jbm4.10254.

[59] T. Sanui, U. Tanaka, T. Fukuda, K. Toyoda, T. Taketomi, R. Atomura, K. Yamamichi, F. Nishimura, Mutation of Spry2 induces proliferation and differentiation of osteoblasts but inhibits proliferation of gingival epithelial cells, J. Cell. Biochem. 116 (2015) 628–639, https://doi.org/10.1002/jcb.25014.

[60] S.Y. Lee, J.K. Yi, H.M. Yun, C.H. Bae, E.S. Cho, K.S. Lee, E.C. Kim, Expression of caveolin-1 in periodontal tissue and its role in osteoblastic and cementoblatic differentiation in vitro, Calcif. Tissue Int. 98 (2016) 497–510, https://doi.org/10.1007/s00223-015-0095-1.

[61] K. Hu, H. Sun, B. Gui, C. Sui, Gremlin-1 suppression increases BMP-2-induced osteogenesis of human mesenchymal stem cells, Mol. Med. Rep. 15 (2017) 2186–2194, https://doi.org/10.3892/mmr.2017.6253.

[62] L.A. Khayal, J. Grünhagen, I. Provazník, S. Mundlos, U. Kornak, P.N. Robinson, C.E. Ott, Transcriptional profiling of murine osteoblast differentiation based on RNA-seq expression analyses, Bone 113 (2018) 29–40, https://doi.org/10.1016/j.bone.2018.04.006.

[63] H. Zhao, Q. Chen, A. Alam, J. Cui, K.C. Suen, A.P. Soo, S. Eguchi, J. Gu, D. Ma, The role of osteopontin in the progression of solid organ tumour, Cell Death Dis. 9 (2018) 356, https://doi.org/10.1038/s41419-018-0391-6.

[64] E.M. Lotz, M.B. Berger, Z. Schwartz, B.D. Boyan, Regulation of osteoclasts by osteoblast lineage cells depends on titanium implant surface properties, Acta Biomater. 68 (2018) 296–307, https://doi.org/10.1016/j.actbio.2017.12.039.

[65] D. Li, J. Liu, B. Guo, C. Liang, L. Dang, C. Lu, X. He, H.Y. Cheung, L. Xu, C. Lu, B. He, B. Liu, A.B. Shaikh, F. Li, L. Wang, Z. Yang, D.W. Au, S. Peng, Z. Zhang, B. Zhang, X. Pan, A. Qian, P. Shang, L. Xiao, B. Jiang, C.K. Wong, J. Xu, Z. Bian, Z. Liang, D. Guo, H. Zhu, W. Tan, A. Lu, G. Zhang, Osteoclast-derived exosomal miR-214-3p inhibits osteoblastic bone formation, Nat. Commun. 7 (2016) 10872, https://doi.org/10.1038/ncomms10872.

[66] W. Sun, C. Zhao, Y. Li, L. Wang, G. Nie, J. Peng, A. Wang, P. Zhang, W. Tian, Q. Li, J. Song, C. Wang, X. Xu, Y. Tian, D. Zhao, Z. Xu, G. Zhong, B. Han, S. Ling, Y. Chang, Y. Li, Osteoclast-derived microRNA-containing exosomes selectively inhibit osteoblast activity, Cell Discov. 2 (2016) 16015, https://doi.org/10.1038/celldisc.2016.15.

[67] J.X. Yang, P. Xie, Y.S. Li, T. Wen, X.C. Yang, Osteoclast-derived miR-23a5p-containing exosomes inhibit osteogenic differentiation by regulating Runx2, Cell. Signal. 70 (2020), 109504, https://doi.org/10.1016/j.cellsig.2019.109504.

[68] Q. Bao, A. Li, S. Chen, J. Feng, H. Liu, H. Qin, J. Li, D. Liu, Y. Shen, Z. Zong, Disruption of bone morphogenetic protein type IA receptor in osteoblasts impairs bone quality and bone strength in mice, Cell Tissue Res. 374 (2018) 263–273, https://doi.org/10.1007/s00441-018-2873-3.

[69] Q. Hu, M. Ecker, Overview of MMP-13 as a promising target for the treatment of osteoarthritis, Int. J. Mol. Sci. 22 (2021) 1742, https://doi.org/10.3390/ijms22041742.

[70] N. Higashihori, B. Lehnertz, A. Sampaio, T.M. Underhill, F. Rossi, J.M. Richman, Methyltransferase G9A regulates osteogenesis via twist gene repression, J. Dent. Res. 96 (2017) 1136–1144, https://doi.org/10.1177/0022034517716438.

1.2.1 SUPPLEMENTARY MATERIAL 1

Titanium with nanotopography attenuates the osteoclast-induced disruption of osteoblast differentiation by regulating histone methylation

Rayana L. Bighetti-Trevisan[a], Luciana O. Almeida[a], Larissa M. S. Castro-Raucci[b], Jonathan A. R. Gordon[c], Coralee E. Tye[c], Gary S. Stein[c], Jane B. Lian[c], Janet L. Stein[c], Adalberto L. Rosa[a], Marcio M. Beloti[a,*]

[a]Bone Research Lab, School of Dentistry of Ribeirão Preto, University of São Paulo, Ribeirão Preto, SP, Brazil
[b]School of Dentistry, University of Ribeirão Preto, Ribeirão Preto, SP, Brazil
[c]Department of Biochemistry and Vermont Cancer Center, University of Vermont Larner College of Medicine, Burlington, VT, USA

[*]**Corresponding author:**
Marcio M. Beloti (ORCID: 0000-0003-0149-7189)
School of Dentistry of Ribeirão Preto, University of São Paulo
Av. do Café, s/n, 14040-904, Ribeirão Preto, SP, Brazil
Tel.: +55 16 33154785
E-mail: mmbeloti@usp.br

Table s1. Primer sequences and product size (bp) for real-time polymerase chain reaction.

Gene	Sense sequence / anti-sense sequence	bp
Runx2	CTT CAC AAA TCC TCC CCA AGT G GGA ATG CGC CCT AAA TCA CTG	150
Dlx5	CTA CCC GGC CAA GGC TTA T TAC CAT TCA CCA TCC TCA CCT C	140
Alpl	GGG GTA CAA GGC TAG ATG GC CGG GCT CAA AGA GAC CTA AGA	150
Ibsp	AGC ATG CCT ACT TTT ATC CTC CT TTC GTT TGA AGT CTC CTC TTC CT	125
Bglap	TTC TGC TCA CTC TGC TGA CC GCT TGG ACA TGA AGG CTT TGT	99
Opg	GAA TGC CGA GAG TGT AGA GAG G CAC GCT GCT TTC ACA GAG GT	148
Bmpr1a	TGG GAG TGG ATC TGG ATT GC TCA CCA CGC CAT TTA CCC AT	120
Id3	CTA CGA GGC GGT GTG CTG GCG AGT AGC AGT GGT T	119
Jund	TCA AGA CCC TCA AAA GCC AGA CGT GGC TGA GGA CTT TCT GTT	96
Mmp13	CAT CCA TCC CGT GAC CTT AT TCA TAA CCA TTC AGA GCC CA	65
Actb	CCC TGA ACC CTA AGG CCA AC TGT GGT ACG ACC AGA GGC AT	122

Runx2: runt related transcription factor 2, *Dlx5*: distal-less homeobox 5, *Alpl*: alkaline phosphatase, *Ibsp*: bone sialoprotein, *Bglap*: osteocalcin, *Opg*: osteoprotegerin, *Bmpr1a*: bone morphogenetic protein receptor type 1A, *Id3*: inhibitor of DNA binding 3, *Jund*: jun D proto-oncogene, *Mmp13*: matrix metallopeptidase 13 and *Actb*: actin, beta.

Table s2. Primer sequences and product size (bp) for chromatin immunoprecipitation assay**.**

Gene	Sense sequence / anti-sense sequence	bp
Runx2	GCT CAG AAC GCC ACA CAC TCA G TAG AAC ACA AAT GCT GAA GG	222
Alpl	GGG ATA GTG TCT GCG GGT TAT A TTG TCC GTC ACC ATG TGC ACC	299
Ibsp	TGG CAT CAA CTC ATT TCC TAA ATT GAA GGG TGA GGA GAA GAT GG	210
Id3	TTT GGT TCT ATG TAT GCC CGT G GAT TTG GGC TAG GCG CTG AGA TTG	300
Bglap	AGC GGG CTC CTC ACA CTC TGA A ATC CGG TTG TAG GGC ATT TCT TG	300
Jund	CCA CAC ATC CCA TCC TCA GTT T ACT TCT GTG GCG TGA TGT GTG GAGC	283

Runx2: runt related transcription factor 2, *Alpl*: alkaline phosphatase, *Ibsp*: bone sialoprotein, *Id3*: inhibitor of DNA binding 3, *Bglap*: osteocalcin and *Jund*: jun D proto-oncogene.

Table s3. Number of upregulated and downregulated genes by comparing osteoblasts grown on polished titanium (Ti Control) or titanium with nanotopography (Ti Nano) either in the presence or absence of osteoclasts.

Comparison	Upregulated	Downregulated
OB / Ti Control *vs.* OB / Ti Nano	116	34
OB / Ti Control *vs.* OC→OB / Ti Control	305	322
OB / Ti Nano *vs.* OC→OB / Ti Nano	1825	1629
OC→OB / Ti Control *vs.* OC→OB / Ti Nano	934	471

OB / Ti Control: osteoblasts grown on Ti Control, OC→OB / Ti Control: osteoblasts grown in the presence of osteoclasts on Ti Control, OB / Ti Nano: osteoblasts grown on Ti Nano, OC→OB / Ti Nano: osteoblasts grown in the presence of osteoclasts on Ti Nano.

1.2.2 SUPPLEMENTARY MATERIAL 2

Titanium with nanotopography attenuates the osteoclast-induced disruption of osteoblast differentiation by regulating histone methylation

Rayana L. Bighetti-Trevisan[a], Luciana O. Almeida[a], Larissa M. S. Castro-Raucci[b], Jonathan A. R. Gordon[c], Coralee E. Tye[c], Gary S. Stein[c], Jane B. Lian[c], Janet L. Stein[c], Adalberto L. Rosa[a], Marcio M. Beloti[a,*]

[a]Bone Research Lab, School of Dentistry of Ribeirão Preto, University of São Paulo, Ribeirão Preto, SP, Brazil
[b]School of Dentistry, University of Ribeirão Preto, Ribeirão Preto, SP, Brazil
[c]Department of Biochemistry and Vermont Cancer Center, University of Vermont Larner College of Medicine, Burlington, VT, USA

[*]Corresponding author:
Marcio M. Beloti (ORCID: 0000-0003-0149-7189)
School of Dentistry of Ribeirão Preto, University of São Paulo
Av. do Café, s/n, 14040-904, Ribeirão Preto, SP, Brazil
Tel.: +55 16 33154785
E-mail: mmbeloti@usp.br

MATERIALS AND METHODS

Cell treatment with UNC1999

To investigate the effect of EZH2 inhibition, and consequently the reduction of H3K27me3 in osteoblasts grown on Ti Nano in the presence of osteoclasts, MC3T3-E1 pre-osteoblastic cells and RAW 264.7 macrophage cells were cultured as described in section 2.3.1 of the manuscript. On day 5, the inserts containing the osteoclasts were positioned above osteoblast cultures, thereby establishing an indirect co-culture system, and kept in α-MEM supplemented with osteoblast and osteoclast differentiation factors and 40 nM of UNC1999 (Cayman Chemical), an EZH2 inhibitor, for further 2 days, completing 7 days of culture in differentiation media. The controls were cocultured osteoblasts grown on Ti Nano, in α-MEM supplemented with osteoblast and osteoclast differentiation factors and UNC1999 vehicle (ethyl alcohol pure, Sigma-Aldrich). The concentration of UNC1999 (Cayman Chemical) was selected from a dose-response experiment, being 40 nM the higher concentration that kept around 80% of viable cells 2 days post-treatment (data not shown).

Protein expression by western blotting

The protein expression of EZH2, H3K27me3 and RUNX2 was detected by western blotting on day 7 (2 days of co-culture in the presence of either UNC1999 or its vehicle), as described in sections 2.3.5 and 2.4.1 of the manuscript.

Statistical analysis

The data of (n =3) were compared using Student's t-test using the SigmaPlot software (Systat Software Inc.) and the level of significance was set at 5% ($p \leq 0.05$).

RESULTS

Changes in protein expression of osteoblasts grown on Ti Nano either in the presence or absence of osteoclasts are shown in Figure 4B (RUNX2), and 5B (H3K27me3) and 5C (EZH2) of the manuscript. To better visualize the effect of UNC1999 treatment, these results are also presented here (Figure s1A-C). The presence of osteoclasts increased the protein expression of EZH2 ($p = 0.029$, Figure s1A) and H3K27me3 ($p = 0.002$, Figure s1B), and reduced RUNX2 ($p = 0.001$, Figure s1C) in osteoblasts grown on Ti Nano. The UNC1999 treatment reversed the

negative effect of osteoclasts on osteoblast differentiation, inhibiting the protein expression of EZH2 ($p = 0.001$, Figure s1D) and H3K27me3 ($p = 0.001$, Figure s1E) and consequently increasing RUNX2 ($p = 0.001$, Figure s1F) in osteoblasts grown on Ti Nano in the presence of osteoclasts.

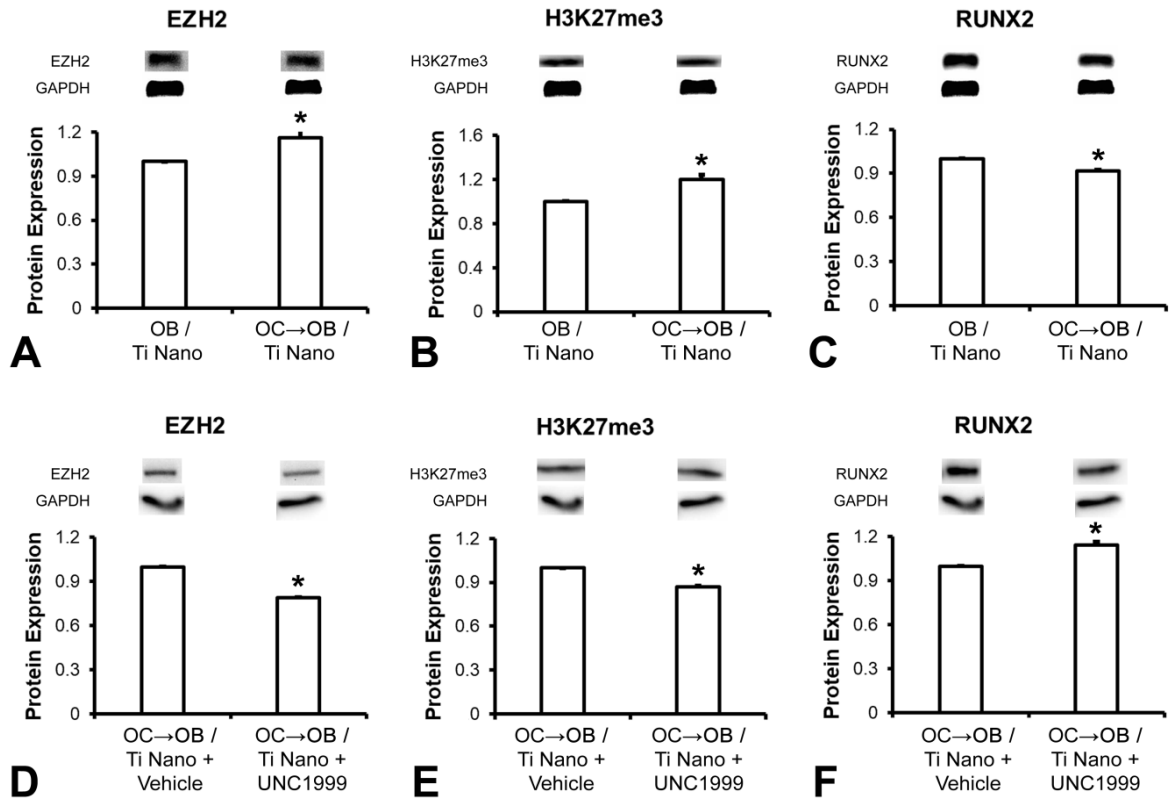

Figure s1. UNC1999 treatment reversed the H3K27me3 increase and RUNX2 reduction induced by osteoclasts (OC) in osteoblasts (OB) grown on titanium with nanotopography (Ti Nano). Protein expression of EZH2 (A), H3K27me3 (B) and RUNX2 (C) of OB grown on Ti Nano and OB grown in the presence of OC (OC→OB) on Ti Nano. Protein expression of EZH2 (D), H3K27me3 (E) and RUNX2 (F) of OB grown in the presence of OC (OC→OB) on Ti Nano and treated with either 40 nM of UNC1999 or vehicle. The data are presented as mean ± standard deviation (n = 3) and asterisks (*) indicate statistically significant differences ($p \leq 0.05$).

Capítulo 2

CAPÍTULO 2 – EFEITO DE OSTEOBLASTOS SOBRE OSTEOCLASTOS CRESCIDOS NO TI NANO

2.1 OBJETIVOS ESPECÍFICOS

- Avaliar o efeito do Ti Nano, comparado ao Ti Controle, na diferenciação osteoclástica de células da linhagem RAW 264.7, em culturas isoladas.
- Avaliar o efeito das células osteoblásticas da linhagem MC3T3-E1 sobre a formação e atividade osteoclástica de células da linhagem RAW 264.7 crescidas sobre o Ti Nano, comparado ao Ti Controle, em modelo de co-cultura indireta.
- Avaliar o efeito do meio condicionado por células osteoblásticas da linhagem MC3T3-E1 crescidas sobre o Ti Nano, comparado ao Ti Controle, sobre a formação e atividade osteoclástica de células da linhagem RAW 264.7.

2.2 MATERIAL E MÉTODOS

2.2.1 Obtenção das amostras de Ti

Discos de Ti comercialmente puro, grau 2, usinados, apresentando 1 mm de altura e 13 mm de diâmetro (Realum, Brasil), foram lixados utilizando lixas de carbeto de silício de gramatura 180, 320 e 600, lavados em ultrassom e submetidos a condicionamento em solução de H_2SO_4 10 N e H_2O_2 30%, sob agitação constante por 4 horas (YI et al., 2006; KATO et al., 2014). Na sequência, houve lavagem dos discos em água destilada e secagem ao ar. Discos usinados apenas lixados e lavados foram utilizados como controle. Previamente à utilização nos experimentos, os discos de ambos os grupos foram autoclavados.

2.2.2 Avaliação do efeito das células osteoblásticas da linhagem MC3T3-E1 sobre a formação e atividade osteoclástica de células da linhagem RAW 264.7 crescidas sobre o Ti Nano, comparado ao Ti Controle, em modelo de co-cultura indireta

2.2.2.1 Cultura de células osteoblásticas da linhagem MC3T3-E1

Células osteoblásticas da linhagem MC3T3-E1, subclone 14, obtidas da American Type Culture Collection (ATCC, EUA), foram cultivadas conforme descrito previamente (BIGHETTI-TREVISAN et al., 2021). Na subconfluência da cultura (4–5

dias), houve remoção do meio de cultura e adição de solução de tripsina a 0,25% (Gibco) e EDTA 1 mM (Gibco) para obtenção da suspensão de células que foram plaqueadas para a realização dos experimentos descritos abaixo. Após o plaqueamento, as células foram mantidas em meio osteogênico, composto por meio de expansão suplementado com 5 µg/mL de ácido ascórbico (Gibco) e beta-glicerofosfato a 7 mM (Sigma-Aldrich, EUA) e sua progressão foi avaliada em microscópio de fase invertido Axiovert 25 (Zeiss, Alemanha). A cada 48 horas, houve troca do meio de cultura e as células foram mantidas a 37 °C e atmosfera umidificada contendo 5% de CO_2 e 95% de ar atmosférico.

2.2.2.2 Cultura de células osteoclásticas da linhagem RAW 264.7

Células da linhagem osteoclástica RAW 264.7, obtidas da American Type Culture Collection (ATCC), também foram cultivadas conforme anteriormente descrito (BIGHETTI-TREVISAN et al., 2021). Na subconfluência da cultura (4–5 dias), houve remoção do meio de cultura e adição de solução de tripsina a 0,25% (Gibco) e EDTA a 1 mM (Gibco) para obtenção da suspensão de células que foram plaqueadas para a realização dos experimentos descritos abaixo. Após o plaqueamento, as células foram mantidas em meio osteoclastogênico, composto por meio de expansão suplementado com 50 ng/mL de RANKL (PeproTech, EUA) e sua progressão foi avaliada em microscópio de fase invertido Axiovert 25 (Zeiss). A cada 48 horas, houve troca do meio de cultura e as células foram mantidas a 37 °C e atmosfera umidificada contendo 5% de CO_2 e 95% de ar atmosférico.

2.2.2.3 Co-cultura indireta

As células osteoclásticas da linhagem RAW 264.7 foram cultivadas conforme descrito no item 2.2.2.2. Em seguida, foram plaqueadas na densidade de $1x10^4$ células/poço sobre discos de Ti Nano e Ti Controle, em meio de cultura osteoclastogênico e mantidas isoladas por 5 dias para permitir a adesão celular. As células osteoblásticas da linhagem MC3T3-E1 foram cultivadas em meio osteogênico, conforme descrito no item 2.2.2.1, sobre membranas de Transwell® (Greiner Bio-One, Alemanha), com poros de 0,4 µm, na densidade de $1x10^4$ células/membrana, e também foram mantidas isoladas por 5 dias para permitir a adesão celular. No dia 5, os Transwell® (Greiner Bio-One) contendo as células osteoblásticas foram posicionados sobre as culturas de células osteoclásticas,

estabelecendo-se assim a co-cultura indireta. As co-culturas osteoblastos-osteoclastos foram mantidas em D-MEM (Gibco), suplementado com 10% de soro fetal bovino (Gibco), 100 U/mL de penicilina (Gibco), 100 µg/mL de estreptomicina (Gibco), β-glicerofosfato a 7 mM (Sigma-Aldrich), 5 µg/mL de ácido L-ascórbico (Sigma-Aldrich) e 50 ng/mL de RANKL (PeproTech) por mais 2 dias, completando 7 dias de cultura em meio de diferenciação. O meio de co-cultura utilizado foi D-MEM suplementado com fatores de diferenciação de osteoblastos e osteoclastos. Os controles foram células osteoclásticas da linhagem RAW 264.7 crescidas sobre os discos de Ti na ausência de células osteoblásticas da linhagem MC3T3-E1, ou seja, não mantidas em co-cultura.

2.2.2.4 Expressão gênica por PCR em tempo real

Ao final de 2 dias de co-cultura (7 dias de cultura total, considerando os 5 dias de culturas isoladas), foi avaliada a expressão gênica de *Rank*, catepsina K (*Ctsk*), receptor associado ao osteoclasto (*Oscar*), fator de necrose tumoral α (*Tnf-α*), *Trap*, metaloproteinase de matriz 9 (*Mmp9*), oncogene de osteossarcoma FBJ (*cFos*), fator de transcrição associado à melanogênese (*Mitf*), fator nuclear de células T ativadas citoplasmático dependente de calcineurina 1 (*Nfatc1*), fator nuclear de células T ativadas citoplasmático dependente de calcineurina 2 (*Nfatc2*), fator 6 associado ao receptor de TNF (*Traf6*) e semaforina 4d (*Sema4d*).

Para este ensaio, houve remoção do meio de cultura dos poços e foi adicionado o reagente TRIzol (Invitrogen, EUA) sob agitação por pipetagem. A extração do RNA total foi realizada, considerando as especificações do fabricante, através do kit SV Total RNA Isolation System (Promega, EUA). Na sequência, houve quantificação do RNA total em espectrofotômetro (GE Healthcare, EUA) e avaliação da integridade, através do aparelho Agilent 2100 BioAnalyzer (Agilent Technologies, EUA), que foi checada a partir de 100 ng do RNA total, seguindo as orientações do fabricante e, considerando adequados, valores de RIN (RIN, do inglês: *RNA Integrity Number*) superiores a 7 (FLEIGE; PFAFFL, 2006; SCHROEDER et al., 2006). Em seguida, foi realizada a confecção da fita de cDNA, partindo de 1 µg de RNA total, no termociclador Mastercycler Gradient (Eppendorf) por meio de reação com a enzima transcriptase reversa, utilizando o kit High-capacity cDNA Reverse Transcription (Applied Biosystems, EUA). Para a reação de PCR em tempo real, foi utilizado sistema SYBR e para isso foram utilizados primers previamente

desenhados e sintetizados para os genes-alvo e de referência (Life Technologies). As reações foram realizadas no aparelho StepOne Plus (Life Technologies), em triplicata (n=3), utilizando 7 µL de Fast SYBR Green Master Mix (Life Technologies), 0,5 µL de primer Foward, 0,5 µL de primer Reverse e 5 µL de cDNA (12,5 ng), para um volume final de 13 µL/reação. As reações de amplificação consistiram em 20 segundos a 95 ºC e quarenta ciclos de 3 segundos a 95 ºC (denaturação) e de 30 segundos a 60 ºC (anelamento e extensão). Como controle endógeno, a expressão gênica de beta (ß) actina (*Actb*) foi utilizada para normalizar os níveis de expressão dos genes avaliados. Para comparar a expressão gênica das células dos diferentes grupos experimentais, foi utilizado o método comparativo de 2^{-ddCt} (LIVAK; SCHMITTGEN, 2001). As sequências dos primers são apresentadas na Tabela 1.

Tabela 1. Sequência de primers e tamanho do fragmento (pb) para PCR em tempo real.

Gene alvo	Sequência Forward e Reverse	Pb
Rank	TGGCTACCACTGGAACTCAGA ACCGTATCCTTGTTGAGCTGC	102
Ctsk	TCAAGTTTCTGCTGCTACCCA ACGCCGAGAGATTTCATCCA	131
Oscar	GTCGACTCTCTGTGAGCTGTC GAGTCACAACTGCAGCAGGAT	122
Tnf-α	CTCACACTCAGATCATCTTCTCAA CTTTGAGATCCATGCCGTTGG	139
Trap	TGCGACCATTGTTAGCCACA AGGGATCCATGAAGTTGCCG	129
Mmp9	GAAAACCTCCAACCTCACG GACTGCTTCTCTCCCATCA	96
cFos	CAGAGCGGGAATGGTGAA GCAGCCATCTTATTCCGTTC	132
Mitf	TACCCGTCTCTGGAAACTTGAT TTTATGTTGGGAAGGTTGGCTG	103
Nfatc1	GGAGACAGACATCGGGAGGAAG CTGACCGCTGGGAACACTCG	128
Nfatc2	ACAGCACTTTACCTACCACC TTGGGTGCTGTGGGTAATA	128
Traf6	GCAGAGGAATCACTTGGCACG CACGGACGCAAAGCAAGGTTA	102
Sema4d	GCCCTGGTGGTAGTGTTG CCTGGCTTGTGAAACTGC	101
Actb	CCCTGAACCCTAAGGCCAAC TGTGGTACGACCAGAGGCAT	122

2.2.2.5 Expressão proteica por western blot

Ao final de 2 dias de co-cultura (7 dias de cultura total, considerando os 5 dias de culturas isoladas), foi avaliada a expressão proteica de CTSK e TRAP. Através do tratamento com solução de tripsina a 0,25% (Gibco) e EDTA a 1 mM (Gibco), as células foram removidas dos discos, transferidas para tubos falcon (Corning Incorporated) de 15 mL e centrifugadas por 5 minutos a 2000 rpm. Houve descarte do sobrenadante e novas lavagens (n=3) do pellet de células com 5 mL de PBS aquecido (Gibco). Após a última centrifugação, houve remoção do PBS, adição do tampão de lise (NaCl a 150 mM (Sigma-Aldrich); Nonidet P 40 a 1% (Sigma-Aldrich); Deoxicolato sódico a 0,5% (Sigma-Aldrich); SDS a 0,1% (Sigma-Aldrich); e Tris base 50 mM, pH 8, (Roche, EUA)) e extração da proteína total através de lise celular, por meio do aparelho de ultrassom (Misonix, EUA). Primeiramente, para identificação da concentração de proteínas das amostras, em µg/µL, utilizou-se o kit comercial DC™ Protein Assay (BioRad, EUA) seguindo as orientações do fabricante e espectrofotômetro (BioTek Instruments Inc., EUA), considerando comprimento de onda de 750 nm. Em seguida, géis de acrilamida a 10% foram preparados, posicionados em suporte próprio e receberam o tampão de corrida e as amostras, que foram preparadas considerando 50 µg de proteína de cada grupo, contidas em um volume final de 35 µL, dos quais 7 µL eram tampão de amostra, e aquecidas em banho-maria a 95 °C por 5 minutos. A separação das proteínas foi realizada por eletroforese com aplicação de 80 Volts por aproximadamente 2 horas e foi utilizado, como referência, um marcador de peso molecular que identifica bandas entre 10 e 250 kDa (BioRad). As proteínas foram transferidas dos géis para membranas de PVDF 0,2 µm (BioRad) com o aparelho Trans-Blot® Turbo (BioRad), operado com 25 Volts por 10 minutos e três incubações foram realizadas, a primeira referente ao bloqueio dos sítios inespecíficos com leite desnatado a 5% diluído em tampão salino de Tris com Tween 20 (TBS-T), por 1 hora, a segunda referente aos anticorpos primários anti-TRAP (1:500, monoclonal de coelho, Abcam, United Kingdom (ab191406)) diluído em solução de leite desnatado a 2,5% em TBS-T e anti-CTSK (1:500, policlonal de coelho, Abcam (ab19027)) diluído em solução de leite desnatado a 2,5% em TBS-T, overnight e a terceira referente ao anticorpo secundário conjugado com peroxidase (1:2000, anti-coelho IgG HRP; Cell Signaling, EUA (7074S)) diluído em solução de leite desnatado a 2,5% em TBS-T, por 1 hora. Após cada incubação, foram realiadas três lavagens das membranas, durante 5

minutos, com TBS-T. Para identificação das marcações, ao final as membranas foram incubadas com solução quimiluminescente Clarity™ Western ECL Substrate (BioRad) por 1 minuto e levadas para o aparelho G:BOX (SynGene, EUA). O programa GeneSnap (SynGene) foi utilizado para obtenção das imagens das bandas relativas às proteínas-alvo e o programa ImageJ (National Institutes of Health, EUA) foi utilizado para obtenção dos dados quantitativos. A expressão da proteína alvo foi normalizada pela expressão da proteína constitutiva gliceraldeído-3-fosfato desidrogenase (GAPDH). Para isso, houve o tratamento das membranas com solução Re-Blot Plus Strong Solution (Milipore, EUA) por 20 minutos, à temperatura ambiente, para a remoção dos anticorpos, e então, incubadas conforme descrito acima, utilizando-se anticorpo primário anti-GAPDH (1:1000, policlonal de coelho IgG; Santa Cruz Biotechnology, EUA (25778)) e anticorpo secundário conjugado com peroxidase (1:2000, anti-coelho IgG HRP; Cell Signaling (7074S)), ambos diluídos em solução de leite desnatado a 2,5% em TBS-T.

2.2.2.6 Marcação histoquímica para TRAP

Ao final de 2 dias de co-cultura (7 dias de cultura total, considerando os 5 dias de culturas isoladas), foi avaliada a formação de osteoclastos através da marcação histoquímica para TRAP, utilizando o kit de fosfatase ácida, leucócitos (procedimento 387, Sigma-Aldrich). Após a remoção dos meios de cultura, as células aderidas aos poços foram lavadas com água deionizada aquecida a 37 ºC e fixadas com uma solução de fixação composta por solução de citrato, acetona e formaldeído 37% durante 30 segundos, à temperatura ambiente. Então, houve nova lavagem com água deionizada aquecida a 37 ºC e acrescentados 1 mL da solução de coloração, preparada seguindo as orientações do fabricante. As células foram mantidas em incubadora, nas condições ideais, por 1 hora. Em seguida, após nova lavagem com água deionizada, os poços foram deixados à temperatura ambiente para secagem. Os discos foram removidos das placas e as imagens foram obtidas digitalmente com um estéreo-microscópio utilizando uma câmera digital de alta resolução DC 300F (Leica, Alemanha). A coloração de TRAP foi quantificada através do software LASV 4.0 (Leica).

2.2.3 Avaliação do efeito do meio condicionado por células osteoblásticas da linhagem MC3T3-E1 crescidas sobre o Ti Nano, comparado ao Ti Controle, sobre a formação e atividade osteoclástica de células da linhagem RAW 264.7

2.2.3.1 Cultura de células

Para avaliar o efeito do meio condicionado por células osteoblásticas da linhagem MC3T3-E1, crescidas sobre o Ti Nano comparado ao Ti Controle, em células osteoclásticas da linhagem RAW 264.7, as células osteoclásticas foram cultivadas conforme descrito no item 2.2.2.2, em placas de cultura de 24 poços (Corning Incorporated) na presença de meio osteoclastogênico por um período de 5 dias. Em seguida, foram expostas ao meio condicionado pelas células osteoblásticas da linhagem MC3T3-E1 (preparo conforme descrito no item 2.2.3.2), que foi coletado após 1, 3 e 5 dias. Como controle, foram utilizadas células osteoclásticas da linhagem RAW 264.7 crescidas em meio não condicionado (meio osteoclastogênico).

2.2.3.2 Preparo do meio condicionado por células osteoblásticas da linhagem MC3T3-E1

As células osteoblásticas da linhagem MC3T3-E1 em suspensão foram plaqueadas na densidade de $1x10^4$ células/poço sobre os discos de Ti Nano e Ti Controle, em placas de 24 poços e mantidas em meio osteogênico. Os meios foram coletados após 1, 3 e 5 dias de cultura, centrifugados a 2000 rpm por 5 minutos em centrífuga modelo 5702 (Eppendorf), transferidos para tubos de 50 mL (Corning Incorporated) e armazenados em freezer a -80 ºC. No momento do uso, os meios foram descongelados e um pool dos meios dos três períodos foi preparado. Em seguida, o meio foi filtrado em filtro de baixa retenção de proteínas (Millex GV – 0,22µm, Millipore) e diluído na proporção de 1:1, com meio de cultura osteoclastogênico.

2.2.3.3 Expressão gênica por PCR em tempo real

Ao final de 2 dias de cultura (7 dias de cultura total, considerando os 5 dias iniciais em meio não condicionado) foi avaliada a expressão gênica de *Rank*, *Ctsk*, *Oscar*, *Tnf-*α, *Trap*, *Mmp9*, *cFos*, *Mitf*, *Nfatc1*, *Nfatc2*, *Traf6* e *Sema4d* conforme descrito no item 2.2.2.4.

2.2.3.4 Expressão proteica por western blot

Ao final de 2 dias de cultura (7 dias de cultura total, considerando os 5 dias iniciais em meio não condicionado), foi avaliada a expressão proteica de CTSK e TRAP, conforme descrito no item 2.2.2.5.

2.2.3.5 Marcação histoquímica para TRAP

Ao final de 2 dias de cultura (7 dias de cultura total, considerando os 5 dias iniciais em meio não condicionado) foi realizada a marcação para TRAP, conforme descrito no item 2.2.2.6.

2.2.4 Análise Estatística

Os dados quantitativos referentes aos experimentos realizados no modelo de co-cultura entre osteoblastos e osteoclastos foram comparados através do teste two-way ANOVA, seguido de pós-teste Holm-Sidak quando apropriado. Já para os resultados referentes ao meio condicionado de osteoblastos em osteoclastos, houve comparação através do teste one-way ANOVA, seguido de pós-teste Holm-Sidak quando necessário. O software SigmaPlot (Systat Software Inc., EUA) foi utilizado para realização das análises e o nível de significância adotado foi de 5% ($p \leq 0,05$).

2.3 RESULTADOS

2.3.1 Caracterização da superfície de Ti Nano

Análises em nanoescala permitiram a detecção de uma superfície polida, irregular e lisa no Ti Controle, enquanto a superfície de Ti Nano apresentou nanoporos distribuídos em toda superfície, conforme apresentado no capítulo 1, nos subitens 2.2 e 3.1.

2.3.2 Osteoblastos induzem a expressão de genes relacionados à diferenciação osteoclástica, que foi acentuada pelo Ti Nano

Para investigar o papel do Ti Nano no efeito de osteoblastos em osteoclastos, foram realizadas análises de expressão gênica de marcadores osteoclásticos e de genes relacionados à via de sinalização Rank/Rankl (Figura 1). A expressão gênica de *Rank* e *Ctsk* em osteoclastos foi aumentada ($p = 0,001$ para ambos) pelo Ti Nano, e a presença de osteoblastos aumentou a expressão no Ti Controle ($p = 0,001$ para ambos os genes) e no Ti Nano ($p = 0,011$ para o gene

Rank) (Figura 1A). A expressão gênica de *Oscar* foi afetada (p = 0,002) apenas pelas superfícies de Ti, de maneira mais pronunciada no Ti Nano (Figura 1A), não sofrendo influência dos osteoblastos no Ti Controle e Ti Nano (p = 0,738 e p = 0,116, respectivamente). A expressão gênica de *Tnf-*α em osteoclastos não foi afetada (p = 0,211) pelas superfícies e a presença dos osteoblastos aumentou sua expressão no Ti Nano (p = 0,001) (Figura 1A). A expressão gênica de *Trap* e *Mmp9* em osteoclastos não foi afetada (p = 0,716 e p = 0,055, respectivamente) pelas superfícies e a presença dos osteoblastos diminuiu a expressão no Ti Controle (p = 0,001 e p = 0,049, respectivamente) e Ti Nano (p = 0,001 e p = 0,002, respectivamente) (Figura 1A). Para os genes relacionados à via de sinalização Rank/Rankl e diferenciação osteoclástica, pode-se observar um padrão na modulação gênica, uma vez que a expressão dos genes *cFos*, *Mitf*, *Nfatc1*, *Traf6* e *Sema4d* foi aumentada pelo Ti Nano (p = 0,001, p = 0,001, p = 0,006, p = 0,001 e p = 0,016, respectivamente), e a presença dos osteoblastos aumentou a expressão dos genes *cFos*, *Mitf*, *Nfatc1*, *Traf6* no Ti Controle (p = 0,001 para todos os genes) e no Ti Nano (p = 0,004, p = 0,001, p = 0,001, e p = 0,001, respectivamente) (Figura 1B). Vale ressaltar que a expressão gênica de *Sema4d* em osteoclastos crescidos no Ti Controle e no Ti Nano não foi afetada pela presença dos osteoblastos (p = 0,199 e p = 0,406, respectivamente) (Figura 1B). Com relação ao gene *Nfatc2,* a expressão gênica em osteoclastos foi diminuída (p = 0,019) pelo Ti Nano, e a presença de osteoblastos aumentou a expressão no Ti Controle (p = 0,001) e no Ti Nano (p = 0,001) (Figura 1B).

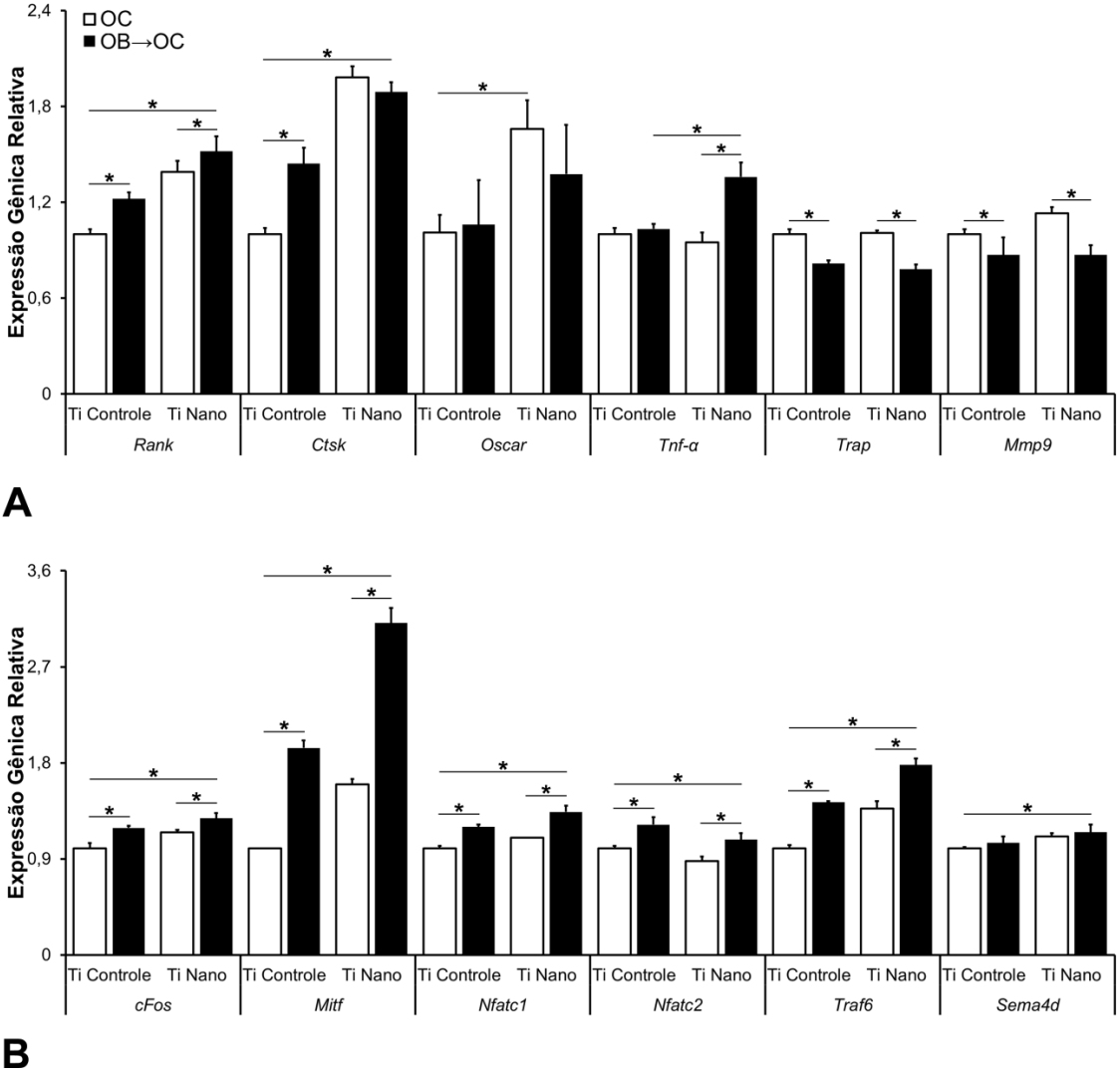

Figura 1. Expressão gênica dos marcadores da diferenciação osteoclástica *Rank*, *Ctsk*, *Oscar*, *Tnf-*α, Trap e Mmp9 (A) e *cFos*, *Mitf*, *Nfatc1*, *Nfatc2*, *Traf6* e *Sema4d* (B) de osteoclastos (OC) crescidos no Ti Controle, osteoclastos crescidos na presença de osteoblastos (OB→OC) no Ti Controle, OC crescidos no Ti Nano e OB→OC no Ti Nano. Os dados representativos da expressão gênica (n = 3) são demonstrados com média ± desvio padrão. (*) indica diferença estatisticamente significante ($p \leq 0,05$).

2.3.3 O Ti Nano inibe a atividade osteoclástica de maneira mais acentuada na presença dos osteoblastos

Para investigar o papel do Ti Nano no fenótipo osteoclástico, na presença ou ausência de osteoblastos, análises de expressão proteica de marcadores osteoclásticos e da atividade de TRAP foram realizadas (Figura 2). A expressão proteica de CTSK em osteoclastos não foi afetada ($p = 0,551$) pelas superfícies de Ti e a presença de osteoblastos aumentou a expressão no Ti Controle ($p = 0,001$) e diminuiu no Ti Nano ($p = 0,001$) (Figura 2A). Já para a proteína TRAP, a expressão

proteica foi menor no Ti Nano (p = 0,001) e a presença de osteoblastos diminuiu sua expressão no Ti Controle e Ti Nano (p = 0,001 para ambos) (Figura 2B). A atividade de TRAP em osteoclastos foi menor no Ti Nano (p = 0,001) e, assim como encontrado na expressão gênica e proteica, a presença de osteoblastos reduziu a atividade osteoclástica no Ti Controle e Ti Nano (p = 0,001 para ambos), de maneira mais pronunciada no Ti Nano (Figura 2C).

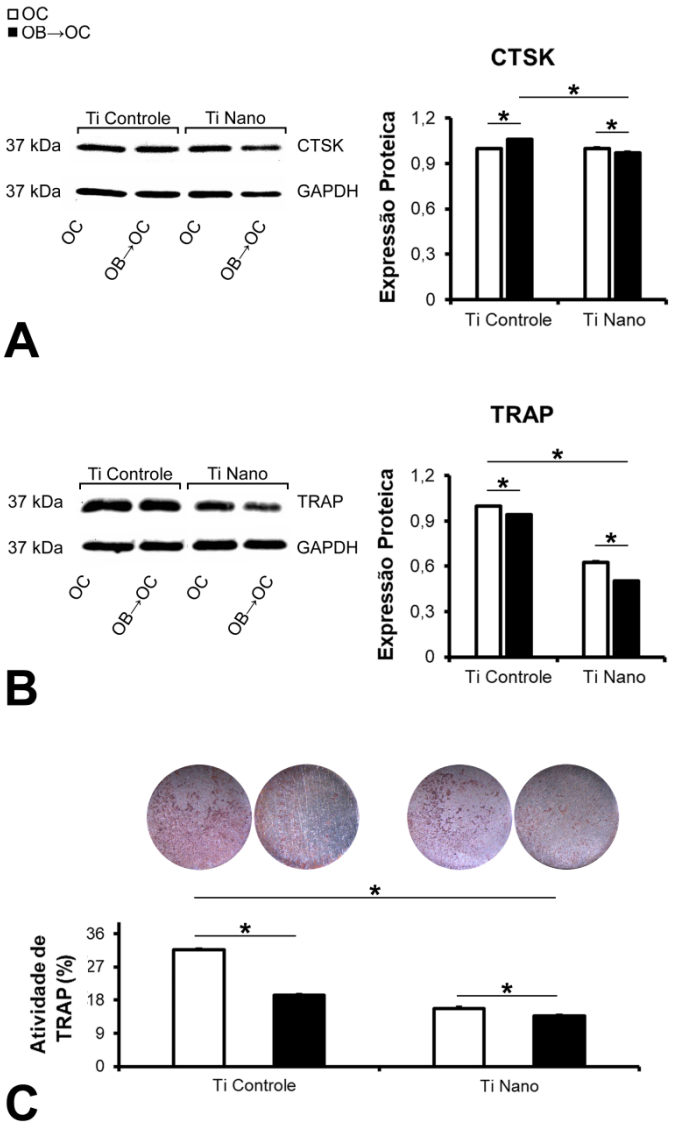

Figura 2. Expressão proteica dos marcadores da diferenciação osteoclástica CTSK (A) e TRAP (B) e atividade de TRAP (C) de osteoclastos (OC) crescidos no Ti Controle, osteoclastos crescidos na presença de osteoblastos (OB→OC) no Ti Controle, OC crescidos no Ti Nano e OB→OC no Ti Nano. Os dados representativos da expressão proteica (n = 3) e atividade de TRAP (n = 4) são demonstrados com média ± desvio padrão. (*) indica diferença estatisticamente significante (p ≤ 0,05).

2.3.4 O meio condicionado por osteoblastos crescidos sobre as superfícies de Ti Nano e Ti Controle favorece a expressão de genes relacionados à diferenciação osteoclástica

Para avaliar o papel do meio condicionado por osteoblastos crescidos sobre o Ti Nano e Ti Controle em osteoclastos, foram realizadas análises de expressão gênica de marcadores osteoclásticos e de genes relacionados à via de sinalização Rank/Rankl (Figura 3). A expressão gênica de *Rank* e *Ctsk* em osteoclastos foi maior na presença do meio condicionado por osteoblastos crescidos sobre as superfícies de Ti Nano ($p = 0,01$ e $p = 0,001$, respectivamente) e Ti Controle ($p = 0,007$ e $p = 0,001$, respectivamente) em relação ao meio não-condicionado (D-MEM). Na comparação entre os grupos de células cultivadas na presença dos diferentes meios condicionados, a expressão dos genes não foi afetada ($p = 0,938$ e $p = 0,187$, respectivamente) (Figura 3A). A expressão gênica de *Oscar* em osteoclastos foi maior na presença do meio condicionado por osteoblastos crescidos no Ti Controle ($p = 0,001$) em relação aos meios não-condicionado e condicionado por osteoblastos crescidos no Ti Nano ($p = 0,001$) (Figura 3A). A expressão do gene *Tnf-*α foi maior na presença do meio condicionado por osteoblastos crescidos no Ti Nano ($p = 0,001$) em relação aos meios não-condicionado e condicionado por osteoblastos crescidos no Ti Controle ($p = 0,001$) (Figura 3A). A expressão gênica de *Trap* e *Mmp9* em osteoclastos foi maior na presença do meio condicionado por osteoblastos crescidos sobre as superfícies de Ti Nano ($p = 0,001$ para ambos os genes) e Ti Controle ($p = 0,002$ para ambos os genes) em relação ao meio não-condicionado (D-MEM). Na comparação entre os grupos de células cultivadas na presença dos diferentes meios condicionados, a expressão dos genes não foi afetada ($p = 0,131$ e $p = 0,951$, respectivamente) (Figura 3A). Para os genes relacionados à via de sinalização Rank/Rankl, pode-se observar que a expressão gênica de *cFos* foi maior na presença do meio condicionado por osteoblastos crescidos no Ti Nano ($p = 0,033$) em relação aos meios não-condicionado e condicionado por osteoblastos crescidos no Ti Controle ($p = 0,016$) (Figura 3B). A expressão dos genes *Mitf* e *Traf6*, foi menor em osteoclastos, na presença do meio condicionado por osteoblastos crescidos sobre as superfícies de Ti Nano ($p = 0,001$ para ambos os genes) e Ti Controle ($p = 0,001$ para ambos os genes) em relação ao meio não-condicionado (D-MEM). Na comparação entre os grupos de células cultivadas na presença dos diferentes meios condicionados, a expressão dos genes

foi maior na presença do meio condicionado por osteoblastos crescidos no Ti Nano ($p = 0,002$ e $p = 0,001$, respectivamente) (Figura 3B). A expressão gênica de *Nfatc1* em osteoclastos foi maior na presença do meio condicionado por osteoblastos crescidos sobre as superfícies de Ti Nano ($p = 0,001$) e Ti Controle ($p = 0,001$) em relação ao meio não-condicionado (D-MEM). Na comparação entre os grupos de células cultivadas na presença dos diferentes meios condicionados, a expressão do gene não foi afetada ($p = 0,111$) (Figura 3B). A expressão gênica de *Nfatc2* não foi afetada pela presença do meio condicionado por osteoblastos crescidos sobre ambas as superfícies ($p = 0,058$) e, com relação ao gene *Sema4d*, foi observada maior gênica em osteoclastos, na presença do meio condicionado por osteoblastos crescidos sobre as superfícies de Ti Nano ($p = 0,001$) e Ti Controle ($p = 0,001$) em relação ao meio não-condicionado (D-MEM). Na comparação entre os grupos de células cultivadas na presença dos diferentes meios condicionados, a expressão do gene foi maior na presença do meio condicionado por osteoblastos crescidos no Ti Controle ($p = 0,014$) (Figura 3B).

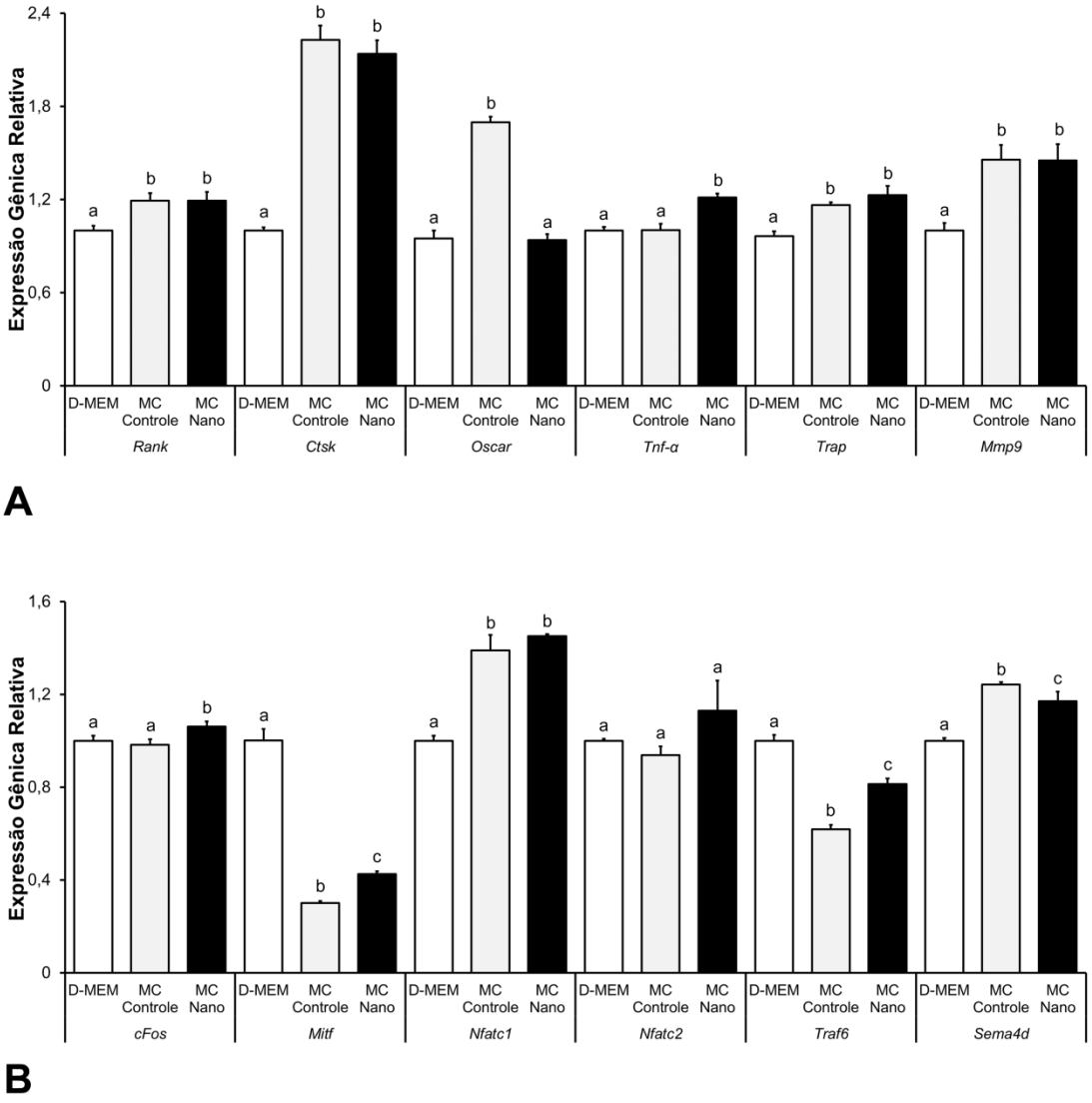

Figura 3. Expressão gênica dos marcadores da diferenciação osteoclástica *Rank*, *Ctsk*, *Oscar*, *Tnf-*α, Trap e Mmp9 (A) e *cFos*, *Mitf*, *Nfatc1*, *Nfatc2*, *Traf6* e *Sema4d* (B) de osteoclastos crescidos na presença do meio controle (D-MEM), osteoclastos crescidos na presença do meio condicionado por osteoblastos crescidos no Ti Controle (MC Controle) e osteoclastos crescidos na presença do meio condicionado por osteoblastos crescidos no Ti Nano (MC Nano). Os dados representativos da expressão gênica (n = 3) são demonstrados com média ± desvio padrão. Letras distintas indicam diferença estatisticamente significante ($p \leq 0,05$).

2.3.5 O meio condicionado por osteoblastos crescidos sobre a superfície de Ti Nano afeta, de maneira mais acentuada, o fenótipo osteoclástico

Para investigar o papel do meio condicionado por osteoblastos crescidos sobre o Ti Nano no fenótipo osteoclástico, análises de expressão proteica de marcadores osteoclásticos e da atividade de TRAP foram realizadas (Figura 4). A expressão proteica de CTSK (Figura 4A) e TRAP (Figura 4B) em osteoclastos foi menor pela presença do meio condicionado por osteoblastos crescidos sobre as superfícies de Ti Nano ($p = 0,001$ para ambos os genes) e Ti Controle ($p = 0,001$

para ambos os genes) em relação ao meio não-condicionado (D-MEM). Na comparação entre os grupos de células cultivadas na presença dos diferentes meios condicionados, a expressão proteica foi menor na presença do meio condicionado por osteoblastos crescidos no Ti Nano (p = 0,002 e p = 0,001, respectivamente) (Figura 4A e 4B, respectivamente). Com relação à atividade de TRAP, houve uma menor marcação em osteoclastos, na presença do meio condicionado por osteoblastos crescidos sobre as superfícies de Ti Nano (p = 0,001) e Ti Controle (p = 0,001) em relação ao meio não-condicionado (D-MEM). Na comparação entre os grupos de células cultivadas na presença dos diferentes meios condicionados, a marcação foi menor na presença do meio condicionado por osteoblastos crescidos no Ti Nano (p = 0,018) (Figura 4C).

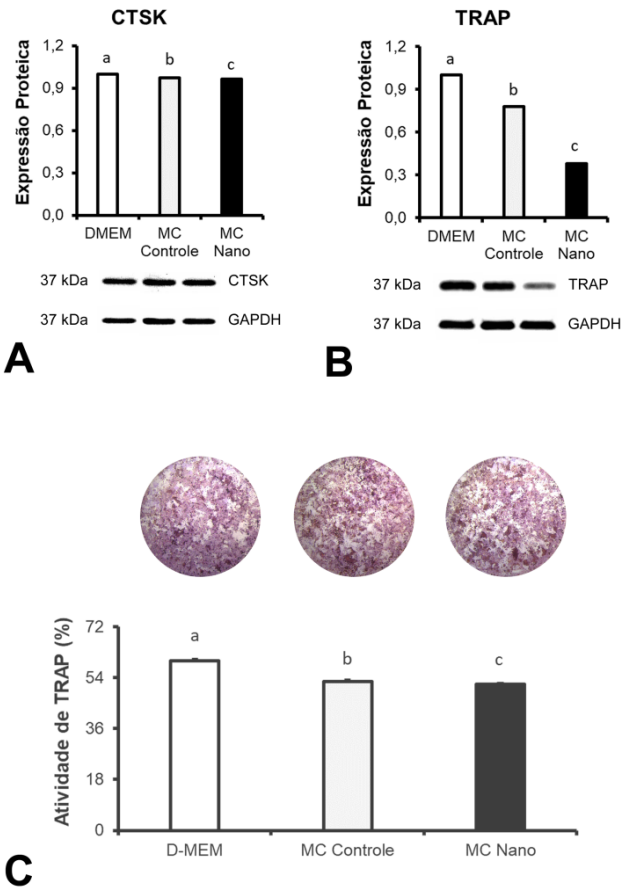

Figura 4. Expressão proteica dos marcadores da diferenciação osteoclástica CTSK (A) e TRAP (B) e atividade de TRAP (C) de osteoclastos crescidos na presença do meio controle (D-MEM), osteoclastos crescidos na presença do meio condicionado por osteoblastos crescidos no Ti Controle (MC Controle) e osteoclastos crescidos na presença do meio condicionado por osteoblastos crescidos no Ti Nano (MC Nano). Os dados representativos da expressão proteica (n = 3) e atividade de TRAP (n = 4) são demonstrados com média ± desvio padrão. Letras distintas indicam diferença estatisticamente significante (p ≤ 0,05).

2.4 DISCUSSÃO

As alterações topográficas das superfícies de Ti desempenham papel fundamental na interação célula-material durante a osseointegração de implantes dentários e ortopédicos, processo biológico complexo que envolve a comunicação entre diversos tipos celulares, dentre eles osteoblastos e osteoclastos (HOU et al., 2022; LOTZ et al., 2020; SILVERWOOD et al., 2016). Para os osteoblastos, nosso grupo de pesquisa tem demonstrado que a nanotopografia, obtida através de tratamento com solução de H_2SO_4/H_2O_2, apresenta propriedades benéficas como substrato, por favorecer a diferenciação através de diversos mecanismos celulares (ABUNA et al., 2019; LOPES et al., 2019; CASTRO-RAUCCI et al., 2016; ROSA et al., 2014). Entretanto, até o momento, não existiam evidências do papel dessa superfície sobre osteoclastos, assim como durante a sua interação com células osteoblásticas, responsáveis pela remodelação óssea, o que motivou a realização desse estudo.

Modelos experimentais de co-cultura e meios condicionados por células têm sido amplamente reportados na literatura, uma vez que permitem a elucidação de alguns aspectos das complexas interações entre diferentes tipos celulares, na presença ou ausência de diferentes topografias de superfície, criando uma representação mais acurada do microambiente *in vivo* (ABE et al., 2019; HEINEMANN et al., 2011; PARK et al., 2017; SILVERWOOD et al., 2016; TU; CHEN; SHIE, 2015; YOUNG et al., 2015). Sabe-se que, a atividade combinada de células osteoblásticas e osteoclásticas e as interações que ocorrem entre elas são relevantes para os processos de remodelação e regeneração óssea (ZHANG et al., 2018). Visando o entendimento desse processo na presença do Ti com nanotopografia, os modelos de co-cultura indireta e utilização de meios condicionados por células foram selecionados para a realização desse estudo.

O efeito de diferentes topografias de implante na osteoclastogênese têm sido demonstrado; entretanto, ainda não há um padrão referente ao efeito das diferentes rugosidades na fusão e capacidade reabsortiva dessas células. Para determinar o papel do Ti com nanotopografia na diferenciação osteoclástica, foram realizados ensaios de expressão gênica, seguidos de ensaios fenotípicos para detecção das proteínas CTSK e TRAP e de marcação histoquímica TRAP, enzimas proteolíticas abundantemente expressas em osteoclastos ativos, que degradam colágeno e outras proteínas de matriz durante a reabsorção (KIM et al., 2020;

MINKIN, 1982). Os resultados indicam que a nanotopografia favorece a diferenciação osteoclástica, uma vez que houve aumento dos níveis de expressão de genes relacionados à via de sinalização Rank/Rankl, como os fatores de transcrição *cFos*, *Mitf*, *Nfatc1*, *Nfatc*2 e a molécula adaptadora *Traf6*, e dos marcadores *Rank*, *Ctsk*, *Tnf-α* e *Oscar*, diferentemente das evidências descritas por ZHANG et al. (2018), cujo estudo visou avaliar os efeitos combinados entre diferentes rugosidades em superfície de Ti na osteoclastogênese e osteogênese. Os autores observaram que as diferentes rugosidades induziram a formação de osteoclastos com distintos fenótipos; entretanto, houve diminuição dos níveis de expressão gênica de *Rank*, *Trap*, *Ctsk* e *Mmp9* quando células osteoclásticas foram plaqueadas sobre as diferentes rugosidades de Ti, e essa diminuição ocorreu de maneira intensa com o aumento da rugosidade. Por outro lado, os autores observaram uma diminuição da atividade de TRAP quando da presença das diferentes rugosidades, o que corrobora com os achados de nosso trabalho, ao menos em parte, pela diminuição da marcação de TRAP em osteoclastos cultivados sobre o Ti com nanotopografia. Ainda, a diminuição da expressão proteica de TRAP e CTSK, e da marcação de TRAP encontrada em nossos resultados são corroborados por evidências do papel deletério de superfícies nanoestruturadas na diferenciação osteoclástica, através da inibição da expressão da integrina β1, diminuição da fosforilação de FAK e redução da expressão da fosforilação de p38 (HE et al., 2022). Os autores discutem informações relevantes acerca do efeito substrato, da topografia, no comportamento dos osteoclastos, uma vez que depende da capacidade perceptiva da superfície mediada por adesão focal, para desenvolvimento da zona de vedação permitindo a adequada reabsorção óssea. No presente estudo, os mecanismos envolvidos na adesão dos osteoclastos e na formação dos anéis de actina e zona seladora não foram avaliados, mas investigações futuras podem contribuir para a elucidação da diminuição da atividade dessas células, em contato com a nanotopografia.

Em nosso trabalho, a presença dos osteoblastos nos modelos de co-cultura indireta favoreceu a expressão de genes relacionados à via de sinalização Rank/Rankl e marcadores osteoclásticos, de maneira mais acentuada na presença da nanotopografia. Entretanto, assim como observado nas culturas isoladas, a presença dos osteoblastos diminuiu a expressão proteica e a marcação de TRAP. Em estudo utilizando o modelo de co-cultura direta entre osteoblastos e osteoclastos

em contato com uma superfície de polímero nanotopográfico observou-se uma expressão ligeiramente superior de TRAP e OSCAR em osteoclastos; porém, não houve aumento da intensidade de marcação de TRAP quando essas células permaneceram na presença da nanotopografia e dos osteoblastos, reforçando os achados do nosso estudo (YOUNG et al., 2015). Um segundo estudo, também utilizando o modelo de co-cultura direta demostrou que uma superfície de Ti com nanopilares favoreceu a osteogênese, evidenciada através do aumento da expressão de ALP, detecção de OPN e de deposição de cálcio, sem afetar a osteoclastogênese, uma vez que houve diminuição da expressão gênica de TRAP e uma tendência de redução da expressão de outros marcadores como OSCAR, CTSK e TNF-α. Assim como evidenciado em nossos resultados, esse estudo também observou uma menor marcação de TRAP nas co-culturas realizadas na presença do substrato com nanopilares e osteoblastos (SILVERWOOD et al., 2016). Os autores ainda abordaram que trata-se de uma superfície nanotopográfica bioativa para a formação óssea, não assumindo o mesmo perfil para todos os tipos de células em contato, sendo relevante para a formação óssea sem aumento da reabsorção, fatores importantes para o implante ideal.

Um outro fator importante no microambiente osteoblasto-osteoclasto é o meio de cultura celular. HEINEMANN et al. (2011) estabeleceram procedimento de co-cultivo entre osteoblastos e osteoclastos e discutiram sobre a influência significativa da composição do meio de cultura na proliferação e diferenciação de osteoclastos. Os autores fazem referência ao trabalho realizado por TAKEYAMA et al. (2001) que observaram efeito inibitório do fosfato inorgânico na matriz extracelular e fosfato extracelular na osteoclastogênese, uma vez que o número de células osteoclásticas diminuiu com o aumento da concentração de beta-glicerofosfato no meio de cultura, e com a liberação de fosfato catalisada pela ALP. Possivelmente, a inibição da atividade osteoclástica, independentemente da superfície avaliada, pode também estar relacionada a esse mecanismo em nosso estudo.

Nossos resultados referentes à cultura de células osteoclásticas na presença de meio condicionado por células osteoblásticas crescidas nas diferentes superfícies de Ti mostraram que, assim como observado nos modelos de co-cultura indireta, a presença do meio condicionados por osteoblastos aumentou a expressão de genes relacionados à via de sinalização Rank/Rankl, como os fatores de transcrição *cFos* e

Nfatc1, e a molécula *Sema4d*, e dos marcadores *Rank*, *Ctsk*, *Tnf-α*, *Trap* e *Mmp9*. Entretanto, uma diminuição do fenótipo relacionado à marcação histoquímica e quantidade das proteínas CTSK e TRAP, foi observada, similar ao observado no modelo de co-cultura. Nossos achados estão parcialmente em acordo com os descritos por LOTZ et al. (2018), que utilizaram meios condicionados obtidos de culturas de células-tronco e osteoblastos em contato com superfícies de Ti microrrugosas em células osteoclásticas humanas. Os autores observaram que a superfície microestruturada regulou indiretamente a atividade osteoclástica, uma vez que após o reconhecimento de superfície por integrinas, a produção de proteínas das células-tronco e osteoblastos foi modulada, sendo responsável pela supressão da atividade e redução da fusão de novos osteoclastos. A atividade reduzida de osteoclastos ocorreu de maneira dependente da superfície, como ocorreu em nosso estudo, nos achados referentes à marcação da proteína TRAP.

Células envolvidas na remodelação óssea também secretam vesículas extracelulares, uma população heterogênea de vesículas com membrana de bicamada lipídica, classificadas na dependência de sua origem, tamanho e função, que afetam o *crosstalk* entre elas, regulando diversos mecanismos celulares, dentre eles a diferenciação (UENAKA et al., 2022; VIG; FERNANDES, 2022). Um estudo demostrou que pequenas vesículas de osteoblastos contendo o microRNA 143 (miR-143) aumentaram significativamente a expressão de *Rankl* em osteoblastos tratados com essas vesículas, sugerindo que o miR-143-3p, presente nas vesículas, induziu uma mudança fenotípica de osteoblastos que indiretamente favoreceu a osteoclastogênese (UENAKA et al., 2022). Em nosso estudo, observamos claras alterações genotípicas e fenotípicas em osteoclastos, crescidos na presença dos meios condicionados por osteoblastos cultivados nas diferentes superfícies de Ti. Futuras abordagens são necessárias para identificação de proteínas, RNAs codificadores e não-codificadores e\ou outros componentes das vesículas que estejam atuando no processo de diferenciação de osteoclastos.

Em conclusão, nossos resultados demonstraram, pela primeira vez, que a nanotopografia afeta direta e indiretamente a diferenciação de osteoclastos, gerando mudanças de perfis genotípico e fenotípico, as quais são mais intensamente moduladas por osteoblastos quando comparadas às células crescidas sobre Ti Controle.

3. Conclusões

3. CONCLUSÕES

- Osteoclastos inibem osteoblastos crescidos sobre superfícies de titânio (Ti).
- Ti Nano protege os osteoblastos do efeito negativo dos osteoclastos por prevenir o aumento do acúmulo de H3K27me3 nas regiões promotoras de *Runx2* e *Alpl.*
- Ti Nano favorece a expressão de genes relacionados à diferenciação osteoclástica; no entanto, os osteoclastos são menos ativos quando crescidos sobre a nanotopografia.
- Osteoblastos favorecem a expressão de genes relacionados à diferenciação osteoclástica em osteoclastos crescidos sobre superfícies de Ti.
- A atividade osteoclástica é inibida de forma mais intensa por osteoblastos quando os osteoclastos crescem sobre Ti Nano comparado ao Ti Controle.

Referências Bibliográficas

REFERÊNCIAS BIBLIOGRÁFICAS*

As referências bibliográficas aqui apresentadas correspondem aos itens **Introdução e **Capítulo 2** da presente tese. As referências bibliográficas correspondentes ao **Capítulo 1** estão apresentadas ao final do artigo científico.*

ABE, T. *et al*. The effect of mesenchymal stem cells on osteoclast precursor cell differentiation. **Journal of Oral Science**, v. 61, n. 1, p. 30–35, 28 mar. 2019.

ABUNA, R. P. F. *et al*. The Wnt/β-catenin signaling pathway is regulated by titanium with nanotopography to induce osteoblast differentiation. **Colloids and Surfaces. B, Biointerfaces**, v. 184, p. 110513, 1 dez. 2019.

ABUNA, R. P. F. *et al.* Frizzled 6 disruption suppresses osteoblast differentiation induced by nanotopography through the canonical Wnt signaling pathway. **Journal of Cellular Physiology**, v. 235, n. 11, p. 8293–8303, nov. 2020.

BIGHETTI-TREVISAN, R. L. *et al*. Titanium with nanotopography attenuates the osteoclast-induced disruption of osteoblast differentiation by regulating histone methylation. **Materials Science & Engineering. C, Materials for Biological Applications**, p. 112548, 13 nov. 2021. Ahead of print. DOI https://www.sciencedirect.com/science/article/abs/pii/S0928493121006883?via%3Dihub. Acesso em: 29 maio 2022.

BRANEMARK, P. I. Osseointegration and its experimental background. **The Journal of Prosthetic Dentistry**, v. 50, n. 3, p. 399–410, set. 1983.

CASTRO-RAUCCI, L. M. S *et al*. Titanium with nanotopography induces osteoblast differentiation by regulating endogenous bone morphogenetic protein expression and signaling pathway. **Journal of Cellular Biochemistry**, v. 117, n. 7, p. 1718–1726, jul. 2016.

CIAPETTI, G. *et al.* Osteoclast differentiation from human blood precursors on biomimetic calcium-phosphate substrates. **Acta Biomaterialia**, v. 50, p. 102–113, 1 mar. 2017.

COSTA-RODRIGUES, J. *et al*. Osteoclastogenic differentiation of human precursor cells over micro- and nanostructured hydroxyapatite topography. **Biochimica et Biophysica Acta**, v. 1860, n. 4, p. 825–835, abr. 2016.

DALBY, M. J. *et al*. Nanotopographical control of human osteoprogenitor differentiation. **Current Stem Cell Research & Therapy**, v. 2, n. 2, p. 129–138, maio 2007.

DE OLIVEIRA, P. T. *et al*. Enhancement ofin vitro osteogenesis on titanium by chemically produced nanotopography. **Journal of Biomedical Materials Research Part A**, v. 80, n. 3, p. 554–564, 1 mar. 2007.

DETSCH, R.; MAYR, H.; ZIEGLER, G. Formation of osteoclast-like cells on HA and TCP ceramics. **Acta Biomaterialia**, v. 4, n. 1, p. 139–148, jan. 2008.

ERIKSEN, E. F. Cellular mechanisms of bone remodeling. **Reviews in Endocrine & Metabolic Disorders**, v. 11, n. 4, p. 219–227, dez. 2010.

FLEIGE, S.; PFAFFL, M. W. RNA integrity and the effect on the real-time qRT-PCR performance. **Molecular Aspects of Medicine**, v. 27, n. 2–3, p. 126–139, jun. 2006.

HE, Y. *et a*l. Nanoporous titanium implant surface promotes osteogenesis by suppressing osteoclastogenesis via integrin β1/FAKpY397/MAPK pathway. **Bioactive Materials**, v. 8, p. 109–123, fev. 2022.

HEINEMANN, C. *et al*. Development of an osteoblast/osteoclast co-culture derived by human bone marrow stromal cells and human monocytes for biomaterials testing. **European Cells & Materials**, v. 21, p. 80–93, 25 jan. 2011.

HOU, C. *et al*. Surface modification techniques to produce micro/nano-scale topographies on Ti-based implant surfaces for improved osseointegration. **Frontiers in Bioengineering and Biotechnology**, v. 10, p. 835008, 25 mar. 2022.

KATO, R. B. *et al*. Nanotopography directs mesenchymal stem cells to osteoblast lineage through regulation of microRNA-SMAD-BMP-2 circuit. **Journal of Cellular Physiology**, v. 229, n. 11, p. 1690–1696, nov. 2014.

KIM, J.-M. *et al*. Osteoblast-Osteoclast Communication and Bone Homeostasis. **Cells**, v. 9, n. 9, p. 2073, 10 set. 2020.

LIVAK, K. J.; SCHMITTGEN, T. D. Analysis of relative gene expression data using real-time quantitative PCR and the 2(-Delta Delta C(T)) Method. **Methods (San Diego, Calif.)**, v. 25, n. 4, p. 402–408, dez. 2001.

LOPES, H. B. *et al*. Participation of integrin β3 in osteoblast differentiation induced by titanium with nano or microtopography. **Journal of Biomedical Materials Research. Part A**, v. 107, n. 6, p. 1303–1313, jun. 2019.

LOTZ, E. M. *et al*. Regulation of osteoclasts by osteoblast lineage cells depends on titanium implant surface properties. **Acta Biomaterialia**, v. 68, p. 296–307, 1 mar. 2018.

LOTZ, E. M. *et al*. Regulation of mesenchymal stem cell differentiation on microstructured titanium surfaces by semaphorin 3A. **Bone**, v. 134, p. 115260, maio 2020.

MARTIN, J. Y. *et al*. Effect of titanium surface roughness on proliferation, differentiation, and protein synthesis of human osteoblast-like cells (MG63). **Journal of Biomedical Materials Research**, v. 29, n. 3, p. 389–401, mar. 1995.

MATSUO, K.; IRIE, N. Osteoclast-osteoblast communication. **Archives of Biochemistry and Biophysics**, v. 473, n. 2, p. 201–209, 15 maio 2008.

MAVROGENIS, A. F. *et al.* Biology of implant osseointegration. **Journal of**

Musculoskeletal & Neuronal Interactions, v. 9, n. 2, p. 61–71, jun. 2009.

MENDONÇA, G. *et al*. The combination of micron and nanotopography by H(2)SO(4)/H(2)O(2) treatment and its effects on osteoblast-specific gene expression of hMSCs. **Journal of Biomedical Materials Research. Part A**, v. 94, n. 1, p. 169–179, jul. 2010.

MINKIN, C. Bone acid phosphatase: tartrate-resistant acid phosphatase as a marker of osteoclast function. **Calcified Tissue International**, v. 34, n. 3, p. 285–290, maio 1982.

MORANDINI RODRIGUES, L. *et al*. Nanoscale hybrid implant surfaces and Osterix-mediated osseointegration. **Journal of Biomedical Materials Research. Part A**, v. 110, n. 3, p. 696–707, mar. 2022.

NAGASAWA, M. *et al.* Topography influences adherent cell regulation of osteoclastogenesis. **Journal of Dental Research**, v. 95, n. 3, p. 319–326, mar. 2016.

PARK, H.-C. *et al*. Effects of osteogenic-conditioned medium from human periosteum-derived cells on osteoclast differentiation. **International Journal of Medical Sciences**, v. 14, n. 13, p. 1389–1401, 2 nov. 2017.

REN, B. *et al*. Improved osseointegration of 3D printed Ti-6Al-4V implant with a hierarchical micro/nano surface topography: An in vitro and in vivo study. **Materials Science & Engineering. C, Materials for Biological Applications**, v. 118, p. 111505, jan. 2021.

ROSA, A. L. *et al*. Nanotopography drives stem cell fate toward osteoblast differentiation through α1β1 integrin signaling pathway. **Journal of Cellular Biochemistry**, v. 115, n. 3, p. 540–548, mar. 2014.

SCHROEDER, A. *et al*. The RIN: an RNA integrity number for assigning integrity values to RNA measurements. **BMC Molecular Biology**, v. 7, p. 3, 31 jan. 2006.

SILVERWOOD, R. K. *et al.* Analysis of osteoclastogenesis/osteoblastogenesis on nanotopographical titania surfaces. **Advanced Healthcare Materials**, v. 5, n. 8, p. 947–955, 20 abr. 2016.

SOUZA, J. C. M. *et al*. Nano-scale modification of titanium implant surfaces to enhance osseointegration. **Acta Biomaterialia**, v. 94, p. 112–131, ago. 2019.

TAKEYAMA, S. *et al*. Phosphate decreases osteoclastogenesis in coculture of osteoblast and bone marrow. **Biochemical and Biophysical Research Communications**, v. 282, n. 3, p. 798–802, 6 abr. 2001.

TU, M.-G.; CHEN, Y.-W.; SHIE, M.-Y. Macrophage-mediated osteogenesis activation in co-culture with osteoblast on calcium silicate cement. **Journal of Materials Science. Materials in Medicine**, v. 26, n. 12, p. 276, dez. 2015.

UENAKA, M. *et al*. Osteoblast-derived vesicles induce a switch from bone-formation to bone-resorption in vivo. **Nature Communications**, v. 13, n. 1, p. 1066, 24 fev. 2022.

VARIOLA, F. *et al*. Tailoring the surface properties of Ti6Al4V by controlled chemical oxidation. **Biomaterials**, v. 29, n. 10, p. 1285–1298, abr. 2008.

VIG, S.; FERNANDES, M. H. Bone Cell Exosomes and Emerging Strategies in Bone Engineering. **Biomedicines**, v. 10, n. 4, p. 767, 24 mar. 2022.

YI, J.-H. *et al*. Characterization of a bioactive nanotextured surface created by controlled chemical oxidation of titanium. **Surface Science**, v. 600, n. 19, p. 4613–4621, 1 out. 2006.

YOUNG, P. S. *et al*. Osteoclastogenesis/osteoblastogenesis using human bone marrow-derived cocultures on nanotopographical polymer surfaces. **Nanomedicine (London, England)**, v. 10, n. 6, p. 949–957, 2015.

ZHANG, Y. *et al*. Combinatorial surface roughness effects on osteoclastogenesis and osteogenesis. **ACS Applied Materials & Interfaces**, v. 10, n. 43, p. 36652–36663, 31 out. 2018.

ZHANG, Y. *et al.* Species-independent stimulation of osteogenic differentiation induced by osteoclasts. **Biochemical and Biophysical Research Communications**, v. 606, p. 149–155, 28 maio 2022.

Apêndices

APÊNDICE A

Resultados relativos aos RNAs não-codificadores longos identificados no RNAseq que estão sendo utilizados para o preparo de novo manuscrito.

Preliminary results

The effect of osteoclasts on transcriptional regulation of non-coding RNAs in osteoblasts grown on titanium with nanotopography

Rayana Longo Bighetti-Trevisan[a], Emanuela Prado Ferraz[b], Jonathan Gordon[c], Coralee Tye[c], Jane Barbara Lian[c], Gary Stephen Stein[c], Janet Stein[c], Adalberto Luiz Rosa[a], Marcio Mateus Beloti[a]

[a]Bone Research Lab, School of Dentistry of Ribeirão Preto, University of São Paulo, Ribeirão Preto, SP, Brazil
[b]Department of Oral and Maxillofacial Surgery, Prosthesis and Traumatology, School of Dentistry, University of São Paulo, São Paulo, SP, Brazil
[c]Department of Biochemistry and Vermont Cancer Center, University of Vermont Larner College of Medicine, Burlington,VT, USA

Background: Titanium (Ti) osseointegration depends on the crosstalk between osteoclasts and osteoblasts that may be affected by epigenetic mechanisms, including long non-coding RNAs (lncRNAs) and microRNAs (miRNAs). Ti with nanotopography (Ti Nano), generated by H_2SO_4/H_2O_2 treatment, induces osteoblast differentiation that is inhibited by osteoclasts in a less pronounced way than in osteoblasts grown on Ti Control. Thus, we hypothesized that osteoclasts affect transcriptional regulation of non-coding RNAs (ncRNAs) in osteoblasts grown on Ti Nano.

Purpose: We aimed to investigate the effect of osteoclasts on the regulation of ncRNAs in osteoblasts grown on Ti Nano.

Methods and results: Osteoblasts were cultured on Ti Nano and Ti Control and osteoclasts into inserts in a co-culture model for 48 h, and non-cocultured osteoblasts were used as control. Using RNAseq (DESeq2: FC>1.7; p<0.05), we identified 252 modulated lncRNAs, plotted in a heatmap according to their expression

patterns. Many genes were regulated by osteoclasts, mainly in osteoblasts grown on Ti Nano (Figure 1). The real-time PCR (p≤0.05) showed that osteoclasts upregulated the gene expression of *H19*, *Snhg1*, *Neat1* and *Zfas1* and downregulated *Carmn*, *Tug1*, *Dnm3os* and *Kcnq1ot1* in osteoblasts grown on Ti Nano (Figure 2). There were inverse correlations between the expression of *Kcnq1ot1*, a lncRNA that contribute to osteogenic differentiation by sponging miR-214, and the osteogenic genes *Alpl*, *Bglap*, *Bmp8a*, *Col1a1* and *Vim* in osteoblasts grown in presence of osteoclasts on Ti Nano (Figure 3A). Although osteoclasts downregulated *Kcnq1ot1* and upregulated miR-214 in osteoblasts grown on both Ti surfaces (p≤0.05, Figure 3B), such effects were more pronounced on Ti Nano.

Conclusions: Ti Nano induces resistance in osteoblasts to the negative effects of osteoclasts due to, at least in part, the modulation of osteogenic mRNAs through a Kcnq1ot1/miR-214 circuit. **Financial support:** FAPESP (# 2017/23888-8, 2018/17356-6 and 2019/09349-2).

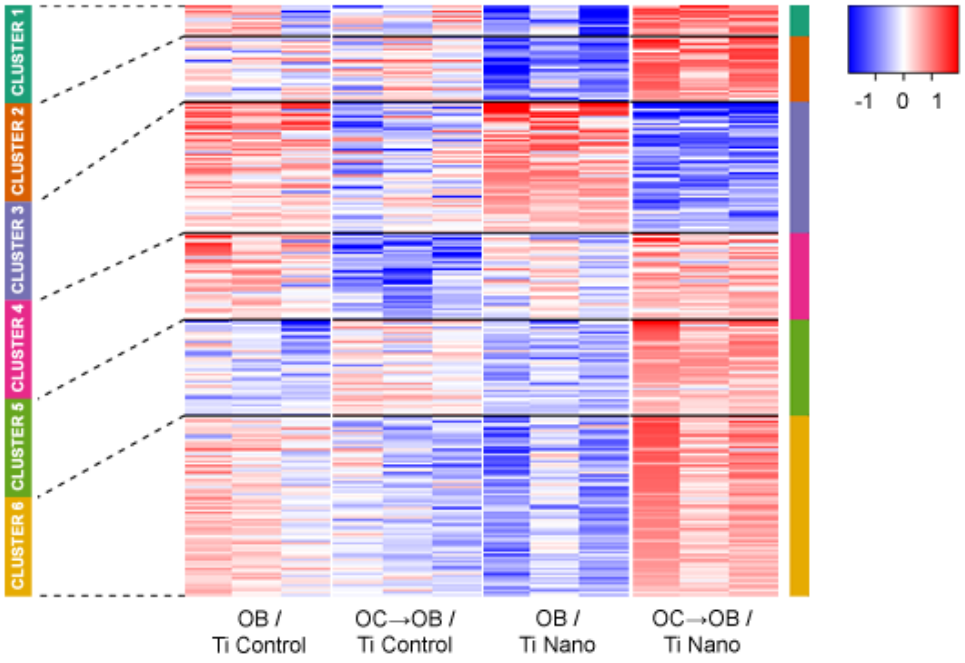

Figure 1. Heatmap showing the differential lncRNAs gene expression in osteoblasts grown on Ti Control (OB / Ti Control), osteoblasts grown on Ti Control in presence of osteoclasts (OC→OB / Ti Control), osteoblasts grown on Ti Nano (OB / Ti Nano) and osteoblasts grown on Ti Nano in presence of osteoclasts (OC→OB / Ti Nano) (n=3).

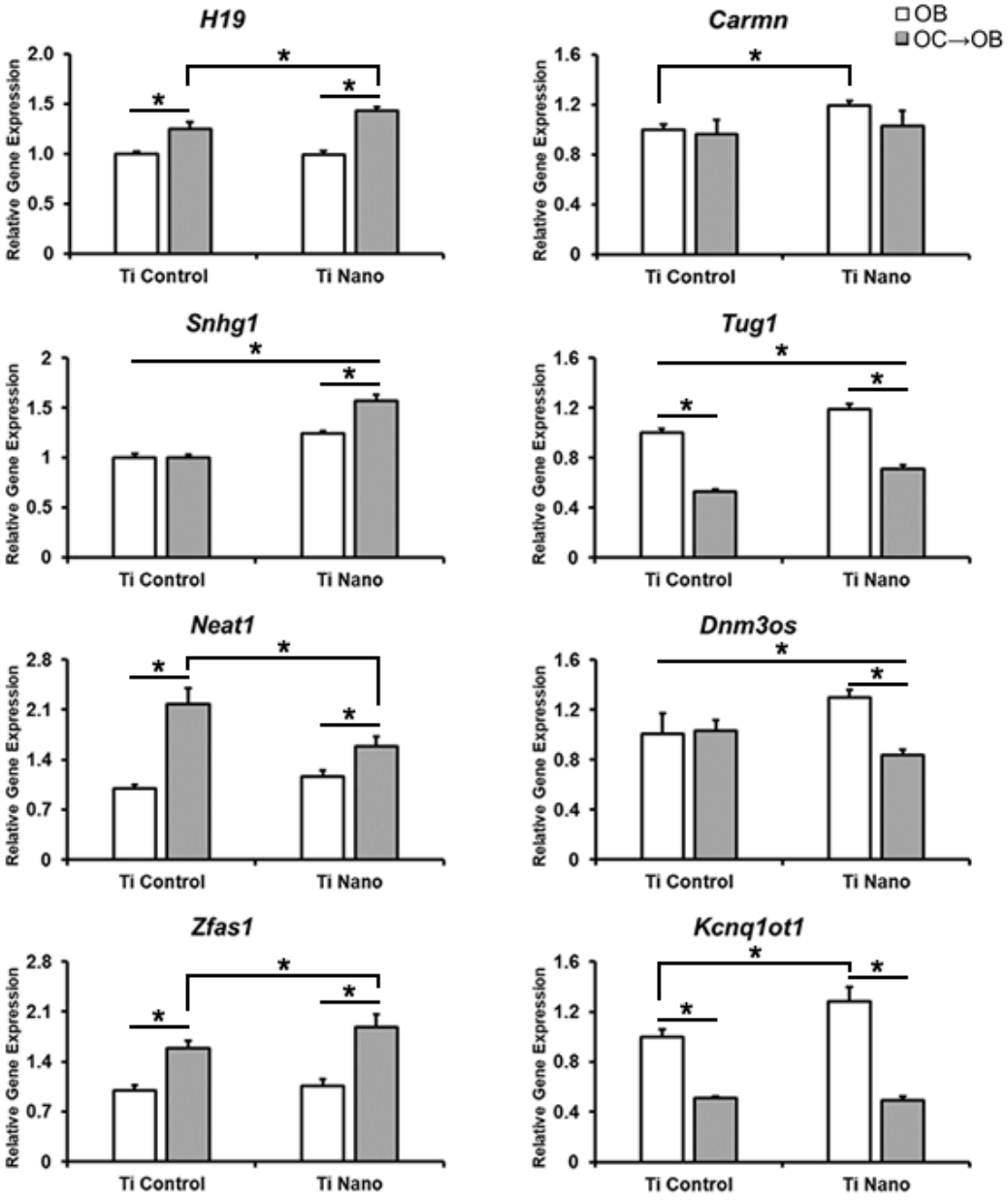

Figure 2. Gene expression of *H19*, *Snhg1*, *Neat1*, *Zfas1*, *Carmn*, *Tug1*, *Dnm3os* and *Kcnq1ot1* of osteoblasts (OB) grown on Ti Control, osteoblasts grown in presence of osteoclasts (OC→OB) on Ti Control, OB grown on Ti Nano and OC→OB on Ti Nano. The data of gene expression (n=3) is presented as mean ± standard deviation and asterisks (*) indicate statistically significant differences ($p \leq 0.05$).

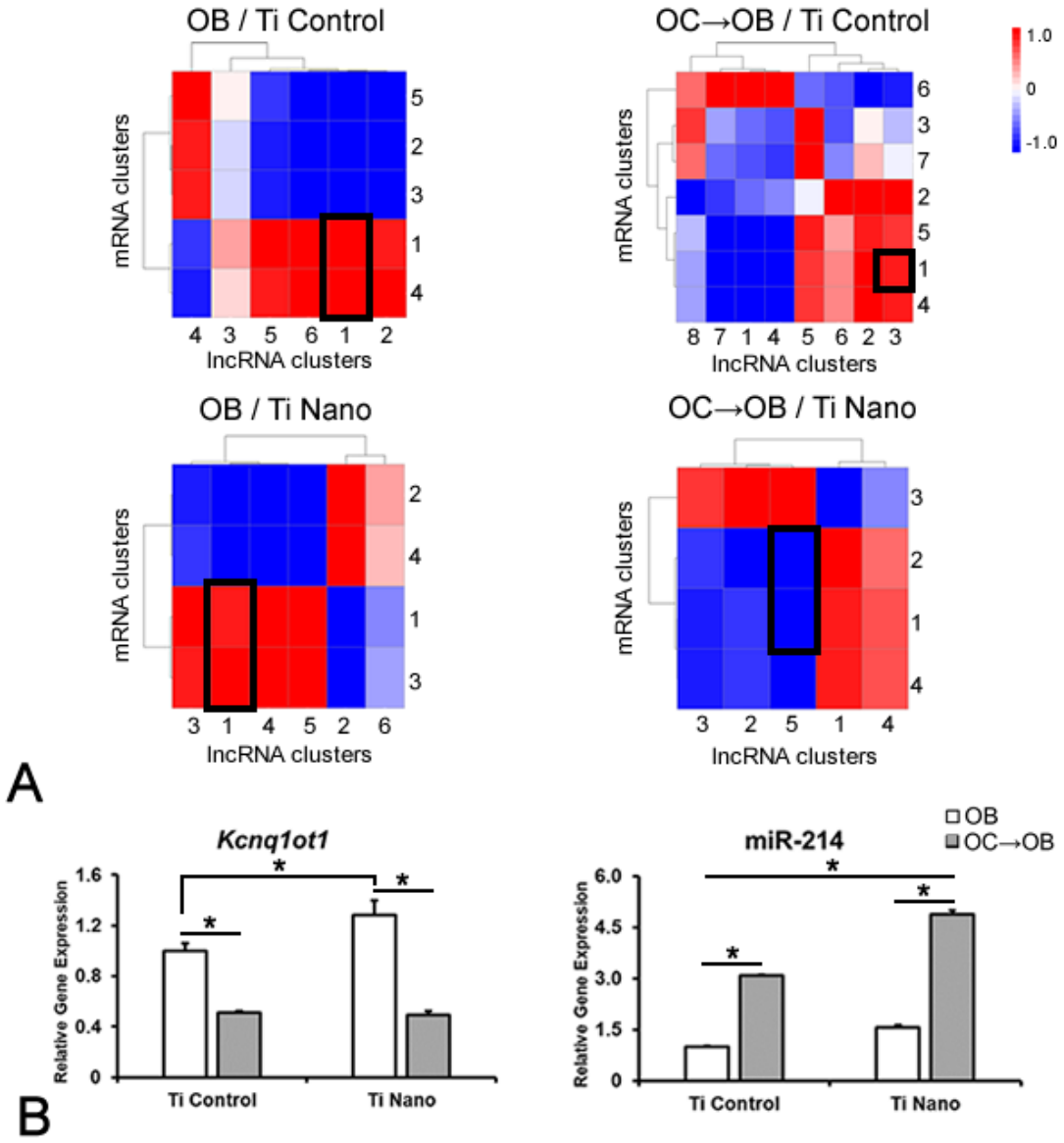

Figure 3. Correlation analysis of lncRNAs and mRNAs differentially expressed in osteoblasts (OB) grown on Ti Control, osteoblasts grown in presence of osteoclasts (OC→OB) on Ti Control, osteoblasts grown on Ti Nano and OC→OB on Ti Nano (Pearson; coefficients 1.0 and -1.0) (A). Gene expression of *Kcnq1ot1* and miR-214 of osteoblasts (OB) grown on Ti Control, osteoblasts grown in presence of osteoclasts (OC→OB) on Ti Control, OB grown on Ti Nano and OC→OB on Ti Nano (B). The data of gene expression (n=3) is presented as mean ± standard deviation and asterisks (*) indicate statistically significant differences ($p \leq 0.05$).

APÊNDICE B

Artigos publicados durante o período do Doutorado

ARTICLE IN PRESS

Materials Science & Engineering C xxx (xxxx) xxx

Contents lists available at ScienceDirect

Materials Science & Engineering C

journal homepage: www.elsevier.com/locate/msec

Titanium with nanotopography attenuates the osteoclast-induced disruption of osteoblast differentiation by regulating histone methylation

Rayana L. Bighetti-Trevisan [a], Luciana O. Almeida [a], Larissa M.S. Castro-Raucci [b], Jonathan A. R. Gordon [c], Coralee E. Tye [c], Gary S. Stein [c], Jane B. Lian [c], Janet L. Stein [c], Adalberto L. Rosa [a], Marcio M. Beloti [a,*]

[a] Bone Research Lab, School of Dentistry of Ribeirão Preto, University of São Paulo, Ribeirão Preto, SP, Brazil
[b] School of Dentistry, University of Ribeirão Preto, Ribeirão Preto, SP, Brazil
[c] Department of Biochemistry and Vermont Cancer Center, University of Vermont Larner College of Medicine, Burlington, VT, USA

ARTICLE INFO

Keywords:
Histone
Nanotopography
Osteoblast
Osteoclast
Titanium

ABSTRACT

The bone remodeling process is crucial for titanium (Ti) osseointegration and involves the crosstalk between osteoclasts and osteoblasts. Considering the high osteogenic potential of Ti with nanotopography (Ti Nano) and that osteoclasts inhibit osteoblast differentiation, we hypothesized that nanotopography attenuate the osteoclast-induced disruption of osteoblast differentiation. Osteoblasts were co-cultured with osteoclasts on Ti Nano and Ti Control and non-co-cultured osteoblasts were used as control. Gene expression analysis using RNAseq showed that osteoclasts downregulated the expression of osteoblast marker genes and upregulated genes related to histone modification and chromatin organization in osteoblasts grown on both Ti surfaces. Osteoclasts also inhibited the mRNA and protein expression of osteoblast markers, and such effect was attenuated by Ti Nano. Also, osteoclasts increased the protein expression of H3K9me2, H3K27me3 and EZH2 in osteoblasts grown on both Ti surfaces. ChIP assay revealed that osteoclasts increased accumulation of H3K27me3 that represses the promoter regions of *Runx2* and *Alpl* in osteoblasts grown on Ti Control, which was reduced by Ti Nano. In conclusion, these data show that despite osteoclast inhibition of osteoblasts grown on both Ti Control and Ti Nano, the nanotopography attenuates the osteoclast-induced disruption of osteoblast differentiation by preventing the increase of H3K27me3 accumulation that represses the promoter regions of some key osteoblast marker genes. These findings highlight the epigenetic mechanisms triggered by nanotopography to protect osteoblasts from the deleterious effects of osteoclasts, which modulate the process of bone remodeling and may benefit the osseointegration of Ti implants.

1. Introduction

A focus of biomaterial investigation is the interactions between titanium (Ti) implants and bone tissue, an essential component of osseointegration [1–4]. To improve the integrative ability of Ti, modifications of implant surfaces have been made, such as functionalization with molecules and creation of different topographies. These modifications affect signaling pathways and cellular events involved in cell adhesion and proliferation, as well as osteoprogenitor cell differentiation, which ultimately regulate the formation of mineralized extracellular matrix [5–9].

Chemical conditioning with H_2SO_4/H_2O_2 solution creates a Ti surface with nanotopography that reduces the contaminants, increases the oxide layer (TiO_2) from 5 to 32-40 nm and generates nano-sized pits of 20-22 nm average diameters [6,10,11]. This nanotopography favors cell adhesion and osteoblast differentiation by modulating several signaling pathways such as integrins, bone morphogenetic proteins (BMPs) and Wnt [6,7,11–14]. To date, there are no investigations on the effects of this nanotopography on the crosstalk between osteoblasts and osteoclasts, which may have a direct impact on bone remodeling and consequently on Ti osseointegration.

Bone remodeling is a physiological process regulated by continuous cycles of bone resorption and formation and depends on complex interactions between osteoblasts and osteoclasts [15]. Osteoblasts are derived from mesenchymal stem cells and osteoclasts are derived from hematopoietic cells through the fusion of macrophages after contact

* Corresponding author at: School of Dentistry of Ribeirão Preto, University of São Paulo, Av. do Café, s/n, 14040-904 Ribeirão Preto, SP, Brazil.
E-mail address: mmbeloti@usp.br (M.M. Beloti).

https://doi.org/10.1016/j.msec.2021.112548
Received 28 July 2021; Received in revised form 11 October 2021; Accepted 9 November 2021
Available online 13 November 2021
0928-4931/

Received: 1 June 2017 | Revised: 30 September 2017 | Accepted: 17 October 2017

DOI: 10.1002/jemt.22963

RESEARCH ARTICLE

WILEY MICROSCOPY RESEARCH & TECHNIQUE

Effects of EDTA gel and chlorhexidine gel on root dentin permeability

Rayana Longo Bighetti Trevisan[1] | Renata Siqueira Scatolin[1] | Larissa Moreira Spinola de Castro Raucci[2] | Walter Raucci Neto[2] | Izabel Cristina Froner[1]

[1]School of Dentistry of Ribeirão Preto, Department of Restorative Dentistry, University of São Paulo, Ribeirão Preto, SP, Brazil

[2]School of Dentistry, Department of Dentistry, University of Ribeirão Preto, Ribeirão Preto, São Paulo, Brazil

Correspondence
Rayana Longo Bighetti Trevisan, Faculdade de Odontologia de Ribeirão Preto – USP, Av. do Café, s/n Monte Alegre, 14040-904, Ribeirão Preto – SP, Brasil.
Email: rayana.longo@gmail.com

Review Editor: Dr. Mingying Yang

Abstract

The aim of this study was to evaluate the effect of 24% ethylenediaminetetraacetic acid (EDTA) gel and 2% chlorhexidine gel (CHX) in dentin permeability and smear layer removal from root canals instrumented with NiTi rotary system using histochemical staining and scanning electron microscopy (SEM) analysis. Overall, 43 premolars were classified into two experimental groups, EDTA ($n = 20$) and CHX ($n = 20$), and a negative control (NC) ($n = 3$). All specimens were instrumented and the irrigant solutions were used after each file change. The EDTA group received a final rinse with 5-ml 1% NaOCl followed by a 5-ml 0.9% saline solution; the CHX group received a final rinse with 10-ml 0.9% saline solution; and the negative control group received a final rinse with only 0.9% saline solution. Fifteen teeth from each group were prepared for histochemical staining and evaluation of dentin permeability using the image-scanning software Axion Vision (v.4.8.2). Five remaining teeth were prepared for analysis using SEM for morphological analysis. The study found that 24% EDTA gel increased the permeability of dentin in all thirds evaluated and also demonstrated an increased cleaning ability, with dentinal walls free of smear layer and open dentinal tubules, as compared to 2% CHX gel. It was concluded that EDTA was efficient in cleaning the dentinal tubules and increased dentin permeability.

KEYWORDS

dentin staining, irrigant solution, optical microscopy, scanning electron microscopy

1 | INTRODUCTION

Root canal treatment comprises complete removal of sound, contaminated, or necrotic pulp tissue through biomechanical preparation, which is performed using manual and/or mechanical instrumentation of the root canal. To achieve this, specific instruments are used in combination with irrigation solutions, aspiration, and flooding, which is necessary for complete cleaning and disinfection to create an environment that permits hermetic sealing of the root canal system (Beraldo, Silva, Antunes, Silveira, & Nunes, 2017; Cecchin et al., 2015; Nasher, Franzen, & Gutknecht, 2016).

Endodontic instrumentation techniques, both manual and rotary, produce a smear layer, i.e., debris on the dentin walls. *Smear layer* is defined as dentin microfragments, vital or necrotic pulp remains, and bacterial components that are retained on the dentin wall during root canal preparation. Microfragments, pulp remnants, and particles freely found within the root canals are defined as *debris* (Kim et al., 2013; Nasher et al., 2016; Schäfer & Zapke, 2000). The smear layer and debris presence in the root canal's interior can reduce dentin permeability (Carrasco, Pécora, & Fröner, 2004; Galvan et al., 1994; Pascon, Kantovitz, Cavallaro, & Puppin-Rontani, 2012; Pécora, Sousa-Neto, Saquy, Silva, & Cruz-Filho, 1993; Ribeiro, Marchesan, Silva, Sousa-Neto, & Pécora, 2010). Nonremoval of this layer may interfere with penetration of drugs into the dentinal tubules and adaptation of the sealing materials into root canal walls (Violich & Chandler, 2010). Subsequently, the debris and smear layer removal requires use of irrigating solutions that can eliminate microorganisms and dissolve organic and inorganic components, thereby allowing intracanal medication interaction and a hermetic sealing of the root canal system (Dotto, Travassos, de Oliveira, Machado, & Martins, 2007; Lottanti, Gautschi, Sener, & Zehnder, 2009; Violich & Chandler, 2010).

Received: 16 March 2018 | Accepted: 23 April 2018
DOI: 10.1002/jcb.27060

RESEARCH ARTICLE

WILEY Journal of Cellular Biochemistry

Effect of bone morphogenetic protein 9 on osteoblast differentiation of cells grown on titanium with nanotopography

Alann T.P. Souza | **Barbara L.S. Bezerra** | **Fabiola S. Oliveira** | **Gileade P. Freitas** | **Rayana L. Bighetti Trevisan** | **Paulo T. Oliveira** | **Adalberto L. Rosa** | **Marcio M. Beloti**

Cell Culture Laboratory, School of Dentistry of Ribeirão Preto, University of São Paulo, Ribeirão Preto, São Paulo, Brazil

Correspondence
Marcio M. Beloti, Cell Culture Laboratory, School of Dentistry of Ribeirão Preto, University of São Paulo, Av do Café s/n, 14040-904, Ribeirão Preto, SP, Brazil.
Email: mmbeloti@usp.br

Funding information
Fundação de Amparo à Pesquisa do Estado de São Paulo, Grant numbers: 2016/14477-1, 2016/14171-0

Abstract

Among bone morphogenetic proteins (BMPs), BMP-9 has been described as one with higher osteogenic potential. Here, we aimed at evaluating the effect of BMP-9 on the osteoblast differentiation of cells grown on titanium (Ti) with nanotopography, a well-known osseoinductive surface. MC3T3-E1 cells were grown either in absence or presence of BMP-9 (20 nM) on Ti with nanotopography (Ti-Nano) or machined Ti (Ti-Machined) for up to 21 days to evaluate the gene expression of RUNX2, osterix, osteocalcin, bone sialoprotein, SMAD6 and SMAD4, protein expression of SMAD4, ALP activity and extracellular matrix mineralization. As expected BMP-9 increased osteoblast differentiation irrespective of Ti surface topography; however, the cells grown on Ti-Nano were more responsible to BMP-9 compared with cells grown on Ti-machined. This could be, at least in part, due to the fact that Ti-Nano may act on both ways, by increasing the activation (SMAD4) and decreasing the inhibition (SMAD6) of the signaling pathway triggered by BMP-9, while Ti-Machined only decrease the inhibition (SMAD6) of this pathway. In conclusion, the combination of the osteogenic potential of BMP-9 with the osseoinductive capacity of Ti-Nano could be a promising strategy to favor the osseointegration of Ti implants.

KEYWORDS
bone, bone morphogenetic protein, nanotopography, osteoblast, titanium

1 | INTRODUCTION

In the last decades, several regulatory pathways involved in the osteoblast differentiation have been investigated.[1–5] Transcription factors, chromatin structure modifiers and signaling molecules such as bone morphogenetic proteins (BMPs) play a key role in this event.[6–8] BMPs are growth factors belonging to the transforming growth factor beta (TGF-β) family and some members are potent osseoinductive agents.[9–13]

The BMP canonical or SMAD-dependent signaling pathway is activated by the binding of a BMP to heterodimeric complexes of serine/threonine kinase receptors composed by type I and type II receptors.[10,14] Upon binding of BMP to the receptor complex, the SMAD1/5/8 phosphorylation occurs, which forms heterodimeric complexes with SMAD4 and the active complex is translocated to the nucleus and acts as a transcription factor inducing the expression of BMP target genes.[15,16] The SMAD1/5/8-SMAD4 signaling

Hindawi
Stem Cells International
Volume 2019, Article ID 9618065, 15 pages
https://doi.org/10.1155/2019/9618065

Review Article

Cancer Stem Cells: Powerful Targets to Improve Current Anticancer Therapeutics

Rayana L. Bighetti-Trevisan,[1] **Lucas O. Sousa**,[2] **Rogerio M. Castilho**,[3] **and Luciana O. Almeida**[1]

[1]*Laboratory of Tissue Culture, Department of Basic and Oral Biology, University of Sao Paulo School of Dentistry, Ribeirao Preto, SP 14040-904, Brazil*
[2]*Laboratory of Markers and Cell Signaling of Cancer, Department of Clinical Analyses, Toxicology and Food Sciences, University of Sao Paulo School of Pharmaceutical Sciences, Ribeirao Preto, SP 14040-903, Brazil*
[3]*Laboratory of Epithelial Biology, Department of Periodontics and Oral Medicine, University of Michigan School of Dentistry, Ann Arbor, MI 48109-1078, USA*

Correspondence should be addressed to Luciana O. Almeida; lubio2001@usp.br

Received 22 July 2019; Revised 25 September 2019; Accepted 3 October 2019; Published 12 November 2019

Academic Editor: Sumanta Chatterjee

A frequent observation in several malignancies is the development of resistance to therapy that results in frequent tumor relapse and metastasis. Much of the tumor resistance phenotype comes from its heterogeneity that halts the ability of therapeutic agents to eliminate all cancer cells effectively. Tumor heterogeneity is, in part, controlled by cancer stem cells (CSC). CSC may be considered the reservoir of cancer cells as they exhibit properties of self-renewal and plasticity and the capability of reestablishing a heterogeneous tumor cell population. The endowed resistance mechanisms of CSC are mainly attributed to several factors including cellular quiescence, accumulation of ABC transporters, disruption of apoptosis, epigenetic reprogramming, and metabolism. There is a current need to develop new therapeutic drugs capable of targeting CSC to overcome tumor resistance. Emerging in vitro and in vivo studies strongly support the potential benefits of combination therapies capable of targeting cancer stem cell-targeting agents. Clinical trials are still underway to address the pharmacokinetics, safety, and efficacy of combination treatment. This review will address the main characteristics, therapeutic implications, and perspectives of targeting CSC to improve current anticancer therapeutics.

1. Introduction

Despite the massive amount of research and rapid development of new therapeutic strategies during the past decade, cancer remains a significant public health problem being the second most common cause of death worldwide. It was estimated a total of 18.1 million new cases of cancer in 2018 and 9.6 million deaths worldwide [1].

The carcinogenesis process is driven by a multistep process initiated by the accumulation of successive mutations in normal cells. Despite the extensive efforts in understanding the signaling pathways that control the process of carcinogenesis, and the therapeutic strategies capable of targeting altered signals, the development of new strategies capable of halting cancer progression remains a challenge. Therapy resistance and tumor relapse are frequently observed for most of the malignancies, and they seem to be driven by the cellular heterogeneity that allows drugs to effectively eliminate some, but not all, malignant cells [2].

Malignant tumors are complex systems composed of tumor cells and normal cells of host tissue with different stromal cells, which help to build the phenotypic heterogeneity and malignancy of solid tumors [3]. Intertumor heterogeneity is responsible for the tumor individuality and the difficulty to establish a molecular signature for groups of tumors [4, 5]. Besides, intratumor heterogeneity presents a distinct molecular signature in every single patient.

Photodiagnosis and Photodynamic Therapy 27 (2019) 455–461

Contents lists available at ScienceDirect

Photodiagnosis and Photodynamic Therapy

journal homepage: www.elsevier.com/locate/pdpdt

Effect of curcumin-mediated photodynamic therapy on *Streptococcus mutans* and *Candida albicans*: A systematic review of in vitro studies

Daniele de Cassia Rodrigues Picco, Leonardo Lobo Ribeiro Cavalcante, Rayana Longo Bighetti Trevisan, Aline Evangelista Souza-Gabriel, Maria Cristina Borsatto, Silmara Aparecida Milori Corona*

Department of Pediatric Dentistry, Ribeirão Preto School of Dentistry, University of São Paulo – Café Av, Ribeirão Preto, São Paulo, 14040-904, Brazil

ARTICLE INFO

Keywords:
Curcumin
Biofilms
Streptococcus mutans
Candida albicans
Antimicrobial Photodynamic Therapy

ABSTRACT

Background: There is still no systematized evidence in the literature regarding the combination of curcumin to improve the effects of antimicrobial photodynamic therapy (aPDT) on complex oral biofilms. Therefore, the objective of this review was to systematically assess the antimicrobial effect of curcumin-mediated aPDT on the vitality of biofilms of microorganisms *Streptococcus mutans* and *Candida albicans*.

Methods: The addressed focused question was: "What are the effects of curcumin-mediated antimicrobial therapy on the biofilm viability of *Streptococcus mutans* and *Candida albicans* in vitro models?" A literature search was conducted in the electronic databases Pubmed, Web of Science, Scopus, Cochrane Library and Bireme up to April 2019. In vitro studies evaluating the effect of curcumin-mediated antimicrobial photodynamic therapy on S. mutans and C. albicans biofilms were included.

Results: From 95 citations, 11 full-text articles were screened and 6 studies were included in this review. Because of the heterogeneity observed in the studies selected, meta-analysis was not possible.

Conclusions: The in vitro studies indicate the potential use of curcumin-mediated aPDT to inactivate microorganisms; *Streptococcus mutans* and *Candida albicans*. This survey should be viewed as a starting point for further examinations using standardized parameters to enhance outcomes.

1. Introduction

The oral cavity contains a heterogeneous, copious and complex arrangement of various microbial biological systems that communicate with the host under physiological or pathological conditions [1,2]. Numerous microbial species are sorted out in biofilm structure, which is made for microorganisms by a firmly followed polymer network in dental surface [3]. These structures have specific favorable circumstances that shield them from host protections and treatment [1,4].

The disharmonic connection between oral microbiota parts may prompt the infection process [1]. One of the primary illnesses found in the oral cavity is dental caries [5]. Dental caries often result from a change in metabolic movement brought about by change in biofilm environment, which causes a disruption between dental minerals and biofilm liquids [3].

Streptococcus mutans are the most generally discovered microbes in biofilms that injure dental veneer, being viewed as a primary pathogen [2].So is *Candida albicans*. These organisms pathogenicity is also affected by host conditions [6] and is enhanced by biofilm formation [7].

Photodynamic treatment (PDT) is a treatment methodology that connects a light source with a photosensitizing operator. Appropriate illumination results in generation of reactive oxygen specimens able to oxidize natural atoms [8]. It's an elective treatment that can be connected for various purposes, for example, malignant growth treatment and dermatological conditions [9]. In the oral cavity, PDT is utilized for oral injuries treatment, for example, mucositis and herpes [10,11], and for antimicrobial way to deal with diminish followed biofilms (framed for microbes, organisms, infections and yeasts) in teeth and delicate tissue [12]. Along these lines, PDT rose as an option for treatment of biofilms ailments, for example, dental caries, oral candidiasis, periimplantitis, and periodontal illness, and it is known as antimicrobial photodynamic treatment (aPDT) [13,14]. The utilization of a light hotspot for aPDT is alluring, since blue LED (light emitting diode) is regularly utilized as a dental relieving gadget for polymerization of

* Corresponding author.
E-mail addresses: danielepicco@outlook.com (D.d.C.R. Picco), leonardolobo@usp.br (L.L.R. Cavalcante), rayana.longo@gmail.com (R.L.B. Trevisan), aline.gabriel@forp.usp.br (A.E. Souza-Gabriel), borsatto@forp.usp.br (M.C. Borsatto), silmaracorona@forp.usp.br (S.A.M. Corona).

https://doi.org/10.1016/j.pdpdt.2019.07.010
Received 13 May 2019; Received in revised form 2 July 2019; Accepted 12 July 2019
Available online 25 July 2019

bio-protocol www.bio-protocol.org/e3534 Bio-protocol 10(04): e3534. DOI:10.21769/BioProtoc.3534

Mesenchymal Stromal Cells Derived from Bone Marrow and Adipose Tissue: Isolation, Culture, Characterization and Differentiation

Gileade P. Freitas[1], Alann T. P. Souza[1], Helena B. Lopes[1], Rayana L. B. Trevisan[1], Fabiola S. Oliveira[1], Roger R. Fernandes[1], Fernanda U. Ferreira[2], Felipe A. Ros[2], Marcio M. Beloti[1] and Adalberto L. Rosa[1, *]

[1]Bone Research Lab, School of Dentistry of Ribeirão Preto, University of São Paulo, Ribeirão Preto, SP, Brazil; [2]Hemotherapy Center of Ribeirão Preto, University of São Paulo, Ribeirão Preto, SP, Brazil
*For correspondence: adalrosa@forp.usp.br

[Abstract] Since their discovery, mesenchymal stromal cells (MSCs) have received a lot of attention, mainly due to their self-renewal potential and multilineage differentiation capacity. For these reasons, MSCs are a useful tool in cell biology and regenerative medicine. In this article, we describe protocols to isolate MSCs from bone marrow (BM-MSCs) and adipose tissues (AT-MSCs), and methods to culture, characterize, and differentiate MSCs into osteoblasts, adipocytes, and chondrocytes. After the harvesting of cells from bone marrow by flushing the femoral diaphysis and enzymatic digestion of abdominal and inguinal adipose tissues, MSCs are selected by their adherence to the plastic tissue culture dish. Within 7 days, MSCs reach 70% confluence and are ready to be used in subsequent experiments. The protocols described here are easy to perform, cost-efficient, require minimal time, and yield a cell population rich in MSCs.

Keywords: Adipose tissue, Adipocyte, Bone, Bone marrow, Cell culture, Chondrocyte, Mesenchymal Stromal cell, Osteoblast

[Background] The concept of stem cells dates back to the 19th century, but their existence was confirmed in the 1960s and 1970s following experiments by Friedenstein and collaborators, which showed the presence of stem cells in the bone marrow (Friedenstein, 1970; Bianco *et al*., 2008). Afterward, Caplan (1991) named them as mesenchymal stem cells (here, called mesenchymal stromal cells–MSCs) and proposed their use in regenerative medicine. In the bone marrow, the percentage of MSCc is estimated to be 0.001 to 0.01% of the total mononuclear cells. Because of their scarcity, alternative sources have been described, although bone marrow remains as the main source of MSCs (Nancarrow-Lei *et al*., 2017). Adipose tissue is a very promising source because it contains a large number of MSCs that are relatively easy to harvest with minimal discomfort and risk for donors (Zuk *et al*., 2001). The protocols used to harvest and culture MSCs from either bone marrow (BM-MSCs) or adipose tissue (AT-MSCs), may vary among different species or even among different strains of the same species. The most commonly used methods for obtaining MCSs involve using flow cytometry (Schrepfer *et al*., 2007), multipotent adult progenitor cell media (Harting *et al*., 2008), the ficoll-paque gradient centrifugation method (Pierini *et al*., 2012), and immunomagnetic beads (Wadajkar *et al*., 2014). Here, we describe cost-efficient protocols that are relatively easy and fast to perform and can be used

Thrombosis Research 186 (2020) 45–53

Contents lists available at ScienceDirect

Thrombosis Research

journal homepage: www.elsevier.com/locate/thromres

Full Length Article

Inhibitory effects of dabigatran etexilate, a direct thrombin inhibitor, on osteoclasts and osteoblasts

Amanda Leal Rocha[a], Rayana Longo Bighetti-Trevisan[b], Letícia Fernanda Duffles[c], José Alcides Almeida de Arruda[a], Thaise Mayumi Taira[c], Bruna Rodrigues Dias Assis[d], Soraia Macari[e], Ivana Márcia Alves Diniz[f], Marcio Mateus Beloti[b], Adalberto Luiz Rosa[b], Sandra Yasuyo Fukada[c], Gisele Assis Castro Goulart[d], Daniel Dias Ribeiro[g], Lucas Guimarães Abreu[e], Tarcília Aparecida Silva[a,*]

[a] Department of Oral Surgery and Pathology, Faculty of Dentistry, Federal University of Minas Gerais, Belo Horizonte, MG, Brazil
[b] Bone Research Laboratory, School of Dentistry of Ribeirão Preto, University of São Paulo, Ribeirão Preto, SP, Brazil
[c] Department of Physics and Chemistry, Faculty of Pharmacological Science, University of São Paulo, Ribeirão Preto, SP, Brazil
[d] Department of Pharmaceutics, Faculty of Pharmacy, Federal University of Minas Gerais, Belo Horizonte, MG, Brazil
[e] Department of Pediatric Dentistry and Orthodontics, Faculty of Dentistry, Federal University of Minas Gerais, Belo Horizonte, MG, Brazil
[f] Department of Restorative Dentistry, Faculty of Dentistry, Federal University of Minas Gerais, Belo Horizonte, MG, Brazil
[g] Department of Hematology, Faculty of Medicine, Federal University of Minas Gerais, Belo Horizonte, MG, Brazil

ARTICLE INFO

Keywords:
Anticoagulants
Dabigatran
Thrombin
Osteoclasts
Osteoblasts
Cell Culture Techniques

ABSTRACT

Introduction: Anticoagulants are widely used in orthopedic surgery to decrease the risk of deep vein thrombosis. While significant bone impairment is induced by long-term heparin therapy, little is known about the effects of direct oral anticoagulants (DOACs). Herein, we investigated the effects of dabigatran etexilate (Pradaxa®), a DOAC inhibitor of thrombin, on bone cells using *in vitro* and *ex vivo* cell culture models.

Materials and methods: Osteoblasts and osteoclasts exposed to different concentrations of dabigatran etexilate and untreated cells were assayed for cell differentiation and activity. Favorable osteogenic conditions for osteoblasts were tested using titanium with nanotopography (Ti-Nano). In addition, mice treated with a dabigatran etexilate solution had bone marrow cells analyzed for the ability to generate osteoclasts.

Results: Dabigatran etexilate at concentrations of 1 μg/mL and 2 μg/mL did not impact osteoclast or osteoblast viability. The drug inhibited osteoclast differentiation and activity as observed by the reduction of TRAP+ cells, resorption pits and gene and protein expression of cathepsin K. Consistently, osteoclasts from mice treated with dabigatran showed decreased area, resorptive activity, as well as gene and protein expression of cathepsin K. In osteoblast cultures, grown both on polystyrene and Ti-Nano, dabigatran etexilate reduced alkaline phosphatase (ALP) activity, matrix mineralization, gene expression of ALP and osteocalcin.

Conclusions: Dabigatran etexilate inhibited osteoclast differentiation in *ex vivo* and *in vitro* models in a dose-dependent manner. Moreover, the drug reduced osteoblast activity even under optimal osteogenic conditions. This study provides new evidence regarding the negative overall impact of DOACs on bone cells.

1. Introduction

Long-term oral anticoagulation is indicated for the prevention and treatment of thromboembolic diseases. Coumarins or vitamin K antagonists have been the first choice therapy for over 50 years [1]. Nevertheless, over the last few years, direct oral anticoagulants (DOACs) have been approved, with the advantages of having more predictable pharmacokinetics and fewer drug interactions [2]. These

* Corresponding author at: Department of Oral Surgery and Pathology, School of Dentistry, Universidade Federal de Minas Gerais, Av. Pres. Antônio Carlos, 6627, room 3204, Belo Horizonte, MG CEP: 31.270-910, Brazil.
E-mail addresses: amandaauharek@yahoo.com.br (A.L. Rocha), rayana.longo@gmail.com (R.L. Bighetti-Trevisan), leticia_duffles@hotmail.com (L.F. Duffles), alcides_almeida@hotmail.com (J.A.A. de Arruda), thaise.taira@usp.br (T.M. Taira), brunardias@outlook.com (B.R.D. Assis), soraiamacari@gmail.com (S. Macari), ivanadiniz@ymail.com (I.M.A. Diniz), mmbeloti@usp.br (M.M. Beloti), adalrosa@forp.usp.br (A.L. Rosa), sfukada@usp.br (S.Y. Fukada), giseleacgoulart@gmail.com (G.A.C. Goulart), ddribeiro@terra.com.br (D.D. Ribeiro), lucasgabreu01@gmail.com (L.G. Abreu), tarcilia@ufmg.br (T.A. Silva).

https://doi.org/10.1016/j.thromres.2019.12.014
Received 23 October 2019; Accepted 19 December 2019
Available online 23 December 2019
0049-3848/

Original Research
Basic Implantodontology and Biomaterials

Bioactive glass-ceramic for bone tissue engineering: an *in vitro* and *in vivo* study focusing on osteoclasts

Rayana Longo BIGHETTI-TREVISAN[a]
Alann Thaffarell Portilho SOUZA[a]
Ingrid Wezel TOSIN[a]
Natália Pieretti BUENO[b]
Murilo Camuri CROVACE[c]
Marcio Mateus BELOTI[a]
Adalberto Luiz ROSA[a]
Emanuela Prado FERRAZ[b]

[a]Universidade de São Paulo – USP, School of Dentistry of Ribeirão Preto, Bone Research Lab, Ribeirão Preto, SP, Brazil.

[b]Universidade de São Paulo – USP, School of Dentistry, Department, São Paulo, SP, Brazil

[c]Universidade Federal de São Carlos – UFScar, Vitreous Materials Laboratory, São Carlos, SP, Brazil.

Declaration of Interests: The authors certify that they have no commercial or associative interest that represents a conflict of interest in connection with the manuscript.

Corresponding Author:
Emanuela Prado Ferraz
E-mail: emanuelaferraz@usp.br

https://doi.org/10.1590/1807-3107bor-2020.volXX.0000

Submitted: September 10, 2020
Accepted for publication: June 2, 2021
Last revision: November 4, 2021

Abstract: Despite the crucial role of osteoclasts in the physiological process of bone repair, most bone tissue engineering strategies have focused on osteoblast-biomaterial interactions. Although Biosilicate® with two crystalline phases (BioS-2P) exhibits osteogenic properties and significant bone formation, its effects on osteoclasts are unknown. This study aimed to investigate the *in vitro* and *in vivo* effects of BioS-2P on osteoclast differentiation and activity. RAW 264.7 cells were cultured in osteoclastogenic medium (OCM) or OCM conditioned with BioS-2P (OCM-BioS-2P), and the cell morphology, viability, and osteoclast differentiation were evaluated. BioS-2P scaffolds were implanted into rat calvarial defects, and the bone tissue was evaluated using tartrate-resistant acid phosphatase (TRAP) staining and RT-polymerase chain reaction (PCR) after 2 and 4 weeks to determine the gene expressions of osteoclast markers and compare them with those of the bone grown in empty defects (Control). OCM-BioS-2P favored osteoclast viability and activity, as evidenced by an increase in the TRAP-positive cells and matrix resorption. The bone tissue grown on BioS-2P scaffolds exhibited higher expression of the osteoclast marker genes (*Ctsk*, *Mmp 9*, *Rank*) after 2 and 4 weeks and the *RankL/Opg* ratio after 2 weeks. *Trap* gene expression was lower at 2 weeks, and a higher number of TRAP-stained areas were observed in the newly formed bone on BioS-2P scaffolds at both 2 and 4 weeks compared to the Controls. These results enhanced our understanding of the role of bioactive glass-ceramics in bone repair, and highlighted their role in the modulation of osteoclastic activities and promotion of interactions between bone tissues and biomaterials.

Keywords: Biocompatible Materials; Osteoclasts; Bone and Bones; Tissue Engineering.

Introduction

The increasing clinical demand for bone regeneration has encouraged the development of porous scaffold biomaterials for tissue engineering-based therapies. The ideal biomaterial should be three-dimensional, resorbable, biocompatible, porous, and exhibit sufficient mechanical strength.[1,2] Bioactive glasses have emerged as a promising alternative due to their superior biocompatibility and osteoinductive characteristics,[3,4,5]

Received: 5 November 2021 | Revised: 2 March 2022 | Accepted: 6 April 2022
DOI: 10.1111/odi.14209

ORIGINAL ARTICLE

ORAL DISEASES WILEY

Epithelial–mesenchymal transition and cancer stem cells: A route to acquired cisplatin resistance through epigenetics in HNSCC

Julia Lima de Oliveira[1] | Thaís Moré Milan[1] | Rayana Longo Bighetti-Trevisan[1] | Roger Rodrigo Fernandes[1] | Andréia Machado Leopoldino[2] | Luciana Oliveira de Almeida[1]

[1]Department of Basic and Oral Biology, School of Dentistry of Ribeirão Preto, University of São Paulo, Ribeirão Preto, Brazil

[2]Department of Clinical Analyses, Toxicology and Food Sciences, School of Pharmaceutical Sciences of Ribeirão Preto, University of São Paulo, Ribeirão Preto, Brazil

Correspondence
Luciana Oliveira de Almeida, School of Dentistry of Ribeirão Preto, University of São Paulo, Av. do Café, s/n, 14040-904, Ribeirão Preto, SP, Brazil.
Email: lubio2001@usp.br

Funding information
This study was supported by the State of São Paulo Research Foundation (FAPESP, Brazil, grants # 2017/11780-8, # 2018/02959-7, and # 2018/11303-8)

Abstract

Chemoresistance is associated with tumor recurrence, metastases, and short survival. Cisplatin is one of the most used chemotherapies in cancer treatment, including head and neck squamous cell carcinoma (HNSCC), and many patients develop resistance. Here, we established cell lines resistant to cisplatin to better understand epigenetics and biological differences driving the progression of HNSCC after treatment. Cisplatin resistance was established in CAL-27 and SCC-9 cell lines. Gene expression of HDAC1, HDAC2, SIRT1, MTA1, KAT2B, KAT6A, KAT6B, and BRD4 indicated the cisplatin activates the epigenetic machinery. Increases in tumor aggressiveness were detected by BMI-1 and KI-67 in more resistant cell lines. Changes in cellular shape and epithelial–mesenchymal transition (EMT) activation were also observed. HDAC1 and ZEB1 presented an opposite distribution with down-regulation of HDAC1 and up-regulation of ZEB1 in the course of chemoresistance. Up-regulation of ZEB1 and BMI-1 in patients with HNSCC is also associated with a poor response to therapy. Cancer stem cells (CSC) population increased significantly with chemoresistance. Down-regulation of HDAC1, HDAC2, and SIRT1 and accumulation of Vimentin and ZEB1 were observed in the CSC population. Our results suggest that in the route to cisplatin chemoresistance, epigenetic modifications can be associated with EMT activation and CSC accumulation which originate more aggressive tumors.

KEYWORDS
BMI-1, chemoresistance, epigenetic reprogramming, head and neck cancer, ZEB1

1 | INTRODUCTION

Head and neck squamous cell carcinoma (HNSCC) is classified as the sixth most common cancer worldwide, and despite advances in treatment, the locally progressive disease presents a poor prognosis, with a survival rate of approximately 50% after 5 years (Küçükgüven & Çelebi-Saltik, 2021; Peitzsch et al., 2019). The high mortality rates result from late diagnosis, locoregional failure, disease recurrences, distant metastasis, and the unknown molecular basis involved in acquired resistance to therapy (Chang & Wang, 2016; Datta et al., 2016).

Platinum-based therapies, such as cisplatin, is the primary option to treat various cancers, including head and neck carcinomas, targeting proliferative cells, inhibiting DNA synthesis, RNA transcription, cell cycle, and inducing apoptosis (Galluzzi et al., 2012; Plaks et al., 2015). The treatment is efficient at the beginning; however,

Anexos

ANEXO A

JOURNAL AUTHOR RIGHTS DO PERIÓDICO MATERIALS SCIENCE & ENGINEERING: C, MATERIALS FOR BIOLOGICAL APPLICATIONS

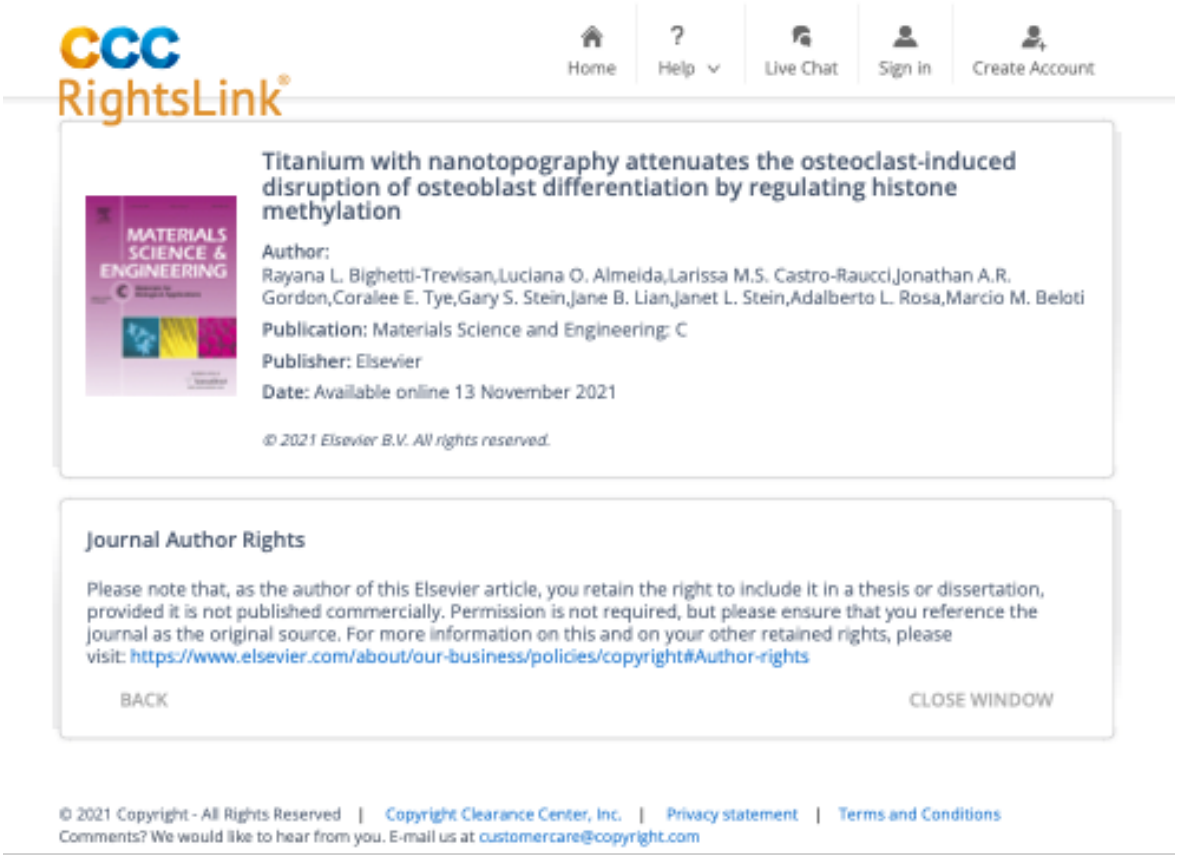

CCC RightsLink®

Home | Help | Live Chat | Sign in | Create Account

Titanium with nanotopography attenuates the osteoclast-induced disruption of osteoblast differentiation by regulating histone methylation

Author:
Rayana L. Bighetti-Trevisan,Luciana O. Almeida,Larissa M.S. Castro-Raucci,Jonathan A.R. Gordon,Coralee E. Tye,Gary S. Stein,Jane B. Lian,Janet L. Stein,Adalberto L. Rosa,Marcio M. Beloti

Publication: Materials Science and Engineering: C

Publisher: Elsevier

Date: Available online 13 November 2021

© 2021 Elsevier B.V. All rights reserved.

Journal Author Rights

Please note that, as the author of this Elsevier article, you retain the right to include it in a thesis or dissertation, provided it is not published commercially. Permission is not required, but please ensure that you reference the journal as the original source. For more information on this and on your other retained rights, please visit: https://www.elsevier.com/about/our-business/policies/copyright#Author-rights

BACK CLOSE WINDOW

© 2021 Copyright - All Rights Reserved | Copyright Clearance Center, Inc. | Privacy statement | Terms and Conditions
Comments? We would like to hear from you. E-mail us at customercare@copyright.com

ANEXO B

RESULTADO DA UTILIZAÇÃO DO SERVIÇO TURNITIN, PARA DETECÇÃO DE PLÁGIO

Turnitin TESE Rayana 24-05-22

RELATÓRIO DE ORIGINALIDADE

22%	18%	15%	%
ÍNDICE DE SEMELHANÇA	FONTES DA INTERNET	PUBLICAÇÕES	DOCUMENTOS DOS ALUNOS

FONTES PRIMÁRIAS

1	teses.usp.br Fonte da Internet	5%
2	www.escavador.com Fonte da Internet	4%
3	Helena Bacha Lopes. "Participação de integrinas na diferenciação osteoblástica induzida por superfícies de titânio com nano e microtopografia", Universidade de Sao Paulo Sistema Integrado de Bibliotecas - SIBiUSP, 2019 Publicação	3%
4	"Análise do potencial osteogênico e adipogênico de células-tronco mesenquimais derivadas de medula óssea e de tecido adiposo", 'Universidade de Sao Paulo, Agencia USP de Gestao da Informacao Academica (AGUIA)' Fonte da Internet	2%
5	Rayana L. Bighetti-Trevisan, Luciana O. Almeida, Larissa M.S. Castro-Raucci, Jonathan	1%

	A.R. Gordon et al. "Titanium with nanotopography attenuates the osteoclast-induced disruption of osteoblast differentiation by regulating histone methylation", Materials Science and Engineering: C, 2021 Publicação	
6	www.tcc.sc.usp.br Fonte da Internet	1 %
7	"2019 Annual Meeting of the American Society for Bone and Mineral Research Orange County Convention Center, Orlando, Florida, USA September 20–23, 2019", Journal of Bone and Mineral Research, 2019 Publicação	1 %
8	Natália Pieretti Bueno. "Efeito da terapia de fotobiomodulação na diferenciação osteoblástica de células-tronco mesenquimais derivadas da medula óssea de ratos diabéticos", Universidade de Sao Paulo, Agencia USP de Gestao da Informacao Academica (AGUIA), 2020 Publicação	1 %
9	bv.fapesp.br Fonte da Internet	1 %
10	repositorio.ufrn.br Fonte da Internet	1 %

11	pt.scribd.com Fonte da Internet	1 %

Excluir citações	Desligado	Excluir correspondências	< 1%
Excluir bibliografia	Em		